Expecting the Unexpected

- Investigating Functional Magnetic Resonance Imaging (fMRI) Signals During Repetition Suppression, Expectation and Attention, using Arterial Spin Labelling and Spectroscopy.

Hanna J. Rooslien

Royal Holloway University of London

31^{st} of October 2019

A thesis presented for the degree of

Doctor of Philosophy

Declaration

I declare that this work was carried out in accordance with the Regulations of the University of London. I declare that this submission is my own work, and to the best of my knowledge does not represent the work of others, published or unpublished, expect where duly acknowledged in the text. No part of this thesis has been submitted for a higher degree at another university of institution.

Signed:..... Date:.....

Hanna J Rooslien

Royal Holloway University of London

Abstract

This thesis explored the fMRI blood oxygenation level dependent (BOLD) signal in various scenarios by simultaneously measuring cerebral blood flow (CBF) using arterial spin labelling (ASL). The first empirical chapter contains two experiments that used a repetition suppression (RS) paradigm to investigate how the coupling between CBF and the BOLD signal varies with expectation when attention is focused on the stimuli (experiment 1) and when attention is diverted away (experiment 2). The stimuli consisted of pairs of face identities that were either repeated or alternated. The probability of repetition was manipulated so that some runs had a 75% probability of repetition and some runs had a 75% probability of alternation. Experiment 1 showed that BOLD effects do not map onto CBF effects and hence suggests that expectation effects may be, in part, hemodynamically driven. Experiment 2 showed that when attention is diverted, CBF data consistently showed expectation effects.

The second empirical chapter demonstrates an experiment that used ASL and spectroscopy to assess the relationship between gamma-aminobutyric acid (GABA), CBF and positive and negative BOLD signals. This experiment used a blocked design where bow-tie shaped flickering checkerboards were shown in either horizontal or vertical orientation. This allowed for selecting positively and negatively responding voxels. This experiment demonstrated that there was a positive relationship between the BOLD signal and CBF in both positive and negative voxels,

and moreover that neurovascular coupling varies with GABA levels.

The third empirical chapter describes an experiment that adapted an electroencephalogram (EEG) mismatched negativity (MMN) experiment into a RS paradigm using fMRI. It used duration pairs that either repeated or alternated while attention was diverted. This experiment failed to replicate any RS effects.

Acknowledgements

First of all, obviously, I would like to thank Dr. Jonas Larsson and Dr. Szonya Durant for their supervision and support. Without you this research endeavour would not have been possible. Thank you for letting me explore and express my scientific creativity, however crazy my ideas have been. Thank you, Royal Holloway University of London, for investing in me and giving me the opportunity to work on something this cool.

Thereafter, I would like to thank Matt who has been my comrade in arms. With you, this journey sucked significantly less.

I would also like to extend my gratitude to the examiners, Professor Alex Wade and Dr Joshua Balsters, for their insightful comments and advice. The thesis is now a much better piece of research.

A special thank you goes to my friends who have endured me throughout this process. Suzanna, you are my rock. Kathrin, you've got my back. Suzie, you are inspirational as Fraiser. Thank you to everyone in the PhD office who have been by my side and indulged my fMRI nerdiness. Thank you, Ari, for great conversations and always keeping my spirits high during the countless (∼85) scanning hours. Thank you, Coach Lloyd and Coach Serge, for keeping me grounded and pushing me to do more. Thank you, Goggins for teaching me the art of taking souls. And of course, my godparents and family, I am eternally grateful for your support and guidance.

Finally, thank you to Professor Tamar Pincus and Veli Inov for helping me print this thesis during the campus-wide printer failure.

Thanks to you all for your contribution to this journey. I am a fundamentally different person now than I was three years ago.

Contents

List of Figures

List of Tables

List of Abbreviations

AMPA - alpha-amino-3-hydroxy-5-methyl-4-isoxazole-propionic acid

ANOVA - Analysis of Variance

ASL - Arterial Spin Labelling

ATP - Adenosine Triphosphate

AUC - Area Under the Curve

B0 - Magnetic Field

BK Channel - Big Potassium Channel

BOLD - Blood Oxygenation-Level Dependent

Ca^{2+} - Calcium

CBF - Cerebral Blood Flow

CBV - Cerebral Blood Volume

$CMRO_2$ - Cerebral Metabolic Rate of Oxygen

CO2 - Carbon Dioxide

CSF - Cerebral Spinal Fluid

EEG - Electroencephalography

EPI - Echo Planar Imaging

EPISTAR - Echo Planar Imaging and Signal Targeting with Alternating Radiofrequency

EPSP - Excitatory Postsynaptic Potentials

ERP - Event Related Potential

ES - Expectation signals

ES - Expectation signals

F - Female

FA - Flip Angle

FDR - False Discovery Rate

FFA - Fusiform Face Area

FID - Free Induction Decay

FLAIR - Flow-sensitive Alternating Inversion Recovery

fMRI - Functional Magnetic Resonance Imaging

fNIRS - Functional Near-Infrared Spectroscopy

FoV - Field of View

FRA - Face Responding Area

FreqAlt - Alternation in Frequent probability of repetition run

FreqRep - Repetition in Frequent probability of repetition run

GABA - Gamma-Aminobutyric Acid

GLM - General Linear Model

Glux - Glutamine Complex

GRAPPA - Generalized Autocalibrating Partial Parallel Acquisition

HC - High Contrast

HRF - Hemodynamic Response Function

InfreqAlt - Alternation in Infrequent probability of repetition run

InfreqRep - Repetition in Infrequent probability of repetition run

IPL - Inferior Parietal Lobule

IPSP - Inhibitory Postsynaptic Potentials

IRF - Impulse Response Function

ISI - Inter-Stimulus Interval

IT - Inferotemporal

IT/TI - Time of Inversion

ITI - Inter-Trial Interval

LFP - Local Field Potential

LGN - Lateral Geniculate Nucleus

LO - Lateral Occipital

LOC - Lateral Occipital Cortex

M - Theoretical Maximum BOLD Response

MatLab - Matrix Laboratories

MEG - Magnetoencephalography

MDEFT - Modified Driven Equilibrium Fourier Transform

mm - millimeter

MMN - Mismatch Negativity

MPRAGE - Magnetization Prepared - Rapid Gradient Echo

MR - Magnetic Resonance

MRI - Magnetic Resonance Imaging

MRS - Magnetic Resonance Spectroscopy

ms - Millisecond

MT - Middle Temporal

MUA - Multi-unit Activity

n-coupling - fractional change ratio between CBF and CMRO2

NMDA - N-methyl-D-aspartate

NO - Nitric Oxid

NOS1 - Nitric Oxide Synthase type-1

NVC - Neurovascular Coupling

O_2 - Oxygen

OFC - Occipital Face Area

PET - Positron Emission Tomography

PICORE - Proximal Inversion with Control of Off-Resonance Effects

PPA - Parahippocampal Place Area

ppm - Parts Per Million

pRF - Population Receptive Fields

RF - Receptive Field

RF pulse - Radiofrequency Pulse ROI - Region of Interest

RS - Repetition Suppression

RSVP - Rapid Serial Visual Presentation

s - Second

se - Standard Error

SPL - Superior Parietal Lobule

SST - Somatostatin

std - Standard Deviation

STS - Superior Temporal Sulcus

SUA - Single Unit Activity

T1w - T1 weighted

TE - Echo Time

TMS - Transcranial Magnetic Stimulation

TR - Repetition Time

V1 - Primary Visual Cortex

VASO - Vascular Space Occupancy

vMMN - Visual Mismatch Negativity

Chapter 1

Chapter One: Introductions

1.1 Overview

Exploring and understanding the brain is the ultimate goal for cognitive neuroscientists. The brain is a complex and intricate system of various biological tissues that communicate through chemical and electrical messaging systems. It is messy to say the least. Additionally, every brain is highly heterogenous and no brain morphology or function is identical. Perhaps therein lies the attraction: "even complex systems follow rules" (Gaehtgens, 2002, pp.4). This may be the justification for continuing the exploration and investigation of the neural environment. The computational and physiological processes occurring that yield perception, cognition and consciousness are not fully understood. The last decades of research into the human brain and its dynamics have uncovered a multitude of elegant mechanistic candidates that aim to explain how this 1.3kg lump of fatty tissue make up the very essence of what makes us uniquely us. In the beautifully worded question by Gaehtgens, 2002, albeit referring to the vascular system, may possibly sum up where the field of cognitive neuroscience currently stands: "do we understand it better, or do we only know

more?" (Gaehtgens, 2002, pp.4).

At the heart of cognitive neuroscience lies the methods and tools we use to unveil fundamental secrets that the brain is hosting. We put our trust in neuroimaging methods, whether they are based on electrical conductance or hemodynamic changes, and carefully designed experiments to give us the sought-after answers. The hope is that neither will betray our trust. Experimental design may seem more in our control, but cannot be overlooked. Neuroimaging methods, however, are also not trivial and their underlying signal source is often complex. Some may say too complex. Some may even doubt their reliability and validity. To date, the field has invested a tremendous amount of resources into generating data based on neuroimaging techniques. The development of the popular technique, functional magnetic resonance imaging (fMRI) has indeed seen ups and downs over the past decades and for good reason. It has become a go-to tool to investigate the human brain, and the research it has yielded is impressive. However, as a responsible scientists it is important to question to what extent we understand what the technique's data are suggesting.

Indeed, focus has slightly shifted to also indulge research into understanding the fMRI signal itself. All in the hope that this investment of time and capital is not sunk cost. Luckily, research is corroborating to suggest that we can rely on the signal to some extent – we know it relates to neural activity in some capacity. But we can do better – we can understand it better. In fact, there are many gaps in our knowledge and understanding of what we are actually measuring when we use fMRI. This thesis is offering one additional bridging step to help fill some of these gaps.

I investigate the hemodynamic contribution to the popular, but debated, visual expectation signal observed through fMRI repetition suppression (RS) paradigms. I thereafter assess how this neurovascular coupling (NVC) relationship changes with

attention. To further understand the potential neural dynamics that underlie various fMRI signals (positive and negative), I additionally explore the hemodynamic patterns during these signals and how those relate to local concentrations of putative inhibitory neurotransmitters in the visual system. Lastly, I explore the effect of attentional control during repetition suppression of visual duration – a study aiming to replicate an electroencephalogram (EEG) study.

These lines of research are important as they offer new knowledge regarding the neuroimaging signals that the field relies on. Specifically, I show that expectation signals are to some extent hemodynamic. This suggests that we need to be cautious when drawing conclusions relating to neural processing when studying these signal-types. Furthermore, expectation signals are still expressed in hemodynamic activity when attention is controlled for. Moreover, there are differences in coupling ratios depending on expectation level. This underscores that the traditional fMRI (the blood oxygenation-level dependent or BOLD) signal alone is not sufficient to appropriately study these fine-grained variations in neural expression.

Consistent with this are findings from the next experiment where I investigate the relationship between the fMRI BOLD signals (positive and negative), hemodynamics and the putative marker for neural inhibition. Again, there is evidence for differential coupling ratio that varies with inhibitory activity.

Lastly, I aimed to determine whether early visual areas can discriminate between short visual durations whilst attention is diverted. An EEG study (Durant, Sulykos, & Czigler, 2018) finds evidence for mismatch negativity (MMN) effects in visual areas when controlling for attention and it was predicted, but not supported, that RS effects would emerge in visual areas when adapting the study for fMRI.

This thesis' empirical experiments exclusively use visual paradigms and different fMRI techniques to understand the relationship between neural activity and vascular

responses – NVC. The story is: traditional fMRI signals are complex and therefore its use does not justify straightforward interpretation. Therefore, it is of utmost importance to also measure other aspects that may contribute to the traditional signal. These arguments do not suggest that fMRI is inherently problematic – it is not. It is highly complicated and it is the interpretation of the signals that is problematic. This thesis' experiments aim to generate an appreciation for the complexity of the traditional fMRI signal and encourage the use of and further research into what intricate dynamics can yield the various signal signatures. Although critical, I hope to convey an optimistic view of how fMRI experiments can be improved, how questions can be improved for using fMRI to investigate the brain, and how hemodynamics may possibly offer a different angle to study and understand the brain.

1.2 Background Chapter: Vision

1.2.1 The Visual System

The visual system is one the most understood parts of the brain and is often studied as an example for basic brain processes, but certain aspects remain elusive. The field has through careful experimentation and observation showed that the visual system demonstrates a hierarchical functional organisation to some extent. Specifically, that each level of this system processes increasingly complex visual features. However, research has also shown that it is unclear where to draw the line of what level of complexity is processed at each visual level. It appears many factors such as feature type, context, attention, brain states, memory, and recency amongst other processes play a part in painting a more complicated picture of how the visual system works. Indeed, the abundance of anatomical feedback connections in addition to feedforward projections between each visual area corroborates this and is indicative of a sophisticated recurrent relationship. This makes the dynamics of the visual system tricky to study and hence warrants careful experimentation and observation in order to draw appropriate conclusions of how the brain processes visual information.

This background chapter aims to provide the reader with an appreciation of the relevant areas of the human visual system and the commonly used measurement tools to study these. First, I will outline the first steps that lead to vision, then I will describe the basic structure and of the visual brain in terms of receptive fields and retinotopy. Thereafter, I will describe and discuss the widely used approach to study visual processing and perception – adaptation and repetition suppression. Then, I will discuss expectation and attention and how these processes may or may not affect adaptation signals. This naturally leads to a discussion of models and theoretical frameworks aiming to explain this. This is not an exhaustive review, but rather it aims to provide the necessary basics for understanding the relevance of the

thesis at hand.

1.2.1.1 From Light to Lobe

To fully appreciate the elegance yet simplicity of the visual system it is important to first understand how the brain receives visual input from the external world. Elementary particles known as photons are energy packets that are commonly known as light. These hit the eyes and travel through transparent layers of cells known as the retina – at the back of the retina are photoreceptors. In the human retina there are two photoreceptors; rods and cones which are sensitive to luminance changes and colours, respectively. Once photons, or light, reach a photoreceptor there are pigments inside these receptors that change shape. This shape-change results in a release of protein that cause a cascade of events the lead to phototransduction – namely, the process of letting the next layer of cells know that light has been detected. The next layer, the middle layer, consist of bipolar cells that collect information from photoreceptors at the back of the retina and relays this to the ganglion cells at the front of the retina. The ganglion cells can then integrate and project this through long cell projections, or axons, that make up the optic nerve. This nerve thereafter sends this information from each eye to the opposite brain half, or hemisphere (Bear, Connors, & Paradiso, 2007).

A curious feature of the visual system is that information from each eye is processed in the opposite, or contralateral, hemisphere. In other words, imagine the visual world in front of you, and imagine a vertical line drawn in the middle. This illustrates the left and right visual field. The left visual field that is seen mainly by the left eye is processed in the right hemisphere, and vice versa. This happens because the optic nerves from each eye that cross paths in an anterior portion of the brain known as the optic chiasm, or optic crossing. From there the information is relayed to the lateral geniculate nucleus (LGN) which is a six layered thalamic

structure that projects to the occipital region of the brain (Bear et al., 2007).

The occipital lobe is located in the posterior part of the brain and is divided by the cerebral fissure into its two hemispheric lobes. In each hemisphere, the lobe folds itself inwards creating a groove known as the calcarine sulcus. This is the seat for the first level of visual processing, namely, primary visual cortex, V1, or striate cortex. The next level is V2, followed by V3, V4, and V5 – these are collectively known as the early visual areas. Before discussing how these regions were delineated it is important to describe the concept of receptive fields, as this lays the groundwork for understanding how the early visual areas are defined.

1.2.1.2 Receptive Fields

Receptive fields (RFs) can be viewed as fundamental processing units of sensory modalities. They are defined as a localised sensory region that generates a neural response when stimulated. Careful electrophysiological experiments demonstrated these units in the visual system: using single-cell recording, Kuffler, 1953 found that the cat's retinal ganglion cells responded to visual stimuli in a concentric ON centre (excitatory) and OFF surround (inhibitory) (or OFF centre and ON surround) manner. These units became known as visual RFs (referred to simply as RFs from now on). Interestingly, RFs in V1 responded preferentially to particular features compared to their retinal and LGN counterparts, and their morphology is different. While retinal and LGN RFs are small and concentric, V1 cells are larger and elongated. This led to the conclusion that information must be integrated and relayed in a hierarchical fashion. In other words, V1 cells will receive integrated information pooled from the LGN, which receives information in a similar way from the retina (e.g. Hubel & Wiesel, 1959, 1962) (see figure 1.1 for an illustration of cell pooling).

Interestingly, it seems as though RFs in V1 show a preference to lines and orien-

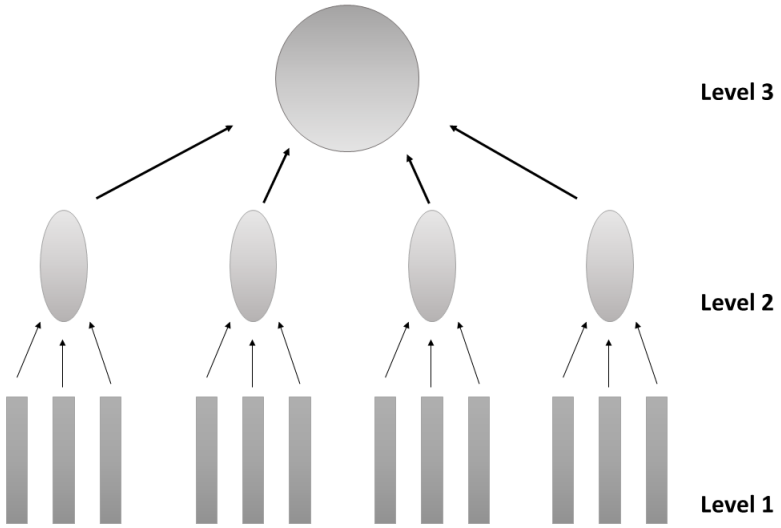

Figure 1.1: Illustration of receptive field pooling. Several small RFs relay information into one larger RF further along the hierarchy. Similarly, these larger RFs send information to another even larger RF. This image is only a simplistic illustration of the process. The image is adapted from Heeger, 2006

tations, while V2 units show stronger responses to combinations of lines for example corners or simple shapes. The higher up the visual hierarchy there seem to be preferences for progressively more complex stimuli. For example, V5 tend to respond well to motion, fusiform face area (FFA) seem to enjoy faces (in comparison to houses, objects, or scrambled face images) and lateral occipital cortex (LOC) respond consistently to objects (compared to e.g. faces or houses). Before discussing higher visual areas that show preference for complex stimulus-types, the story needs to begin with how the it was figured out how to delineate the borders of the early visual areas.

1.2.1.3 Retinotopy

As mentioned, RFs in V1 respond preferentially to lines and orientations, and this activity demonstrate a topographic pattern. In their seminal work Gattass, Gross, and Sandell, 1981 demonstrated features of retinotopy: the property of how the visual world topographically maps onto the visual cortex. They recorded single cells

in the cat's visual cortex and found that the spatial locations of the cat's visual field had the same spatial correspondence in the primary visual cortex as on the retina, hence *retinotopy*. As mentioned previously, the visual world maps onto the visual cortex albeit contralaterally and up-side-down: RFs, or neurons, in the lower bank of the left calcarine sulcus responds to stimulation in the upper right visual field (see figure 1.2). In the right part of figure 1.2, this corresponds to the light-blue and turquoise field in the circular object, and it maps onto the lower bank of the calcarine as see on the colour-matched brain surface below.

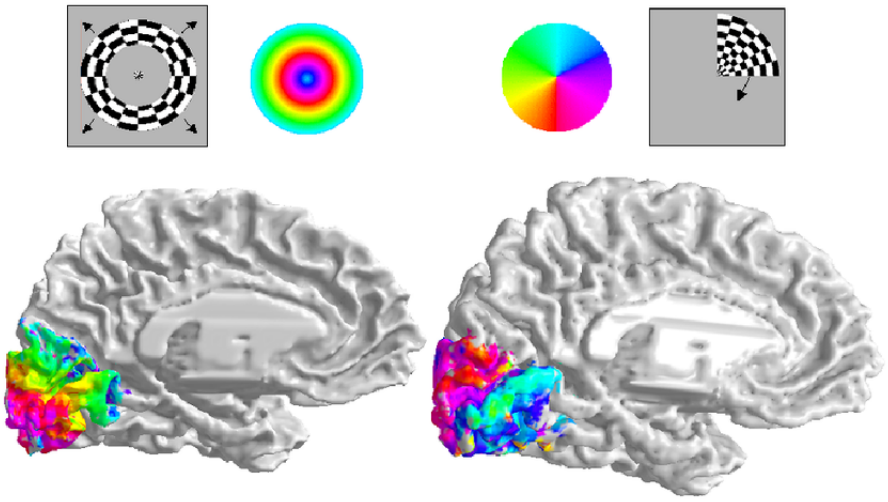

Figure 1.2: Illustration of retinotopy. The square insets reflect the visual field and the stimuli commonly used to map polar angle and eccentricity. The colourful circular objects next to the stimuli are colour-keys linking the visual stimulation to the occipital lobe. For example, when the eccentricity ring reaches the yellow part of the circular object, then this stimulates the yellow part of the occipital lobe. The image is taken from Dougherty et al., 2003

At closer inspection the authors note that cells by the occipital pole part of the calcarine sulcus, respond to stimulation in the middle (or foveal) visual field while cells located more rostrally in the fundus responds to stimuli located further away from central vision – the eccentricity coding feature of the retinotopic map (see figure 1.2 left-hand side for illustration). Additionally, cells located in the innermost part of the sulcus, the fundus, responds to stimulation along the horizontal meridian (imagine again a horizontal line in the middle of the visual world) of the visual field. Cells located progressively further away from the fundus respond to stimulation

progressively closer to the vertical meridian – the retinotopic feature of polar angle (see figure 1.2, right-hand side).

However, as soon as one crosses the vertical meridian the next set of cells stop responding, though, they give responses if the stimulation begins moving away from the vertical meridian back towards the horizontal meridian. Moreover, the cells will respond to larger areas of stimulation. This reveals a border between visual areas V1 and V2. Cells in V2 respond to visual stimulation reaching from the vertical to the horizontal meridian and will then reveal a new border – between V2 and V3. The next sets of cells respond to an increasingly larger area of stimulation as well as changing direction to prefer stimulation from the horizontal to the vertical meridian.

This size increase corroborates the statement that the visual system processes progressively more complex stimulus types. V2 has larger processing units and integrates information from V1, and V3 has larger units than V2 and integrates information from V2. Furthermore, areas further along the visual system have larger RFs and show preferences for behaviourally and functionally more relevant stimuli such as objects (Grill-Spector et al., 1998), scenes (Epstein & Kanwisher, 1998), faces (Eger, Schyns, & Kleinschmidt, 2004), and tools (Rice, Valyear, Goodale, Milner, & Culham, 2007). These features are detectable using adaptation paradigms (more details on this in next sections).

Retinotopic maps, and as such the borders of the early visual areas, are characterisable using fMRI by presenting flickering checkerboard wedges that rotate around a fixation point or rings that expand from a fixation point (Sereno et al., 1995). This reveals polar angle and eccentricity properties, respectively. As information is processed beyond V3 the feature-specific features become less clear-cut. However, two main functional visual processing streams – the ventral and dorsal – have been mapped in animals and in humans (Mishkin, Ungerleider, & Macko, 1983). The ventral stream preferably responds to identification of categories such as faces, objects,

scenes, words etc. (e.g. Baker et al., 2007; Grill-Spector & Weiner, 2014; Peelen & Downing, 2017), while the dorsal stream enjoys spatial locations (discussing the details of the dorsal stream and all characteristics of the ventral stream is beyond the scope of this thesis, but see Rauschecker, 2018 and Peelen and Downing, 2017 for further information and review). Specifically, the ventral stream that project along the lateral inferio-temporal sulcus have revealed areas that encode particular stimulus-types: the FFA and occipital face area (OFC) tend to respond to faces, and LOC responds to objects and tools, and parahippocampal place area (PPA) likes scenes and buildings (Grill-Spector & Weiner, 2014).

1.2.2 Adaptation and Repetition Suppression

Electrophysiological experiments demonstrate that when stimulus features are presented for a long time, or repeated, then neurons that initially respond a lot to this feature tend to have a reduction in activity over time. This is referred to as adaptation, or RS, respectively (e.g. Desimone, 1996). This paradigm continues to be developed to further understand neural representation and preference (Grill-Spector & Malach, 2001). The idea is that if a neuron, or population of neurons, like to respond to a stimulus feature – line orientations or face identity – then the response magnitude will be less with more exposure. For example, by comparing the amount of activity reduction when a feature is repeated to when it is alternated is thought to be a measure of preference (e.g. Kohn, 2007; Kohn & Movshon, 2003). More preference leads to more suppression following a repetition compared to an alternation – repetition *suppression*. We can measure retinotopic properties and complex stimulus preference in animals using invasive methods, and fortunately this is translatable to human non-invasive neuroimaging methods.

As aforementioned, adaptation refers to the observation that neurons that encode

a feature will reduce their responsiveness as a function of feature exposure. For example, neurons in motion sensitive V5 will initially yield a strong response to a particular motion, and if this motion continues to be presented neurons will respond less and less to the same stimulus (Tolias et al., 2005). RS critically depends on this adaptation effect as it assesses the difference in response suppression between repeating and alternating features.

This type of paradigm is commonly used in cognitive neurosciences and has become a cornerstone in experimental designs investigating neural preferences and representations. This is enticing as the ultimate goal of the field is to understand how the brain accomplishes perception, cognition, and consciousness, and thus if certain neurons, populations, or brain regions show preferences for particular computation that gives us important clues. To understand it better, the following paragraphs will discuss different proposed mechanisms and models for explaining RS and how to interpret it (this is however not an exhaustive review, please see Grill-Spector, Henson, and Martin, 2006 and Barron, Garvert, and Behrens, 2016 for this).

1.2.2.1 Models of RS

There are various models aiming to capture the mechanisms that underlie the RS effects. This section will cover three of the more commonly referred to models; the neural fatigue model, neural sharpening model, and predictive model, and discuss it in relation to differences between single neuron and large-scale neural population interactions.

The fatigue model suggests, as the name implies, that neurons tire from firing in response to the feature they prefer (e.g. Grill-Spector et al., 2006). This has been demonstrated through direct neural recording (e.g. Kohn & Movshon, 2003, 2004). Moreover, another study artificially depolarised a set of neurons in a cat's V1

and observed that the firing rate was reduced when these neurons were shown their preferred stimulus, even though it was for the first time (Sanchez-Vives, Nowak, & McCormick, 2000). This idea also applies to larger populations of neurons – if the population prefers a stimulus the whole population is thought to tire over time. The importance of this is that if it is valid at a larger neuronal scale, then it is possible to study this using large-scale measurement tools like as in human neuroimaging.

However, electrophysiological studies have also observed single neurons and populations of neurons exhibiting other patterns, for example sharpening. This refers to the observation of tuning curves narrowing with repeating presentation and widened when a feature is altered (e.g. Krekelberg, Boynton, & van Wezel, 2006; Tolias et al., 2005). Effectively, this means that although the neurons or the neural population show selectivity for a feature, their activity is sustained or increased rather than decreased as in the case with the fatigue model, whilst the non-selective neurons decrease activity. Theoretically, this could lead to overall activity decreasing if it occurs at a population-wide and large-scale neural level – hence, RS would be observed, while the selective neurons are increasing in activation.

Another observation is that some neurons show an increase in activity when presented with their preferred feature: repetition enhancement. This is different to the sharpening model which suggests tuning curves change in response to repetitions and alternations, and as such exhibits sustained or increased activity. The enhancement is rather peculiar as adaptation-based paradigms assume reduced activation. Although, it would make sense for a dynamic organ such as the brain to communicate preferences in various manners. For example, perhaps feature selective neurons communicate their observation by maintaining a high or increasing their firing rate. At a large scale, this may generate an overall increase in activity and thus no RS effects would show, even though the population of neurons prefer a feature (see Segaert, Weber, de Lange, Petersson, and Hagoort, 2013 for a review).

When we consider the complexity of RS on a neuronal and neuronal population level, it is unsurprising that the picture gets even more complicated once we start using large-scale measurement tools such as non-invasive neuroimaging methods. However, the effect has shown to be replicable in humans. Grill-Spector et al., 2006; Grill-Spector and Malach, 2001 demonstrated adaptation and RS paradigms' applicability to fMRI and since then the field has investigated neuronal selectivity using fMRI.

These models describe neural activity largely driven by the input, with minimal influence from other regions, higher or neighbouring. Therefore, it is important to understand how much of a single neuron effect translates to populations of neurons and to more complex stimuli in higher areas. Indeed, analysis of inferotemporal (IT) cortex responses suggest that single neuron activity explain very little of IT variance (De Baene & Vogels, 2009). Moreover, trial-by-trial neuron firing does not correlate with RS magnitude, corroborating that single neural activity may not be predictive of how the neural population acts.

In an attempt to corroborate these findings with the observation that the visual system has a high feedback to feedforward ratio, another theoretical framework suggests that the brain uses external statistical environments to generate internal models that are used to make predictions of future states: predictive coding (e.g. Bastos et al., 2012; Rao & Ballard, 1999). It explains RS effects as being a result of increased statistical certainty, and thus less energy is required to update the model (Kilner, David, & Friston, 2007). Mismatch between the input and model arises when a feature is altered (prediction error) and more neurons are recruited to update the model (e.g. Wacongne, Changeux, & Dehaene, 2012). In other words, this model suggests a largely top-down control of neural computation.

The question of which of these models best explains the RS phenomenon is difficult to answer. The most likely scenario is that the brain utilises and combines

aspects from all the models, perhaps depending on the input as well as on the brain region. It also depends from which perspective one studies the brain. Historically, electrophysiology has informed the field about local neural events in response to repeating stimuli, and the bottom-up models (fatigue, sharpening and enhancement) lend themselves well to describe these observations (Grotheer & Kovács, 2016). However, within human research, the non-invasive neuroimaging methods capture neural events at much larger spatial (and, for fMRI, temporal) scale. This is where a top-down model, such as predictive coding may fare better at describing such system-wide neural mechanisms. As pointed out by Grotheer and Kovács, 2016, the consequences of this type of framework are many, for example, one has to assume that neural communication feeds forward *and* backward. One could argue that this makes more sense on a more global level given the observed high feedback to feedforward ratio, and therefore is a more realistic framework in which to study the human brain, especially with temporally coarser tools such as fMRI. Nevertheless, the simplicity of the bottom-up models are sensible to work with at a local neural scale.

Indeed, when using measurements that capture large pools of neurons, such as fMRI, it is difficult to disentangle these subtle, but important, differences in model predictions. The fMRI signal would reveal activity reduction independent of which model the underlying computation belonged to (e.g. Grill-Spector et al., 2006; Grill-Spector & Malach, 2001). Therefore, using a large-scale measurement tool such as fMRI has received criticism (e.g. Ramsey et al., 2010). Furthermore, these models may combine leading to other problems. The absence of RS fMRI effect does not mean an absence of RS; if one neural population in a region is fatigued, and another is sharpened, this could average to no fMRI signal change (Krekelberg et al., 2006). This highlights the disagreement between direct neural recording and large-scale measurement tools such as fMRI. In addition to this, at large-scales, other influences may have an impact on how each unit of neural population or neuron reacts and

interacts with others. Indeed, in a democracy it is the voice of the many that determines the outcome – not just the single neuron or population. This may mean that the putative preference measure that is RS is weaker than thought.

1.2.3 Attention and Expectation

A potential pitfall of the view that RS reflects neural selectivity is that it assumes the RS effects will remain when context and brain state change. Early animal research show that if a monkey is passively watching a stimulus on a screen, and the stimulus is within a V4 neurons' RF then the neuron will respond to the stimulus (Reynolds, Pasternak, & Desimone, 2000). It will also respond to stimulus changes just outside the cell's RF. However, if the monkey focuses attention to the stimulus in the RF then any changes to the stimulus outside the RF is not processed by the neuron. Along the same line, Vogels, 2016 in fact suggests that RS may be an attentional effect rather than adaptation effect. Perhaps, the RS effect is observed because the repetition is less attended to compared to an alternation. This was assessed in IT neurons in monkeys and they had the monkeys trained to attend equally to adapter and test stimuli (De Baene & Vogels, 2009). The authors found that RS is still present and as such suggest that RS is likely related to adaptation. However, this study does not reject the idea that attention can modulate and affect RS effects in the visual system (De Baene & Vogels, 2009; Vogels, 2016).

At a larger scale, Summerfield, Trittschuh, Monti, Mesulam, and Egner, 2008 manipulated how probable a repetition of a face identity would be. Using fMRI in humans they found that in runs where face repetition was expected, the RS effect was greater than when the repetition was not expected. They named this effect *expectation signals* (ES), and these signals further complicate the picture of RS in large scale measurement. Indeed, it challenges the view that RS is purely a low-level

adaptation effect and a signature of neuronal selectivity. Rather, it suggests that RS effect may be a property of predictive coding. Further research into this have shown that these effects are present in an auditory paradigm measuring with MEG (Todorovic & de Lange, 2012), using face stimuli in fMRI (Larsson & Smith, 2011) and EEG (Summerfield, Wyart, Mareike Johnen, & De Gardelle, 2011), roman letter stimuli (Grotheer & Kovács, 2014), and illustrated objects (Mayrhauser, Bergmann, Crone, & Kronbichler, 2014; Richter, Ekman, & de Lange, 2018).

These ES effects could be explained by either the predictive coding model or a more complex sharpening model. The former suggests, as before, that expected features lead to a reduction in activity, or prediction error (de Lange, Heilbron, & Kok, 2018; Friston, 2005), and the latter suggests that expected features lead to an increase in activity for selective populations and a suppression of populations not showing preference – this results in an overall reduction in activity, or RS (e.g. de Lange et al., 2018; Kok, Jehee, & De Lange, 2012). Walsh and McGovern, 2018 point out the difficulty in assessing these differences, particularly at large scale measurement methods. Though they suggest that the key may lie in how information is suppressed – prediction must mean that the neurons selective for the predicted feature are inhibited, while sharpening means that the non-selective neurons are suppressed. Speculatively, these predictions may be exhibited differently using fMRI in that prediction could lead to suppression effects downstream the visual hierarchy while sharpening may only show suppression in particular feature-sensitive regions.

To further investigate the matter, Larsson and Smith, 2011 replicated Summerfield et al., 2008 study and added an additional manipulation – they diverted attention away from the face stimuli. Doing this they observe that ES disappears while RS effects remain. This could mean that ES are in fact attentional effects. However, it is important to underline that ES have only been observed in humans using fMRI and a subset of stimuli. Face stimuli (Kovács, Iffland, Vidnyánszky,

& Greenlee, 2012; Larsson & Smith, 2011; Summerfield et al., 2008), roman letter stimuli (Grotheer & Kovács, 2014), illustrated objects (Mayrhauser et al., 2014) and voices (Andics, Gál, Vicsi, Rudas, & Vidnyánszky, 2013) seem to elicit ES, while natural objects (e.g. Kovács, Kaiser, Kaliukhovich, Vidnyánszky, & Vogels, 2013) (but see Mayrhauser et al., 2014 for discussion), unfamiliar fonts (Grotheer & Kovács, 2014) do not lead to ES. Furthermore, ES have never been replicable in animal electrophysiological studies (e.g. Kaliukhovich & Vogels, 2010) – even when the experiment uses face stimuli, behaviourally relevant stimuli, and monkeys that are actively engaging with the stimuli (Vinken, de Beeck, & Vogels, 2018).

This line of research also probes an important question: to what extent are these RS effects a result of *reacting* to the stimulus versus *expecting* the next stimulus? At surface level it may not seem like a significant problem. If a neural effect is due to a feature, then we can infer selectivity to the feature. On the other hand, if the neural effect is a combination of the brain's prediction of what the feature would be and the comparison to what it was, then the net measurement is a complex set of signals and thus inferring selectivity is problematic. This is an issue because we are not necessarily measuring what we think we are measuring. If expectation influences RS then we know that the RS effect is not only an adaptation effect, and therefore the field must interpret RS results with caution.

As mentioned, animal studies have failed to replicate ES effects, however, some of these studies reveal that RS may arise in subregions of monkey IT and response enhancement or oddball responses arise in higher IT areas (Vinken, Vogels, & de Beeck, 2017). This further underscores an important aspect of adaptation and RS, namely, whether these processes are intrinsic to the studied region or population, or whether they are inherited from other regions or populations. Indeed, although the RS and ES effects have been shown to be distinct and separable in humans (Larsson & Smith, 2011; Tang, Smout, Arabzadeh, & Mattingley, 2018; Todorovic

& de Lange, 2012), it remains unclear to what extent top-down influences may affect RS activity.

1.2.4 Finding the Neural Substrate

Another issue with using large-scale measurement tools for adaptation paradigms is that the origin of adaption is unclear. Is the adaptation signal to a complex stimulus due to local adaptation at early visual areas or because a higher area is selective for that complex stimulus? Put differently, is the effect intrinsic to the measured region, or is it inherited from another region? This is an important question, particularly for fMRI studies where stimuli tend to be large and cover most of the visual field.

Early electrophysiological studies investigated motion after-effects that are thought to be adaptation effects (e.g. Maunsell & Van Essen, 1983; Zeki, 1974). For example, it has been shown that area V5/MT cell activity was reduced when the cells' preferred stimuli were continually presented (Kohn & Movshon, 2003). Crucially, they demonstrate that adaptation to stimuli moving in a non-preferred direction reduced the ability of MT cells to inhibit response to preferred direction. Because the behaviour of the RFs in this area seem to be affected by both the preferred and non-preferred direction, the authors conclude that the adaptation effect may originate from somewhere else: most likely early visual areas. Furthermore, another study finds motion adaptation effects in V4 neurons (Tolias et al., 2005). This area is normally not associated with motion direction selectivity, as shown by experiments comparing their response to motion vs a no-motion baseline (Desimone & Schein, 1987). By using an adaptation paradigm for motion direction, they show that neurons in area V4 demonstrate motion preference which could be inherited from V5. Hence, there is evidence for inheritance from lower and higher visual areas. This further highlights the complex interactions and computations of visual processing in

the visual cortex, and it underscores the need to dissociate intrinsic and inherited adaptation effects in different areas.

To further understand this in humans, an fMRI study tackled this problem by taking advantage of the retinotopic properties of the visual system and presented grating and motion stimuli of different sizes (Larsson & Harrison, 2015). They show that adaptation seems to be inherited from V1 in all regions, except MT/V5. Specifically, by exploiting the receptive field sizes of each level of the visual cascade and their respective retinotopic nature, the authors develop a spatial specificity paradigm to untangle the origins of adaptation effects throughout the system. The study shows that the areas beyond V1 had significantly narrower population receptive field (pRF) responses to adaptation that what would be expected in each region: the observed pRF size matched that of V1. However, area V5/MT response to direction-selective adaptation showed a significantly broader spatial specificity than V1, which suggests that adaptation in this area is not completely inherited. The authors propose that it may be a combination of intrinsic and inherited adaptation in area V5/MT.

In fact, one of the aforementioned studies using repetition suppression of face identity, controlled for low-level adaptation biases by changing the angle and size of face photographs as well as the face's expression. In other words, the face identity was the same, but the photos were different (Larsson & Smith, 2011). This study revealed RS effects in face sensitive areas but also in all early visual areas. Since the low-level features were different, the adaptation effect is likely to be inherited from face sensitive regions.

In summary, it is unclear to what extent RS effects are low-level adaptation effects independent of top-down influences and to what extent they could be influenced by expectation effects and attention. The strange observation that ES are relatively robust and consistently replicated in humans but not animals may suggest that it is a signal unique to the human brain. Although, the fact that the field

cannot seem to observe ES universally across all feature-sensitive regions may indicate that it is unique to certain stimulus types – indeed some suggest that ES are only observable with stimuli that humans are highly trained in (Grotheer & Kovács, 2016). However, the demonstration that attention affects the signal as well suggest that ES may be a by-product of attention (Larsson & Smith, 2011). This is also supported by accounts suggesting ES to simply be a deviance detection effect rather than expectation suppression (Vogels, 2016) – are the repetitions differentially suppressed or are the alternation responses differentially increased? Although the ES have been documented using EEG (Summerfield et al., 2011) and MEG (Todorovic & de Lange, 2012), most studies use fMRI. The fMRI signal depends on hemodynamic changes in response to stimuli, or, blood oxygenation level changes (hence the name, blood-oxygenated level dependent signal, or BOLD signal). Hemodynamic events can occur both with and without neural events (e.g. Lee et al., 2019; Sirotin & Das, 2009). Importantly, Sirotin and Das, 2009 show that anticipated visual stimuli that fail to be presented generate a hemodynamic event equivalent to when the stimulus is shown, but without the accompanying neural activation. This highlights the importance of further understanding to what extent the observed ES are hemodynamic. Indeed, to better understand these signals and what they may signify and reflect, it is crucial to appropriately understand how neural and hemodynamic activity are generated and interact.

1.3 Background Chapter: Neurophysiology

This chapter aims to illustrate the intricacies and interactions of neural activity and hemodynamic responses. First, I will give a brief description of some of the more important brain cells (in addition to the aforementioned receptive field cells) and their function and roles. Whilst we are interested in the mechanisms of brain cells involved in visual processing, many types of cells contribute to the measured BOLD signal. Thereafter, I will describe how these cells utilise energy. This leads into a description and discussion of the vascular system and how blood is recruited by neural tissue. With this foundation, I will then enter the discussion of the BOLD signal and its origins. This is then followed by weighing advantages and disadvantages of calibrating the BOLD signal. Work into this suggest that calibrating BOLD may offer a window into understanding excitatory and inhibitory interactions. Considering this, I will then discuss the role of gamma-aminobutyric acid (GABA) in relation to positive and negative BOLD signals. This chapter lays the groundwork to the methodology chapter as well as the rest of the thesis.

1.3.1 Cells of the Brain and Their Putative Roles

The brain is a 1.3-1.4kg lump of fat and other tissue. The fat is what makes up cells and encapsulates, or myelinates, the brain cells and facilitates electrical signalling between cells. There are two main cell types in the human brain, namely neurons and glial cells. These cells exist in approximately the same proportions and they differ in structure and function. Specifically, neurons have features such as dendrites and axons; dendrites are the tree-like branching at the top of the cell, and the axons are the elongated processes projecting from the cell body, the soma. In contrast, glial cells only have the dendritic part. Glial cells can modulate their resting potential but not fire potentials like neurons can. This also means that the

glial cells, in contrast to neurons, do not have the ability to transmit information via chemical neurotransmission. Glial cells receive their name from the Greek word and means "glue" - this underscores their role in that they are *supportive* cells in the brain and maintains vital processes such as homeostasis and are thought to play a role in communicating between neurons and the vascular system (Kettenmann & Verkhratsky, 2011; Verkhratsky, Zorec, & Parpura, 2017). There are various types of neurons such as excitatory pyramidal cells and inhibitory interneurons. In general, interneurons are bipolar cells which means that they can transmit information bi-directionally (Ascoli et al., 2008), sensory neurons are unipolar and relays information from the external world to the brain (such as from retina to occipital regions), and pyramidal neurons (as well as motor neurons and Purkinje cells) are multipolar which means that they can integrate information from numerous sources (Sotelo, 1978).

As mentioned previously, the axons are covered in a fatty sheath called myelin and this facilitates electrical conductance. It also gives rise to white matter tracts and reveals an important distinction between in brain matter: there is white and grey matter. The latter consists of neural soma and dendrites. These two matter types convolve across the neocortex creating sulci and gyri, and as such increases the surface area of the neocortex by fully utilising the space inside the skull (Bear et al., 2007).

1.3.1.1 Intracellular Structure and Extracellular dynamics

The neuron can, as aforementioned, transmit electrical signalling through its body in order to release neurotransmitters that can then chemically signal to the efferent neuron. Excitatory input from neighbouring neurons sum at the dendrites of the receiving neuron, and that will make the cell either do nothing or reach a threshold that will trigger an action potential. The action potential is the electrical signal

used for communication. Once the neuron receives enough input, its membrane (the structure surrounding the internal cell structure) will depolarise, meaning that positive ions are let into the cell and negative ions are let out. This is done in a sequential manner whereby the potential travels from the soma (the cell body), along the axon, and then to the axon terminals. The inside of the cell becomes more positively charged along the potential, and the local extracellular environment becomes more negatively charged (Bear et al., 2007; Gazzaniga & Ivry, 2013). Excitatory neurons tend to be excited through receptors that show an affinity for glutamate (these can be α-amino-3-hydroxy-5-methyl-4-isoxazole-propionic acid (AMPA) and N-methyl-D-aspartate (NMDA) types). This input is known as excitatory postsynaptic potentials or EPSPs. Excitatory neurons constitute the majority of neurons at 15-20% (Buzsáki, Kaila, & Raichle, 2007). Interneurons that are inhibitory often carry GABA transmitters – GABAergic interneurons. When GABA binds to an inhibitory receptor it results in a flow of negative ions into the neuron being inhibited and positive ions are pumped out of the cell, in other words, it is the opposite of an action potential. Hence, inhibitory interneurons can counteract the depolarization caused by excitatory input. Moreover, these interneurons modulate excitatory and inhibitory output by binding to GABA-type receptors (e.g. Behrends & Ten Bruggencate, 1993). When inhibitory input is received it is referred to as inhibitory postsynaptic potentials or IPSP. There are two GABA receptors types – type a and b. The type a receptor is a ligand-gated ion channel and type b class is a metabotropic one using G protein-coupling. GABA-type receptors occupy a third of synapses in the central nervous system (Mohler et al., 1996; Schür et al., 2016).

Interneurons can attach to different parts of an excitatory neuron generally in an inhibitory manner. For example, an interneuron can affect information relaying at the dendrites, and this means that input to the excitatory neuron is modulated and/or it can integrate information locally. Interneurons can also influence the region around the soma and can thus affect action potential discharge and phase exci-

tatory synchrony by communication with more than one excitatory neuron. Lastly, these inhibitory neurons can also modulate activity at the axons and thus influence output, the generation of action potentials and their timings (Behrends & Ten Bruggencate, 1993). Interneurons can inhibit other interneurons resulting in various mechanisms such as disinhibition where suppressive processes are inhibited and thus there is an increase in excitation (Pi et al., 2013). Hence there is a dynamic and intricate relationship between these classes of neurons. Once an excitatory neuron fires its action potential it temporarily alters the local charge and a current in generated. The interneurons generate action potentials to inhibit the activity of other neurons, and as such they also change the extracellular potential.

In addition to neurons the brain is also made up of equal numbers of glial cells. This suggests that the glial cells must be as important. Just as this review is not an exhaustive review of neurons, it is also not exhaustive of glial cells (see Kettenmann and Verkhratsky, 2011; von Bartheld, Bahney, and Herculano-Houzel, 2016 for this), but there is one of these cells that is of interest: the astrocyte. These cells are radially configured (star shaped, hence the name "astro" for "star") and play an important role as they communicate with neurons but also have so-called endfeet processes that attach to vessels in the brain (more on this later) (Mulligan & MacVicar, 2004). Although these cells do not generate action potentials, they do alter their resting membrane potential, which means that they can increase or decrease the negativity charge in the surrounding space. Combine this with excitatory and inhibitory neurons changing the local charges and the extracellular environment is a complex interplay of electrical signals that can dynamically and in a structured and organised way receive, transmit, modulate and create information.

1.3.2 Energy Consumption

To accomplish these processes, these cells need to use energy. In fact, although the brain is just 2% of the body it requires 20% of the caloric consumption (Shulman, Rothman, Behar, & Hyder, 2004). There are two main energy production mechanisms to generate energy in the form of adenosine triphosphate (ATP), from glucose – aerobic metabolism makes up 90% of energy production, and anaerobic metabolism makes up 10% (Rich, 2003). The former is also known as oxidative phosphorylation and it produces 38 ATP per each glucose molecule. The latter is known as glycolysis and yields two ATP from a glucose molecule. Different processes need different amounts of energy. Attwell and Laughlin, 2001 estimate that 75% of energy goes to post-synaptic activity, 10% to action potentials, 7% pre-synaptic, 6% glial, and 2% resting activity. Moreover, the grey matter uses five times more oxygen compared to the white matter – which makes sense since most energy is used in post-synaptic processes.

The brain needs glucose and it needs oxygen to metabolise glucose into energy. Most tissue throughout the body has energy reserves and storage in case it requires it. The brain is special in that it cannot store glucose nor oxygen and is as such acutely dependent on the vascular system delivering blood to all areas of the brain on demand. In fact, if the brain is without blood flow for 5-10 seconds it will go unconscious. This is where the vascular system plays the lead part.

1.3.3 Vascular System

The role of the vascular system is delivering the necessary compounds for the body's tissues to perform activity that requires energy. It also transports hormones as well as removing waste products from metabolic processes (e.g. Mader, 2008). There are three circulatory systems that form the vascular system – the pulmonary, coronary,

and systemic and these have specific tasks namely to provide blood to lungs, to the heart and the rest of the body, respectively. This task is carried out through a sophisticated "plumbing" system of vessels. The vessels are different sizes and have different properties. The largest one is the aorta and it transports oxygenated blood from the heart to the body. Following the aorta are arteries, arterioles, capillaries, venules, veins and venae cavae. Arteries are the second largest vessel-type and have strong muscular walls that can deliver lots of blood under lots of pressure. These bring blood to the next vessel-type, the arterioles that form when the artery split into branch-like structures. Arterioles also have strong muscular walls that are elastic – these can expand to allow more blood to travel through. This is especially important if some tissue demands more blood. Arterioles then branch into small vessels with thin walls known as capillaries (S. I. Fox, 2006; Gaehtgens, 2002). This is where the blood-tissue exchange occurs. Blood cells carrying oxygen (i.e. oxygenated blood or oxyhemoglobin) and glucose molecules can release these and they perfuse through the thin walls and can used by tissue to generate necessary energy. Waste products and deoxygenated red blood cells (or deoxyhemoglobin) then continue transportation to the venuoles that are vessels collecting blood to bring back to be re-oxygenated. Venuoles merge into veins that in turn reach the vanae cavae that carries deoxygenated blood to the heart (e.g. Mader, 2008).

The amount of blood present in each part of the vascular system is unequal. Around 64% will be present in the veins, 13% in arteries, 7% in arterioles and capillaries, 7% in the heart and 9% in the pulmonary system (e.g. S. I. Fox, 2006; Mader, 2008). Whereby the deoxygenation occurs in the peripheral capillaries, the reoxygenation occurs in the capillaries of the lungs in the pulmonary system. Oxygen enters the lungs through breathing and enters the blood system in capillary beds in the alveoli (small air-sacks that are found at the end of the respiratory system). The red blood cells reattach four oxygen molecules and is oxygenated – now the process can start again. Blood will go from lungs into the heart and be pumped out

through the aorta to the rest of the body. The blood will then be returned to the heart that pumps it into the lung vessels.

The brain is greedy and has a huge energy requirement and therefore, it also needs about 15% of the cardiac output (Attwell & Laughlin, 2001; Bélanger, Allaman, & Magistretti, 2011). The brain is supplied with blood through the left and right common carotid and vertebral arteries. The two former supply the face, scalp and cerebrum parts, and the two latter transport blood to the brainstem, cerebellum and posterior cerebrum parts. These arteries integrate at the base of the brain and form a structure known as the Circle of Willis. The circular configuration of this structure allows the whole brain to still receive blood in case of any damage or blockages to the arteries.

On the brain surface, inside the skull, are pial vessels and these branch into smaller vessels that penetrate the brain tissue. Once inside the tissue they are parenchymal, or microvessels, and this is where astrocytes use their endfeet to surround the vessels (Mulligan & MacVicar, 2004). Moreover, cerebral spinal fluid (CSF) is created in the choroid plexus and distributes throughout the brain. Because the CSF and blood-plasma have different ionic compositions this leads to various extracellular environments that may play a role in facilitating how neural tissues and the vascular system communicate (Hladky & Barrand, 2016). Once a neuron activates and changes the extracellular ionic composition it signals to the vessel muscles to constrict or dilate. How this mechanism of neural and vascular communication, or NVC, is exactly achieved is unclear.

1.3.4 Thoughts on Neurovascular Coupling

Early scientists suggested that a negative feedback theory is the best explanation for how NVC was accomplished (e.g. Roy & Sherrington, 1890). The putative mech-

anism was that neural activity led to a decrease in oxygen and glucose levels and an increased level of carbon dioxide (CO_2), adenosine and lactate. CO_2, adenosine and lactate are all able to dilate vessels and therefore it made sense as an NVC mechanism. This was further developed into a metabolic hypothesis of NVC that poses that cerebral blood flow (CBF) increases in response to the release of nitric oxide (NO) and ATP when blood is deoxygenated. However, Lindauer et al., 2010 demonstrate that when they remove deoxyhaemoglobin and as such remove the release of NO and ATP, CBF is still recruited in response to neural activity. Moreover, if increase of CO_2 would be mechanistically important to recruit CBF then the extracellular environment should be more acidic during neural activation, but the contrary is observed: it becomes more alkaline (e.g. Siesjö, Kjällquist, Pontén, & Zwetnow, 1968; Yaksh & Anderson, 1987). This is explained by CBF already arriving and washing any CO_2 increases away before acidity increases. This led researchers to ask whether changes in O_2 concentration in the tissue may lead to CBF increase. They kept mitochondrial O_2 stable during neuronal activity they saw that CBF recruitment was not dependent on O_2 concentration but rather the cerebral metabolic rate of oxygen ($CMRO_2$) (Buxton, 2002).

Hence, a new hypothesis formed namely the neuronal hypothesis of NVC. This idea suggests that energy requirements are directly and indirectly signalled by astrocytes to vessels. Furthermore, in contrast to the negative feedback theory, it suggests that the signalling occurs in an anticipatory feedforward fashion through vasoactive neurotransmitters in synaptic signalling. This can happen in several ways, for example, as neurons activate and release glutamate this neurotransmitter binds to a receptor-type on the astrocyte. This leads to a set of channels opening (big potassium (BK) channels) and potassium is released onto the vessels' smooth muscle cells resulting in dilation (Filosa et al., 2006; Girouard et al., 2010). Another way is through potassium release from activated neurons that spreads extracellularly and leads to reduced calcium (Ca^{2+}) influx. This leads to vessel dilation (Girouard

et al., 2010). This could also be done by the extracellular potassium activating astrocytes and they in turn releasing more potassium that moderates dilation of vessels. Although, a study that depolarised glial cells independently observed no vasodilation (Attwell et al., 2010; Metea, Kofuji, & Newman, 2007). Nevertheless, it is important to note that many of these studies investigating vasodynamic processes are done in vitro and as such it is unclear whether the findings would hold in in vivo experiments.

Evidence suggests that the metabolic hypothesis of NVC is weaker than the neuronal hypothesis. However, this does not mean the theories are mutually exclusive. It would make sense for a dynamic system to utilise both metabolic by-product information as well as neuro-vascular communication to recruit CBF. Perhaps the brain primarily relies on feedforward anticipatory signalling for CBF recruitment, but it also samples metabolite concentrations to make appropriate adjustments.

1.3.5 Cerebral metabolic rate of oxygen and the BOLD signal

The brain uses oxidative metabolism for energy and for this to work it will need oxygen. Oxygen must be extracted from the blood and this can be quantified through cerebral metabolic rate of oxygen ($CMRO_2$) and can thus be seen as a close proxy for neural activation (e.g. Lin, Fox, Hardies, Duong, & Gao, 2010; Merola et al., 2016). As aforementioned, as soon as oxygen is extracted and metabolised it is accompanied with an increase in CBF. Importantly, the increase in CBF is disproportionally larger than the extraction of oxygen (Buxton & Frank, 1997; Buxton, Uludağ, Dubowitz, & Liu, 2004). This is important because oxygenated blood is diamagnetic and therefore it does not cause as much magnetic susceptibility as the paramagnetic deoxygenated blood. As a result, when CBF increases it increases the

proportion of oxygenated blood – this changes the local oxygenation to deoxygenation ratio. This gives rise to a change in susceptibility that is detectable with the T2* sequence in fMRI: the *blood-oxygenation level dependent*(BOLD) signal.

What the BOLD signal reflects is highly debated because it depends on oxygenation level changes, and as such depends on different processes such as CBF, cerebral blood volume (CBV), and $CMRO_2$. This casts doubt on whether this signal really captures neural activity. In theory, it sounds elegant – neural activity leads to energy usage which in turn recruits CBF and hence there is a local oxygenation change that the BOLD signal measures (Buxton et al., 2004). It is not this simple and to illustrate, consider the following. The BOLD signal may decrease for different reasons: if CBV increases it is likely to increase in the venules as these can house more volume, and therefore there will be an increase in deoxygenated blood as a result. This means that the BOLD signal will decrease. CBF increases oxygenation and thus increases the BOLD signal, while $CMRO_2$ extracts oxygen from the blood and as such it decreases the BOLD signal. Hence, the BOLD signal decreases, but because of different mechanisms. It may be that increases in $CMRO_2$ also leads to increases in CBV, but this is not always the case (e.g. Derdeyn et al., 2002).

This leads to the question: what if $CMRO_2$ is different between two activations but the CBF is the same? This results in a difference in BOLD signal, namely that the higher neural activation will lead to a smaller BOLD signal change in comparison. This is because the $CMRO_2$ will be higher, reducing the amount of oxygenated blood. This highlights a deep issue with the BOLD measurement: what if $CMRO_2$ is the same between two conditions while CBF is different? If $CMRO_2$s are the same, it implies no difference in neural activation – however a difference in CBF recruitment would lead to a larger BOLD signal for the condition with higher CBF. Differential CBF recruitment in response to the same neural activity is likely a common occurrence considering physiological constraints such as capillary density

and neural density varies across regions (Ekstrom, 2010; Harrison, Harel, Panesar, & Mount, 2002; Koopmans, Barth, & Norris, 2010). This may lead researchers to conclude that there is a difference while there is none. In other words, the BOLD signal relies on a complicated relationship between neural, metabolic and vascular dynamics and can therefore at best be seen as a proxy for neural activity.

Neural activity is often characterised as neural spiking, and the next logical question is to ask whether the BOLD signal reflects spiking or something else. Logothetis, Pauls, Augath, Trinath, and Oeltermann, 2001 measured neural activity directly, local field potentials (LFP) and the BOLD signal simultaneously and found that the BOLD signal correlated with both. They asked what would happen if they removed spiking from the equation (Logothetis, 2008) – would the BOLD signal still be generated? They tested this by raising the action potential threshold. This results in an environment where extracellular activity is the same but the only difference in whether neurons spike. They demonstrate that the BOLD signal was generated in absence of neural spiking, suggesting that the BOLD signal better correlate with LFPs or presynaptic activity. Moreover,Magri, Schridde, Murayama, Panzeri, and Logothetis, 2012 found that 20-60Hz LFP best predicted the BOLD signal compared to single unit activity (SUA) and multi unit activity (MUA), and this was the case even when there was no spiking present.

Thus evidence converges on fact that the BOLD signal correlates with synaptic activity in the form of LFPs, but not necessarily neural spiking. The presence of a correlation is good news for researchers using fMRI to study the human brain. However, the underlying problem remains – the BOLD signal reflects an interaction between many processes such as LFPs, $CMRO_2$, CBV, and CBF. Additionally, research demonstrates that $CMRO_2$ and CBF changes can vary between conditions, tasks, brain region and individuals. Because of this, Buxton, Griffeth, Simon, and Moradi, 2014 highlight the need for finding a stable factor to estimate true neural

activity by quantifying at least one more variable that contribute to the BOLD signal in order to more accurately capture what is going on. Researchers suggest using the perfusion imaging method arterial spin labelling (ASL) to measure CBF simultaneously in order to calibrate it (e.g. Buxton et al., 2014; Davis, Kwong, Weisskoff, & Rosen, 1998).

The authors also propose taking a ratio of CBF and $CMRO_2$ and use that as a stable factor or coupling ratio – n (Buxton et al., 2014). This relies on the idea that if CBF is recruited by neurons in an anticipatory fashion (and not a feedback or metabolic manner) then CBF and $CMRO_2$ can be viewed as parallel processes, and the BOLD signal their interaction. A coupling ratio could facilitate a more quantitative view of condition comparisons by incorporating more information. The authors illustrate this point by demonstrating that the BOLD signal in general overestimates $CMRO_2$ in response to low and high contrast stimulus change, while it underestimates $CMRO_2$ when attention changes. Specifically, the difference in measured $CMRO_2$ when attention is altered is greater than the difference in $CMRO_2$ when stimulus contrast is changed. However, the BOLD signal shows a smaller difference when attention changes, while a larger difference when stimulus contrast switches. This depends on differential CBF changes as CBF is modulated more by contrast changes compared to $CMRO_2$ and modulated less than $CMRO_2$ by attention. By using a coupling ratio – n – this pattern is better approximated in that if CBF is more strongly modulated than $CMRO_2$ then the ratio increases while if CBF is less modulated than $CMRO_2$ then n decreases.

In light of this, the authors also propose that this ratio may shed light on inhibitory and excitatory interactions. For example, when a participant is attending to a feature of a stimulus this may lead to increased inhibition of other features resulting in the ratio increasing (this was also shown in Moradi, Buračas, and Buxton, 2012). Indeed, understanding how inhibitory activity modulates the BOLD signal

and CBF is important as it will help the field better understand the human brain and provides a richer story to the neuroimaging tool.

1.3.6 GABA and Inhibition

GABA is one of the major players in facilitating inhibitory dynamics in the brain. Therefore, it is of interest to understand how this neurotransmitter relates to the BOLD signal. This is possible to investigate by using magnetic resonance spectroscopy (MRS) to measure GABA concentration in a particular region. The literature is mixed as to how GABA concentrations correlate with CBF, BOLD and CBV. Some find a positive relationship between GABA and CBF (Donahue, Near, Blicher, & Jezzard, 2010), others a negative relationship (Krause et al., 2014). While some find that GABA and BOLD negatively correlate (Donahue et al., 2010; Muthukumaraswamy, Evans, Edden, Wise, & Singh, 2012). When directly modulating GABA, one study observes that when injecting GABA in primary sensory cortex led to inhibited CBF increase in this area while other areas enjoy an increase in CBF. Hence, local GABA, in at least primary sensory cortex, exhibits complex modulations of adjacent areas (Barbelivien, Noël, MacKenzie, & Dauphin, 1999). Another study used GABAa receptor antagonists and found that evoked potentials and BOLD increased during sensory stimulation compared to control (Nasrallah, Kaur, Singh, Yeow, & Chuang, 2017). Excitability increased, and CBF also increased but only in areas where receptor density was high. As such, there may be a modulatory relationship between GABA and blood flow (Donahue et al., 2010). Moreover, if GABA affinity is pharmacologically increased it leads to more inhibition and lower BOLD (Walter et al., 2016). In short, the evidence is diverging.

Furthermore, it is important to note that GABA is present in the extracellular environment as a transmitter precursor and metabolite, as well as a neurotrans-

mitter. Indeed, there are two types of GABA – cytoplasmic and vesicular (Stagg, Bachtiar, & Johansen-Berg, 2011). Cytoplasmic GABA is produced from glutamate and is thought to be important for metabolism. The latter can be found in high concentrations in pre-synaptic vesicles and is thought to be crucial for inhibitory neurotransmission. Therefore, it is difficult draw conclusions about the GABA concentrations when using MRS (Myers, Nutt, & Lingford-Hughes, 2016). Crucially however, Harris et al., 2015 investigated GABA and BOLD correlations in various brain regions in response to region-relevant stimulation (visual stimulation for the visual areas, auditory stimulations for the auditory areas, and finger-tapping for motor areas). They demonstrate no relationship between BOLD and GABA in any area. This casts doubt upon research finding a relationship as their study had more power, in terms of sample size and controlling for further confounding variables, compared to the other studies. The authors also point out that methodological differences may play a part.

At any rate, if there is an increase in inhibition this would lead to an increase in energy need and as such increased $CMRO_2$ – hence BOLD signal decrease. Therefore, GABA and $CMRO_2$ should correlate positively (Donahue et al., 2010). Another prediction that can be drawn from this is that negative BOLD is associated with more inhibitory activity: a positive relationship (Logothetis & Wandell, 2004).

1.3.7 Negative BOLD - Neural or Hemodynamic?

The relationship between BOLD, CBF, CBV and $CMRO_2$ is complicated. The observation of negative BOLD responses in addition to the more common positive BOLD responses make the picture even more complex. Particularly, as BOLD signal change is a relative measure that compares signal change between conditions, areas or baseline, it naturally follows to ask whether a negative response is truly neural in

nature or due to differential CBF changes. This led to the proposition that negative BOLD may be an effect of blood-stealing, meaning that areas close to ROI activate and steal blood from ROI and as such the BOLD response will be negative as BOLD shows the relative differences between regions (e.g. Shmuel et al., 2002).

This elusive signal has been a matter of debate for a long time, but research is converging onto the idea that it reflects neuronal deactivation. For example, a recent optogenetic study investigated the effect of stimulating two types of GABAergic interneuron subpopulations (Lee et al., 2019). These were the somatostatin (SST) and nitric oxide synthase type-1 (NOS1) subtypes. SST interneurons communicate with microvessels in superficial layers and when these release GABA it is thought they contribute to stimulation evoked CBF, whilst the NOS1 expressing interneurons release the known vasodilators NO. Unsurprisingly, photic stimulation generated localised hemodynamic responses – however, surprisingly, only SST-activation led to neural activity while NOS1-activation had minimal neural activity. Hence, hemodynamic responses were generated both with and without neural activity. Moreover, when SST stimulation was sustained it sometimes showed local negative hemodynamic responses. This directly supports the idea that negative BOLD has some underlying inhibitory activity. BOLD signals are biased to large draining veins and as these are located towards the brain surface the signal is biased towards the superficial cortical layers (Boillat, Xin, van der Zwaag, & Gruetter, 2019). Moreover, ASL is biased towards middle layers as the vascular density is higher there. Furthermore, maximum CBV and BOLD locations are different during positive and negative BOLD (Huber et al., 2014; Huber, Uludağ, & Möller, 2017), where positive signals were found towards the surface and negative signals in deep layers in monkeys (e.g. Goense, Merkle, & Logothetis, 2012). However, a study investigating layers in humans observe that there was a monotonic increase and decrease in superficial layers during positive and negative BOLD, respectively (Fracasso, Luijten, Dumoulin, & Petridou, 2018). Hence, the relationship between the two BOLD sig-

nals and CBF is further confounded by differential layer bias, meaning that a voxel having a particular BOLD response may not accurately reflect the associated CBF response pattern.

1.4 Background Chapter: Neuroimaging Methods

This section will describe and discuss the methodologies used in the empirical chapters of the thesis. It aims to provide the reader with the fundamentals to appreciate the rationales for using the techniques as well as the critical discussions implication the tools. The current studies used a variety of imaging techniques to probe the question of what neuroimaging signals contain and reflect: traditional functional MRI, perfusion MRI, and MR spectroscopy. Each technique will be described, and some evaluation of technique reliability and validity will be offered. I will also briefly describe and discuss the Davis model (Davis et al., 1998) and its adaptations for use on calibrated BOLD experiments.

1.4.1 Functional Magnetic Resonance Imaging

The previous chapter laid the groundwork for understanding what the literature has uncovered to date about what the underlying neural activity may be that give rise to neuroimaging signals. FMRI is one of the most widely used neuroimaging tools for basic research and clinical applications as can be seen by the publications increases per year since the 90s (e.g. Muckli, 2010). The technique is also becoming more widely available in hospitals and at research institutions. Besides being a non-invasive technique (in contrast to positron emission tomography (PET) scanning), one other attractive aspect of fMRI is its spatial resolution and the fact that it can capture activity in deeper structures. This contrasts with EEG and functional near-infrared spectroscopy (fNIRS) that can only measure superficial activity from the brain. On the other hand, the temporal resolution is lower compared to EEG and MEG techniques. Although, recent research has shown that millisecond resolution

is possible to model in fMRI (Stigliani, Jeska, & Grill-Spector, 2019).

The rationale for using the technique to study cortical dynamics, is because the BOLD signal is shown to correlate closely with LFPs, as covered in the previous section (Logothetis et al., 2001; Logothetis & Wandell, 2004). To briefly recap, LFPs themselves measure pre-synaptic activity, meaning that they capture changes in extracellular voltage. In contrast, single-cell recordings measures firing of neurons and is better correlated with measurements such as EEG. In other words, differing electrophysiological and neuroimaging techniques are measuring different aspects of brain activity. The advantage is that a more complete view of cortical dynamics is captured by using different techniques. The downside is that they do not fully correspond, and care needs to be taken when drawing conclusions. To illustrate, extracellular voltage changes may not lead to neurons firing, though it increases LFP and the BOLD signal (e.g. Logothetis & Wandell, 2004). Hence, LFP and BOLD changes do not necessarily reflect neural firing. EEG would capture neural firing, though only if large pyramidal cells are aligned. If the cells are radially arranged (Herreras, 2016), then the extracellular voltage changes would be observed with BOLD and LFP but missed by EEG. Moreover, LFPs can capture changes in neural population synchrony which would also be measurable with EEG but not BOLD. Since fMRI can capture subthreshold fluctuations it has been suggested that this tool is superior when studying diffuse activity such as feedback, lateral activity, and potentially also expectation signals (e.g. Muckli, 2010). However, despite these strengths, the fundamental problem remains: the BOLD signal is a complex mix of physiological signals.

The BOLD signal is measured in volume pixels – or voxels, and the resolution of these depend on the magnet strength. The signal relies on the ratio change in oxygenated and deoxygenated blood and these have different magnetic properties whereby oxygenated blood is diamagnetic and deoxygenated blood is paramagnetic.

Because paramagnetic material has an unpaired electron this leads to the proton moving randomly as the unpaired electron is attracted to any magnetic momentum: it will have spin. A collection of paramagnetic atoms will spin randomly and attract atoms around them to move randomly. If a strong magnetic field is applied then the protons will spin, or precess, around its axis either parallel or anti-parallel to the magnetic field (B0). The frequency at which the proton precesses is known as the Larmor frequency (Buxton, 2009).

Different material will have different Larmor frequencies and to excite a material one has to apply energy at that frequency. This is known as applying a radiofrequency (RF) pulse. The material, or proton, will absorb the energy, or resonate, and flip itself away from the magnetic field. Now the proton will transition to a high energy state and once the pulse is removed the protons will relax back to align with the magnetic field. This relaxation leads to oscillations in the magnetic field that a coil can capture. There are two relaxation types: spin lattice and spin-spin, referring to longitudinal and transversal relaxation, respectively. These give rise to T1 weighted and T2 weighted images, respectively. T1 and T2 are decay time constants of the RF pulse signal. Echo time (TE) is the time between when the RF pulse was applied to when the signal is acquired and repetition time (TR) refers to the time between RF pulses (i.e. the time between the first slice being excited and it being excited the second time. Each slice receives a RF pulse within on TR) (Buxton, 2009).

Moreover, there are different ways to achieve acquisitions, namely through gradient echo and spin echo. The gradient echo uses one RF pulse and spin echo uses pairs of pulses. Gradient echo uses a rephasing gradient which means that it makes proton spins that were spin-uncoupled or de-phased by the gradient to be phased again. Any phasing/shifting done by tissue susceptibility is not affected or cancelled in gradient echo as in spin echo – this means that this acquisition method is vulner-

able to artefacts from chemical shifts and susceptibilities. However, it also means that the gradient echo is generally quicker to acquire as TE can be short and so can TR.

We know that the BOLD signal is a complex combination of physiological processes and we know that CBF increases disproportionally compared to $CMRO_2$. This response is modelled by the hemodynamic response function (HRF, see figure 1.3). There is an initial dip in the HRF that seems to reflect the initial increase of deoxygenated blood and possibly increased CBV, and then about 6s later the signal peaks, putatively reflecting the increase in oxygenated blood from the recruited CBF (Hu, Le, & Uğurbil, 1997). Thereafter there is a post-stimulus undershoot that is thought to reflect increases in venule CBV and deoxygenated blood (Kim & Ress, 2016). In total the response takes about 15-30s. It is important to highlight that the response lags and happens a relatively long time after the neural event takes place.

A way to better estimate neural activity is to know the cerebral rate of oxygen extraction and this can be estimated by also measuring CBF. This is achieved using perfusion imaging.

1.4.2 Arterial Spin Labelling

CBF, can be measured invasively in humans using radioactive tracers, however, these are not ideal and cannot be used for some clinical populations. Therefore, arterial spin labelling, or ASL, offers a solution as it uses blood water as a tracer. Arterial water is labelled by applying a 180-degree RF pulse making the paramagnetic protons flip – this is applied to a slab-area right before the region of interest. The net magnetisation is inverted and as such labelled. After transit time (time to arrive to an area of interest) the blood water will exchange with tissue water. The

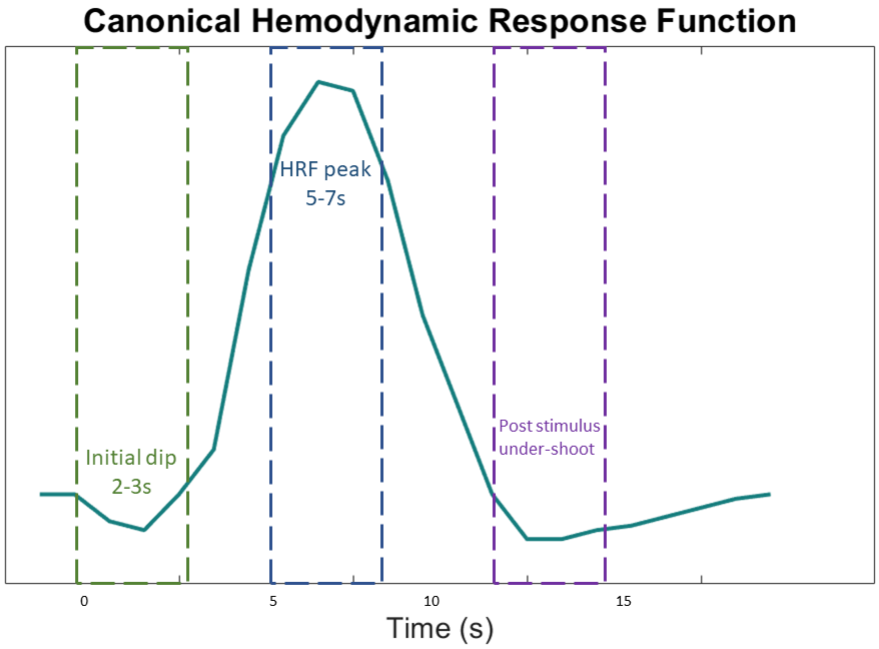

Figure 1.3: Illustration of a canonical hemodynamic response function (HRF). The HRF evolves over a time period of 15-20s. It is characterised by an initial dip about 2-3s after stimulus presentation, and then reaches a peak response at about 6s after presentation. Before returning to baseline the HRF tends to undershoot.

labelled inflow will change the tissue magnetization – specifically, it will reduce it, and this leads to a reduction in the MR signal. An image is taken, and this will be the tag image that is compared to the control image (image without the labelling). In other words, this image the blood water has a different magnetization compared to the static tissue water. The control image has the same magnetization of blood water and tissue water. This difference is proportional to regional CBF amount: a perfusion image (Aguirre & Detre, 2012; Borogovac & Asllani, 2012).

There are different ASL methods: continuous ASL, pulsed ASL, and pseudo-continuous ASL. The former inverts arterial blood continuously by applying RF pulses continuously. The control image is captured by applying the pulse above the region or slice of interest – this is in order to account for distortions from the pulse itself. This is also known as flow-driven inversion. Pulsed ASL uses spatial inversion. This means that the RF pulse is applied in a spatially specific way.

This can be achieved using, for example, echo planar imaging and signal targeting with alternating radiofrequency or EPISTAR or flow-sensitive alternating inversion recovery or FLAIR.

While the BOLD signal is biased by large veins and arteries, ASL reflects parenchymal changes, in other words, it has higher resolution localisation (Duong et al., 2002). However, the temporal resolution is effectively halved, and thus ASL is noisier. On the other hand, the ASL signal is much higher in magnitude, and with stronger magnets the ASL signal-to-noise ratio will improve (Haller et al., 2016). Moreover, because ASL measures CBF it has been shown to capture slow changes in neural activity (e.g. Aguirre & Detre, 2012; Olson et al., 2006; Tjandra et al., 2005), meaning that it may be especially suitable for studying attentional effects, learning, and expectation (e.g. Demeter, Hernandez-Garcia, Sarter, & Lustig, 2011).

1.4.3 The Davis Model

Advancements in fMRI techniques make it more accessible to study various aspects of human brain physiology such as CBF. Characterising CBF signals on their own or in relation to traditional BOLD signals are informative. However, there is also the opportunity to estimate $CMRO_2$ by calibrating the BOLD signal with the use of CBF information. In order to gain such an estimate, researchers are reliant on estimation models that incorporates and captures various other physiological parameters that are not feasible to measure simultaneously in one experiment. Davis et al., 1998 provided the field with a model that does just this.

The Davis model (Davis et al., 1998) is based on experiments where Davis and colleagues induced controlled hypercapnia (elevated CO_2) in participants by letting them breath air with higher than normal CO_2. This leads to vasodilation and as such a controlled removal of some venous deoxyhaemoglobin, giving the authors the

ability to extrapolate a maximum BOLD response. An absolute maximum BOLD response is possible to measure by removing all deoxygenated blood from a voxel – but this is not feasible to do in humans. A theoretical maximum response (M) is important to estimate as there are high inter-individual differences in BOLD signal generations and as such must be scaled (e.g. Hoge, 2012). Many calibration studies use a hypercapnia scan to estimate the scaling factor as hypercapnia is believed to not affect $CMRO_2$ while it does affect CBF (e.g. Blockley, Griffeth, & Buxton, 2012). However, as hypercapnia scans require equipment that is not accessible everywhere, there have been advancements in estimating M from the acquired data. For example, Moradi and Buxton, 2013 conducted an adaptation paradigm and approximated $CMRO_2$ by estimating M for each participant using the BOLD and CBF signals from the stimuli that yielded the highest activation.

Moreover, the Davis model also contains two other physiological parameters namely α and β - constants reflecting CBF-CBV relationship and the BOLD signal and blood oxygenation relationship (e.g. Blockley et al., 2012; Ogawa et al., 1993). These are normally estimated from the literature, although work has been done to empirically estimate these (e.g. Griffeth and Buxton, 2011 suggest α=0.16 and β=1; Griffeth, Perthen, and Buxton, 2011 suggest α=0.2 and β=1.3).

Human NVC is evidently complex and intricate, yet the Davis model is simple. Despite this, it has been shown to be incredibly robust (Buxton et al., 2004). Even in light of advancements in field-strength (e.g. Hare, Blockley, Gardener, Clare, & Bulte, 2015; Huber et al., 2017), MRI sequences (Blockley, Griffeth, Simon, Dubowitz, & Buxton, 2015), physiological parameter measurements (Gauthier & Hoge, 2013), and $CMRO_2$ estimate model developments (Buxton et al., 2004), the Davis model still estimates $CMRO_2$ as well as models that incorporates more parameters (e.g. Blockley et al., 2012; Buxton et al., 2004).

1.4.4 Magnetic resonance spectroscopy

One study in the thesis uses magnetic resonance spectroscopy (MRS) to measure local GABA concentrations in early visual areas. This was to look at how GABA levels correlate with positive and negative BOLD as well as CBF. The first study, to our knowledge, combining all three measures at once.

MRS differs from other MR techniques in that it is not interested in spatial information, but rather it uses frequency information to identify compounds (e.g. Blüml, 2013; Tosetti, Schirmer, d'Alesio, Di Costanzo, & Scarabino, 2006). This is possible due to different compounds having a different electron number and structure. Electrons move around the nucleus and as such create local magnetic susceptibilities, or shields. This means that the observed resonance frequency of different molecules will differ slightly, resulting in a chemical shift, which is what MRS can capture. A chemical shift can be formally defined as the difference between the frequency of interest and a reference frequency through the reference frequency (Blüml, 2013). If a compound has high electron density, they have more shield and thus a lower chemical shift (also known as up field). Lower electron density has less shield and as such a higher chemical shift or a downfield.

Metabolite resonance is measured in parts per million (ppm) which is a dimensionless measure. GABA resonates at 2.2-2.4 ppm, which is the same as glutamine and glutamate (glutamine complex or glux). In comparison, water resonates 4.7ppm. Free induction decay (FID) is a combination of all sample resonance and therefore using a fourier transform will yield a spectrum of frequencies. Different metabolite nuclei resonate at different frequencies, therefore there are different peaks in the spectra. The peaks have an area under their curves, and this reflects the concentration of that frequency. Creatine is a stable metabolite in tissue, and often this is used to calculate a ratio of metabolite to this stable one (e.g. Near, Ho,

Sandberg, Kumaragamage, and Blicher, 2014, although see Li, Wang, and Gonen, 2003 for opposing finding). The issue with using spectroscopy is that it is easily confounded by inter-participant variability such as their size, diet habits, alcohol consumption, lifestyle choices and gender (e.g. Stagg et al., 2011). Moreover, MRS cannot easily detect compounds that occur in low abundance such as neurotransmitters, which is an issue for many neuroimaging studies interested in understanding neurotransmitters' relationship with brain function. Also, sometimes different metabolites have very similar resonance frequencies and as such one metabolite may be hidden. An example of this is GABA and glutamine whereby GABA is hidden behind the glutamine complex's peak. On the other hand, MRS is a direct measurement of metabolite concentrations and it has shown to be robust and reproducible. Moreover, a session is relatively quick, and the participant do not require much preparation beyond the standard MRI preparations.

In summary, there are various ways fMRI can be used to study the human brain and its dynamics – all from the traditional BOLD signal, to calibrating the BOLD by measuring CBF and CBV, to measuring neuro-metabolites through spectroscopy. These approaches help in providing deeper and richer insights into how the brain achieves perception, cognition and consciousness. However, these methods have disadvantages alongside their unique contributions. The BOLD signal is widely available to study while also being coarse, relative and with low temporal resolution. Perfusion imaging has better specificity and can be used in conjunction with traditional BOLD for calibration, but has even lower temporal resolution and $CMRO_2$ estimations are problematic. Spectroscopy can capture metabolite concentration in relation to functional processing but is easily affected by participant heterogeneity. Considering this it becomes apparent that understanding what these signals reflect and how they interact during various cognitive and perceptual processes is paramount. This thesis aims to contribute to the field by investigating NVC of expectation signals with and without focused attention, and by characterising the

NVC of positive and negative BOLD and how this relates to GABA concentration, and by adapting an attentionally-controlled MMN EEG study into fMRI RS. This is important as the BOLD signal is highly complex and as such it is difficult to draw appropriate conclusions based on this measurement alone as neural activation and hemodynamic responses can couple and decouple depending on stimulus type and brain state (e.g. Moradi & Buxton, 2013). Therefore, it is imperative to understand how and if NVC differs depending on expectation, and whether attention affects this, and whether this is the same when the BOLD signal is positive or negative, and whether GABA concentrations relates to NVC. If there are NVC differences then this suggests that the traditional BOLD signal will not reflect neural variation when investigating expectation and attention, as well as positive and negative BOLD.

Chapter 2

Chapter Two: Neurovascular Coupling Varies With Expectation and Attention

2.1 Overview

This chapter contains two experiments where I aimed to replicate the expectation paradigm by Summerfield et al., 2008 and Larsson and Smith, 2011 but also simultaneously acquired CBF data using a pulsed ASL sequence. Expectation signals arise from manipulations of statistical contexts, where frequent repetition of faces elicits a larger repetition suppression effect compared to infrequent repetitions of faces (Larsson & Smith, 2011; Summerfield et al., 2008). These signals are however not present in electrophysiological studies (e.g. Kaliukhovich & Vogels, 2010; Vinken et al., 2018), or when attention is diverted (Larsson & Smith, 2011). This raises the question whether the observed expectation signals are true neural events or only hemodynamic responses (Lee et al., 2019; Sirotin & Das, 2009). Acquiring CBF data

allowed me to investigate whether there are any differences within both the BOLD signal and the CBF signal in response to varying levels of expectation. I find that, in both experiments, that there were differences between the BOLD and CBF signals in that ES were consistently expressed in the CBF data and not the BOLD data. Hence, ES may be more driven by hemodynamics than previously thought. Moreover, we observe that there are differences in n-coupling (i.e. how CBF and $CMRO_2$ couple) depending on expectation, indicating that NVC processes are differentially affected by levels of expectation.

2.2 Introduction

The repetition suppression design is an elegant paradigm to assess and infer neural selectivity (Barron et al., 2016) – a cornerstone in cognitive neuroscience and the efforts to map the brain and its functions. Using this paradigm, the field has gained an understanding about important processing mechanisms in multiple regions of the brain (such as orientation and contrast preferences in the early visual system (Fang, Murray, Kersten, & He, 2005; Larsson, Landy, & Heeger, 2003), object (Grill-Spector et al., 1998), scene (Epstein & Kanwisher, 1998) and face (Eger et al., 2004) preferences of higher visual areas, time perception (Harvey, Dumoulin, & Fracasso, 2018; Hayashi et al., 2015) preferences in parietal areas, pitch (De Martino et al., 2013; Todorovic & de Lange, 2012) preferences in auditory regions). The paradigm rests on the observation that neuronal activation and the BOLD signal change reduce in magnitude when a stimulus feature is repeated – such as a V1 neuron to a bar orientation. Once the feature is altered (for example, by tilting a bar), the signal magnitude increases. Hence, one can present pairs of a stimulus feature and compare the signal magnitude differences between pairs that repeat and pairs that do not. The prediction is that pairs that repeat will show a reduction is signal magnitude

compared to the pairs that do not repeat (Grill-Spector & Malach, 2001; Krekelberg et al., 2006).

Summerfield et al., 2008 challenged this paradigm by demonstrating that, at least in fMRI, the RS paradigm is not only inducing low-level adaptation effects. They showed this by altering the probability of a repetition occurring: pairs of faces have either the same (repeating) or different (alternating) identity, and the relative probability of repeats or alternations are different between fMRI runs. Specifically, half of the runs had a high probability of a face identity to repeat (75% repetition probability), meaning that a repeat was expected, and an alternation was surprising. In the other half of the runs, there was a low probability of a face identity to repeat (25% chance of repetition), hence, a repetition was surprising, while an alternation of face identity is expected. If RS effects are purely feedforward and low-level effects, then it should not matter whether a repetition is expected or not. However, the authors showed that it *does* matter. Specifically, they found that in runs where a repetition was expected, the suppression magnitude was greater than when a repetition was not expected. This has wide implications for the field as it suggests that the measured RS signal may not be purely low-level but can be confounded by higher cognitive functions such as expectations. They name this observed difference in suppression magnitude *expectation signals* (referred to as ES from now on).

Moreover, the observation of ES may indicate that the role of prediction is important in more aspects of sensory processing than previously thought. Indeed, perhaps these findings are important neural correlates, or signatures, of predictive coding – a theoretical framework aiming to explain all aspects of neural functioning. Crucially, the findings highlight that the effects of RS and the use of these to infer selectivity may be unreliable.

ES are replicable – however in human fMRI studies they only replicate using a subset of specific stimuli. For example, Grotheer and Kovács, 2014 found that roman

letters induce ES and illustrated objects can also generate ES (e.g. Mayrhauser et al., 2014; Utzerath, John-Saaltink, Buitelaar, & de Lange, 2017). Moreover, it has been replicated using face identity and voices in fMRI (Andics et al., 2013; Larsson & Smith, 2011), tones in MEG (Todorovic & de Lange, 2012; Todorovic, van Ede, Maris, & de Lange, 2011), shapes and faces in EEG (e.g. Stefanics, Kimura, & Czigler, 2011; Summerfield et al., 2011). However, the effects do not replicate when using other stimuli such as natural objects (Kovács et al., 2013) (as opposed to simple illustrated objects (Mayrhauser et al., 2014)). Furthermore, inferring neural selectivity using large-scale imaging methods benefit from having animal electrophysiological studies supporting the ideas. ES have not been observed in primate research. Using fractal and natural stimuli and changing the probability does not induce ES, while RS remains (Kaliukhovich & Vogels, 2010). However, in animal work, the monkeys are often anesthetised and are as such passively observing the stimuli. This is important as Larsson and Smith, 2011 showed that diverting attention away from the face identity stimuli removes any expectation effects whilst preserving the RS in humans using fMRI. Hence, the animal work may not directly translate, and the fMRI study suggests that ES may be attentional effects (Larsson & Smith, 2011). Furthermore, the stimuli used for the animals were not the same (i.e. faces) and that could explain why they find RS effects and not any expectation effects. Specifically, Kaliukhovich and Vogels, 2010 used fractal shape stimuli as well natural stimuli. Although these stimuli generally drive activity in IT neurons (Kaliukhovich & Vogels, 2010), they are not face stimuli - this is important as this could have resulted in monkeys not paying attention or engaging with the stimuli (Vinken et al., 2018).

Vinken et al., 2018 addressed these issues and trained monkeys to actively engage with face stimuli using a repetition probability paradigm. They found, despite controlling for all these possible confounds, that expectation effects do not replicate while RS consistently do. In summary, ES replicate only using highly specific stimuli

using large-scale imaging methods, and they can be removed by controlling for attention. Hence, these observations may be attentional effects or a function of stimulus-type. Perhaps they could even be a signature of predictive coding, although that may be questionable as the ES only seem to arise with specific stimulus-types.

Interestingly, studies demonstrate that hemodynamic changes can occur without neural activity. Sirotin and Das, 2009 measured blood flow and MUA changes in a paradigm where they showed visual stimuli in a predictive rhythm. From time to time the visual stimulus was omitted. When there was a stimulus then there was accompanying neural activity, and when the stimulus was omitted then the neural activity ceased. However, hemodynamic changes occurred in both conditions, despite there being no neural activity when the stimulus was not present. Lee et al., 2019 showed a similar pattern whereby they optogenetically stimulateed two different subtypes of inhibitory interneurons and found that both induce hemodynamic changes but only one had accompanying neural activation. These studies converge to the idea that hemodynamic signals can happen without neural activation – particularly the study of Sirotin and Das, 2009 suggest that there may be a possibility that expected stimuli could have a hemodynamic response but not necessarily a neural one. This begs the question to what extent ES are neural and to what extent they are hemodynamic.

The aim of the current study was to test this idea by replicating the previous studies using the repetition probability paradigm. We calibrated the BOLD signal using ASL, and as a result we measured CBF alongside the traditional BOLD signal to capture a more informative image of ES. Moreover, we added the attentional diversion condition from Larsson and Smith, 2011's study and measured CBF alongside BOLD. This way we could observe the coupling relationship between expectation levels and attentional levels.

We show that traditional BOLD and CBF signals do not couple the same way

during varying levels of expectation (although it is important to note that we fail to replicate BOLD ES effect in the first study, while we do demonstrate ES in CBF signals). Therefore, we decided that it is important to investigate this relationship when attention is diverted and as such conducted a second experiment where we aimed to replicate Larsson and Smith, 2011's second experiment. The uncoupling observation is also observable during attentional diversion. However, during attentional diversion ES is still consistently expressed in CBF, but not in the BOLD data. Moreover, we find that CBF and neural activity (as estimated by $CMRO_2$) differentially couple and decouple depending on expectation, and this pattern is different when attention is diverted. Taken together this suggest that BOLD alone may not be appropriate for studying fine-grained changes in neural signals, and CBF signals offer a more informative insight into brain activity, particularly for processes that develop over time such as expectation levels.

2.3 Methodology

2.3.1 Participants

2.3.1.1 Experiment 1: Focused attention

15 participants (F=8; mean age=25.6 years old) with normal or corrected-to-normal vision partook, and their written informed consent was obtained. Three datasets had to be excluded due to excessive motion (>3mm artefact). The procedures were in accordance with the Psychology Department Ethics Committee at Royal Holloway University of London.

2.3.1.2 Experiment 2: Diverted attention

15 participants (F=7; mean age=26.1 years old) with normal or corrected-to-normal vision participated, and as per the previous experiment we obtained their written informed consent. The procedures were in accordance with the Psychology Department Ethics Committee at Royal Holloway University of London. One dataset was excluded due to the participant falling asleep in the scanner.

2.3.2 Stimuli - Focused and Diverted Attention

2.3.2.1 Main Experiment

The stimuli consisted of greyscale photographs of 509 individuals (males=414), and each individual had their face photographed from four slightly different angles and distances, resulting in a stimulus-pool of 2036 photographs. These images were gathered from various image databases (Psychological image collection at Stirling; Georgia Teach Face Database; Database of Faces, AT&T Laboratories Cambridge; Yale Face Database B, Yale University; Faces94 collection of facial images, department of Computer Science, Essex University; Faces 1999 database, Computational Vision, Caltech; Indian Face Database; BioID face database, Friedrich-Alexander University of Erlangen-Nuremberg), each image was extracted and scaled to 14x14° visual angle and presented against a grey background. Details of how the images were extracted can be found in previously published procedures (Larsson & Smith, 2011).

2.3.2.2 Face Localiser

The localiser for face-responding areas was created by organising face photographs (different from the experiment) into 16 collages consisting of grids of 6x6 photographs and scrambled versions of the same grids (details of stimulus creations can be found at Larsson and Heeger, 2006). These were then masked by a circular mask extending to 15° visual angle. The photographs in the grid, as well as the scrambled versions, were changing at a rate of 200ms. Photograph grids were presented for 32s, and thereafter the scrambled version was presented for 32s. There were five cycles of faces and scrambled stimuli.

2.3.2.3 Retinotopy

Retinotopic visual areas were mapped using standard phase-encoded mapping stimuli consisting of a high-contrast checker-board wedge subtending 22.5 ° visual angle that rotated around the centre of fixation. Each wedge consisted of two radial strands of checks that moved either outwards or inwards along the eccentricity dimension. Each run included six cycles of a full rotation of the wedge stimuli moving in a single direction (clockwise or counter-clockwise). Each cycle took 26s and wedge stimuli were presented in two blocks of three cycles each. Before, between, and after the blocks there was a 26s baseline during which only a blank screen was shown. Two scans were obtained for retinotopic mapping, one scan with the wedge rotating clockwise and the other counter-clockwise.

The experimental stimuli, face localiser, and retinotopic approach were all the same for the second experiment with diverted attention.

2.3.3 Experimental Design

2.3.3.1 Experiment 1: Focused Attention

The first study was a replication of Summerfield et al., 2008 and Larsson and Smith, 2011's first experiment (not diverting attention), with the exception that timings are modified to fit ASL acquisition.

We used an event-related design where each stimulus pair were shown for 2.5s (1s probe, 0.5 ISI, 1s test) (see figure 2.1). To let the evoked response to return to baseline, and thus avoid making assumption of the impulse response function shape, we randomly varied the interval between events between 12-17s, in 1s steps.

Event stimuli were randomly selected from the pool of photographs with the constraint that once a face identity had been used in one event, it could not be sampled again. Hence, each event always contained unique face identities. If the event was a repeating event, the probe and test showed the same face identity, and if the event was an alternating event, the probe and test were different identities. The probe and test stimuli were each randomly sampling photographs every 200ms from the pool of four photographs per identity.

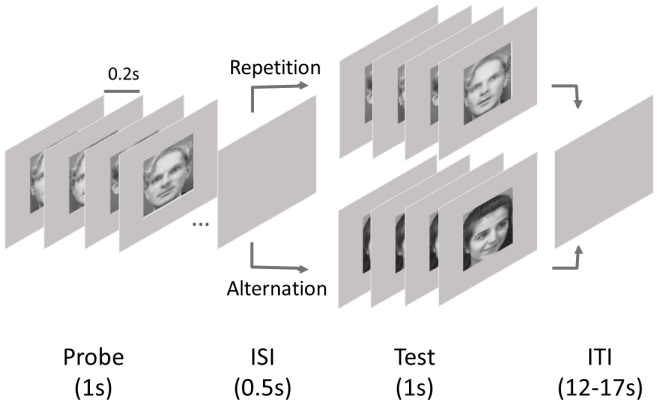

Figure 2.1: Experimental Design. An event consisted of a 1s probe, 0.5s ISI, and 1s test stimulus. The test stimulus was either a repetition of the probe, or an alternation. Each event was separated by an inter-trial interval (ITI) of 12-17s.

To manipulate statistical context, we changed the proportion of repetition and alternation events per run to 3:1 in Frequent repetition runs (18 repetition and 6 alternations), 1:3 in Infrequent repetition runs (6 repetitions and 18 alternations), and 1:1 in equal repetition runs (12 repetitions and 12 alternations), in line with previous research (Larsson & Smith, 2011; Summerfield et al., 2008) (see figure 2.2). The experiment consisted of ten runs, of which four were Frequent repetition runs, four were Infrequent repetition runs, and two were equal repetition runs. The runs were randomly ordered for each participant.

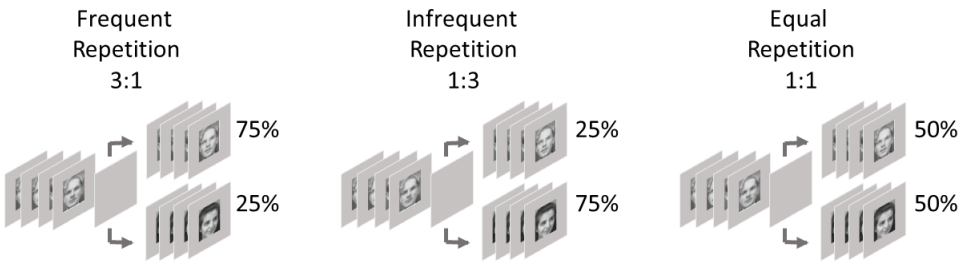

Figure 2.2: Experimental Probability Manipulation. The experiment comprised of three run types of different statistical contexts: Frequent, Infrequent, and equal repetition.

2.3.3.2 Experiment 2: Diverted attention

This experiment replicates Larsson and Smith, 2011's second experiment where attention was diverted. We modified timings to fit ASL acquisition. Event stimuli were randomly selected the same way as in the previous experiment. The only difference is that we excluded the equal repetition condition as this did not yield enough power to be a meaningful control. This resulted in five runs of Frequent repetitions (3:1, 18 repetition and 6 alternations) and five runs of Infrequent repetitions (1:3, 6 repetitions and 18 alternations) (see figure 2.3). The runs were randomly ordered for each participant.

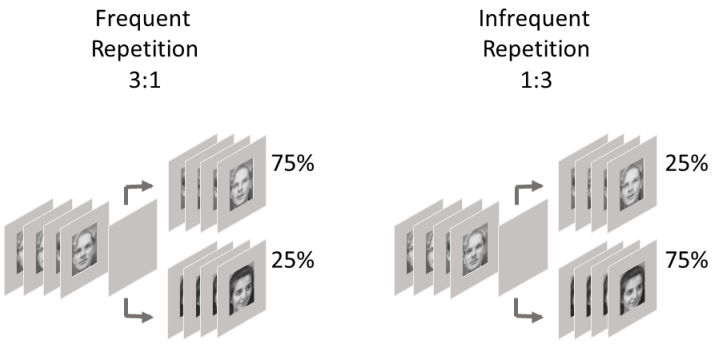

Figure 2.3: Experimental Probability Manipulation for the experiment with diverted attention. It shows the two statistical context runs that were used (note that this is different from experiment 1 in that the "equal probability of repetition" run is excluded).

2.3.4 Task and Procedure

2.3.4.1 Experiment 1: Focused Attention

Participants were asked to fixate, and to report when a photograph was inverted (see figure 2.4). This was employed as an attentional task to ensure the participants were engaging with the stimuli. Inversions occurred randomly at an 8.3% (1 in 12) probability. Behavioural data was recorded using an MR-compatible four-button Lumitouch button-box. None of the participants were aware of the experimental manipulation before the study.

The main session started with an anatomical scan, followed by ten runs of the expectation paradigm. The final run comprised of the face region localiser. The session took about 90 minutes.

Those participants (n=9) who did not already have defined ROIs from previous experiments, underwent a second separate session. During this, one high-resolution anatomical and two retinotopic runs were acquired. This session took about 30

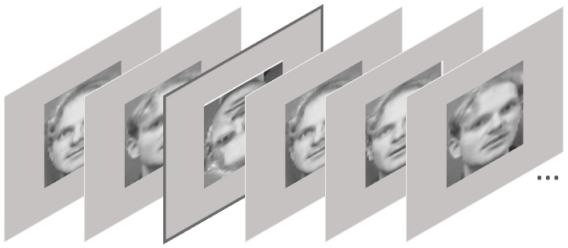

Figure 2.4: Illustration of the task to ensure that the participant was attending to the stimuli.

minutes.

2.3.4.2 Experiment 2: Diverted attention

The task in this experiment was different from that of the previous as the participants were asked to focus on a rapid serial visual presentation (RSVP) of letters (figure 2.5). This was to ensure their attention was diverted away from the face stimuli while still maintaining fixation. The participants had to count how many "X"s (0 through 3) they saw in each RSVP stream and respond by pressing 1 of 4 keys on the Lumitouch button-box. Each letter was shown for 200ms, and each stream trial was four seconds of which three seconds were the stream followed by one second of response time. A fixation cross appeared during the response window and remained there until the next RSVP stream. The fixation cross changed colour to give feedback to the participant – green if their response was correct, red if it was incorrect, and no change if they responded outside the one second response window.

The RSVP trials were independently timed from the main experiment, they were not synched with the face stimulus presentation and they run back-to-back.

As with the previous experiment, the main session started with an anatomical scan, followed by ten runs of the expectation paradigm and a final run comprising of the face region localiser. The session took about 90 minutes.

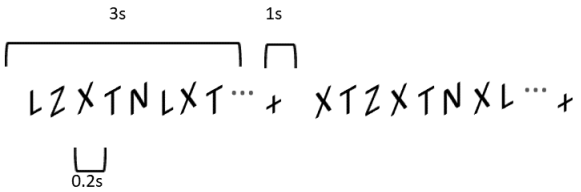

Figure 2.5: Illustration of the the attention task to divert attention. The participant attended to a rapidly presented string of letters and had to indicate how many of the letter "X" they observed.

Participants (n=4) who did not already have defined ROIs from the previous experiments, underwent a second separate session during which one high-resolution anatomical and two retinotopic runs were acquired. The separate session took about 30 minutes.

As with the first experiment, none of the participants were aware of the experimental manipulation before the study.

2.3.5 MRI Acquisition - Focused and Diverted Attention

MRI data were collected using a Siemens 3T TRIO system (Erlangen, Germany; 32-channel head-coil).

2.3.5.1 Anatomical Acquisition

A whole-brain anatomical scan was obtained for each participant for alignment and co-registration between sessions (MPRAGE sequence; 1mm isotropic; 160 slices; TR: 1830ms; TE: 3.03ms; TI: 1100ms; FA: 11°; GRAPPA acceleration of 2; echo space: 8.9ms; 4:52 minutes). Participants that did not have defined retinotopic areas from previous studies, had a high-resolution high contrast anatomical obtained (MDEFT sequence; 1mm isotropic; 176 slices per slab; 1 slab; TR: 7.92ms; TE: 2.48ms; TI:

910ms; FA: 16 °; 13:43 minutes).

2.3.5.2 Functional Acquisition

Functional data was obtained using a standard Siemens pulsed ASL sequence (PICORE; 3mm isotropic; 6:22min; 13 slices; axial acquisition; TR: 2000ms; TE: 15ms; IT1: 700ms; IT2: 1401.6ms; Saturation stop time: 1200ms; FA: 90 °; GRAPPA acceleration factor of 2; gap: 22.1mm; echo shift: 0.53ms). 186 volumes were acquired for the 10 functional runs, and 171 volumes for the face region localiser run.

The bounding box for determining the slab position within which the functional data was acquired was positioned manually for each participant. Anatomical landmarks such as the Calcarine sulcus and inferior temporal regions were used to position the bounding box to capture functional activation from early visual cortices and face responding regions(see figure 2.6 for an example of bounding box positioning). Care was taken to avoid the eye and surrounding regions due to the possible artefacts that can arise (e.g. Chen & Zhu, 1997). The data were checked in retrospect through the retinotopic mapping and face localisation to ensure that the functionally relevant regions were included in the slab. During the pilot phase of the experiment the bounding box was incorrectly positioned in two participants and the face responsive areas were not adequately covered. None of the pilot data-sets were used in the main analysis.

To acquire the volumes, the pulsed ASL sequence alternated tagged and control volumes in an interleaved fashion. CBF responses were estimated by subtracting the control from the tag volume, while BOLD responses were obtained by averaging the tag and control volumes. Surround subtraction was used to estimate CBF at each time point as follows: for tagged volumes, CBF was estimated using a weight of 1 for the tagged volume and -0.5 for the preceding and subsequent control volumes; for

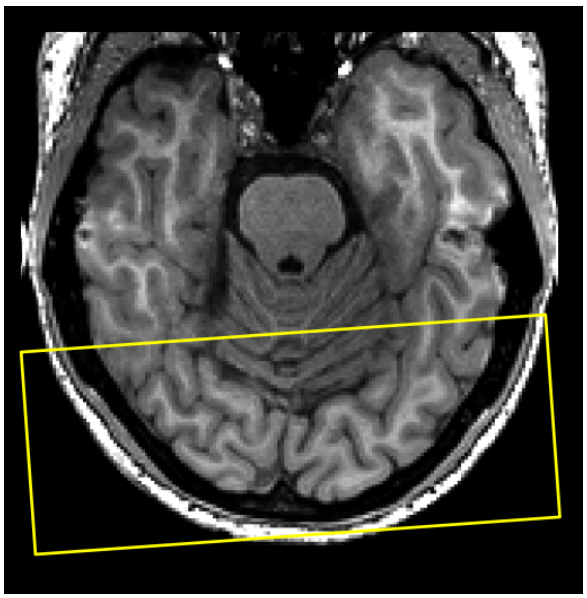

(a) Example of slab position in axial plane

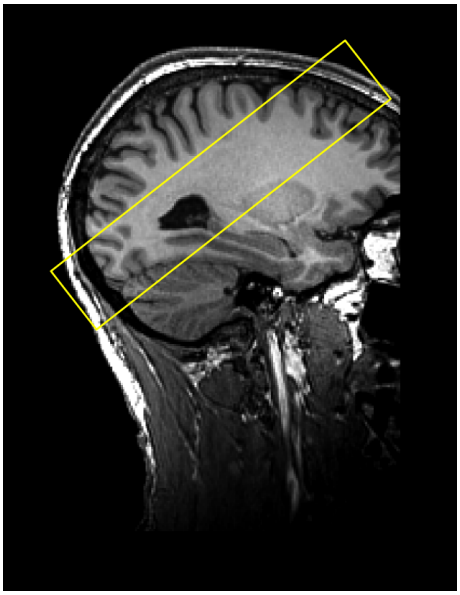

(b) Example of slab position in sagittal plane

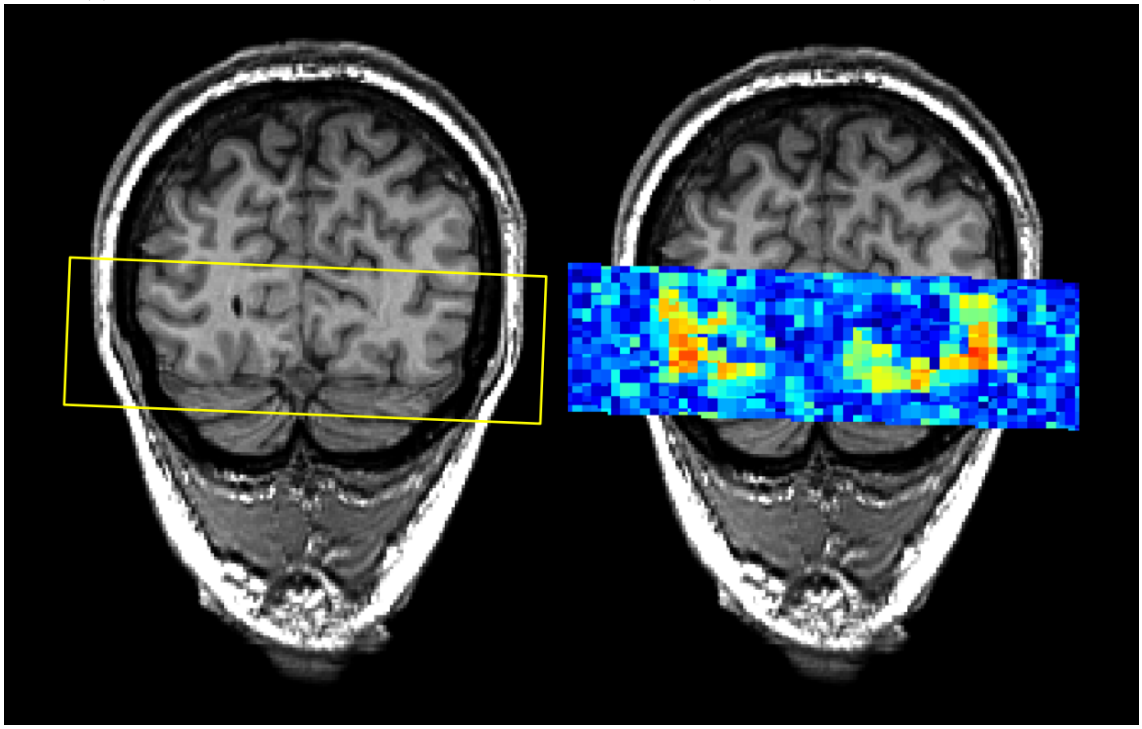

(c) Example of slab position in coronal plane (left) with corresponding activation map (right) in response to the face localiser.

Figure 2.6: Examples of how the acquisition slab was positioned to include relevant brain regions: early visual cortex and face responsive areas. Care was taken to avoid eye regions as these can contribute to acquisition artefacts. The activation map is included to highlight that relevant functional areas were captured.

control volumes, the signs of the weights were inverted (i.e., [0.5 -1 0.5]. For BOLD, the corresponding weights were 0.5 and 0.25 respectively ([0.25 0.5 0.25]). The first and last CBF and BOLD estimates were computed from the two first or last volumes only, respectively, weighting the current and neighbouring volume equally, i.e. [1 -1] for CBF and [0.5 0.5] for BOLD (Liu & Wong, 2005).

Nine participants underwent one additional separate session to acquire two runs of retinotopic mapping data (EPI sequence; 154 volumes; 3mm isotropic; 3:57min; 19 slices; TR: 1500ms; TE: 34ms; FA: 75 °; echo shift: 0.78ms).

2.3.5.3 Pre-processing

Between-scan alignment and motion correction were done using the mcflirt tool (Jenkinson, Bannister, Brady, & Smith, 2002). Slice timing, linear de-trending and high-pass filtering (using a cut-off of 0.022Hz) was applied using in-house software written in MATLAB. Surfaces, used for visualisation and identifying visual areas, of each participant's cortex were reconstructed from the anatomical MR image using SurfRelax (Larsson, 2001).

2.3.6 Analysis

All analyses were done in MATLAB 2020a (MATLAB, 2020).

2.3.6.1 Region of Interest Identification

Experiment 1: Focused Attention Each participant's retinotopic data (maps of phase and coherence) were projected onto a reconstructed flat-map of their occipital area. Identification and drawing of area V1, V2, V3, hV4, LO1, LO2, V3A/B

were done manually based on the acquired maps (Larsson & Heeger, 2006), and ROIs from left and right hemisphere were combined. There were some difficulties in identifying some of the later visual areas (particularly V3AB and hV4) in some participants, therefore, we used V1, V2, and V3 for the analysis as these areas were identifiable in all participants.

The separate face localiser was used to identify face responding areas (FRA) for each participant. In addition to BOLD defined face responding ROIs we also obtained CBF defined ROIs. CBF defined face responding ROIs were identified the same way as the BOLD defined ROI by using the face localiser CBF data. Voxels were chosen based on their preferential response to faces vs scrambled images (as in (Larsson & Smith, 2011)). The threshold was decided based on visual inspection of each participant's data in order to choose the most biologically plausible voxels. Although there was some individual variation in chosen thresholds, they corresponded well across participants such that the mean threshold in this experiment was 0.62 (std=0.0537) for BOLD defined FRA and 0.45 (std=0.026) for CBF defined FRA.

Theoretically the BOLD and CBF defined face ROIs should show overlap, specifically in that BOLD signals seem to have a wider activation area, or point-spread function, compared to CBF signals (e.g. Bandettini, 2012). Based on this logic we also created an additional ROI whereby the overlapping CBF data was removed from the BOLD data. Specifically, we subtracted the CBF activation area from the BOLD activation area, and we expected this to generate an ROI that contained BOLD signal information devoid of direct CBF influences. This was done to assess if and to what extent the CBF signal affects the BOLD signal.

The complete set of six ROIs for each participant were V1, V2, V3, BOLD defined FRA, CBF defined FRA, and BOLD-CBF FRA difference. Although, because there was no consistent overlap between the BOLD and CBF defined FRAs we did not include this ROI in the analysis.

Experiment 2: Diverted Attention This study defined ROIs based on retinotopic mapping data (either from a separate scanning session, or from the previous experiment), and the face localiser. Hence, the complete set of five ROIs are V1, V2, V3, BOLD defined FRA and CBF defined FRA. The mean threshold for choosing face responsive voxels in this experiment were 0.62 (std=0.0625) for BOLD defined FRA and 0.46 (std=0.044) for CBF defined FRA.

2.3.6.2 Main Experiment Analyses

Experiment 1: Focused Attention Data from each run-type (Frequent, Infrequent, and Equal) were combined into three separate data-sets and analysed per participant and ROI. For each set, we used linear deconvolution to estimate the time courses for each event-type (repetition or alternation). We ended up with six conditions: repetition and alteration within Frequent, Infrequent, and Equal run-type. We excluded events that contained a face inversion. Deconvolution was performed to avoid making assumptions of HRF shape (Burock & Dale, 2000). Specifically, a design matrix consisting of 10 columns (time-points) per condition was created, where the first column indicated the start of each trial in that condition and subsequent columns each subsequent time-point. This resulted in 61 columns (1+10*6), where the first represents the mean response. For BOLD and CBF data, a standard GLM was used to estimate response magnitude at each time-point after a trial began yielding a time-course. These estimated response magnitudes at each time-point, measured across all trials, were averaged into a single HRF and use in the next step where beta values were extracted for each trial.

Each trial was modelled in a GLM using the average HRF from the preceding deconvolution analysis, yielding a beta value. This beta value is the response magnitude for that trial. This was done for both BOLD and CBF data. These values were then used for the formal analysis in the next step.

To formally assess any differences in the data we performed a permutation analysis of linear models in MATLAB using the PALM toolbox (Winkler, Ridgway, Webster, Smith, & Nichols, 2014). This non-parametric method was chosen because of the experiments' low sample size and the non-normality issues that come with it. The permutation approach is more robust against violations to normality and independence as it makes fewer assumptions of the data compared to parametric alternatives. The model was built as being more easily compared to previous literature (Larsson & Smith, 2011; Summerfield et al., 2008) and takes the form of a two by two repeated measures model. The main effects assessed were Expectation and RS, and an interaction between the two. Thereafter, pairwise comparisons were performed to assess what differences drive the effects as well as remaining more comparable to previous literature (Larsson & Smith, 2011). 10,000 permutations were run per effect and across conditions (i.e. participants were modelled as blocks for within exchangeability (see Winkler et al., 2014, for further details)). Participants were treated as random effects to allow for generalisation of the effects to the population at large. False discovery rate (FDR) adjustments using the Benjamini-Hochberg method (Benjamini & Hochberg, 1995) were applied to control for multiple tests within each ROI as across ROIs. This was achieved using an external MATLAB function (Groppe, 2020).

Experiment 2: Diverted Attention Data from each run-type (Frequent and Infrequent) were combined into two separate data-sets and analysed per participant and ROI. In experiment 1, we observed that the 'same' or equal repetition run-type did not have enough power to be useful as a control. Therefore, we excluded this run-type for experiment 2 and as such allocated more power to the Frequent and Infrequent run-types. For each set, we used linear deconvolution to estimate the time courses for each event-type (repetition or alternation) as per the previous experiment and we had four conditions: repetition and alteration within Frequent

and Infrequent run-type. This design matrix consisted of 41 columns (1+10*4), where the first column reflects the mean response and the rest are the four conditions by time-points.

The remaining analyses were done as in experiment 1.

2.3.6.3 $CMRO_2$ Estimation

To estimate $CMRO_2$, we used the Davis model (Davis et al., 1998) modified by Moradi and Buxton, 2013. The modification involved using empirical data to estimate certain parameters that can only be obtained with special equipment (such as MRI compatible oxygen-tanks and inhalation-masks) (see Moradi and Buxton, 2013).

$$\Delta b = M(1 - f^{\alpha-\beta} r^{\beta}) \tag{2.1}$$

Just as Moradi and Buxton, 2013 point out, the estimation methods are based on and developed from the David model (Davis et al., 1998). In equation (2.1) Δb refers to the change in normalised BOLD, f to normalised cerebral blood flow, and r to normalised $CMRO_2$. Griffeth and Buxton, 2011 normalised their data based on absolute measurements of CBF, specifically they normalised absolute CBF to equal 1 at rest (based on the approach of Griffeth and Buxton, 2011). The current study only measured relative signal changes, and hence does not have any measure of the absolute CBF signal change. Therefore, to circumvent these methodological differences, the current study normalised the relative BOLD and CBF signal change to each signal's own baseline. In other words, we transformed the raw signals in the percent signal change which conforms to the same properties as a resting baseline equalling 1.

In equation 1, alpha (α) and beta (β) are constants that have been empirically

estimated (Griffeth & Buxton, 2011) and equal 0.16 and 1, respectively. Moradi and Buxton, 2013 estimated a scaling parameter (M) for each participant that was based on a stimulus condition in their experiment, namely the high contrast condition (this is represented with a "HC" subscript in equation (2.2)).

$$M = \frac{(b_{HC} - 1)}{(1 - f_{HC}^{\alpha-\beta}\ r_{HC}^{\beta})} \tag{2.2}$$

In the current study, the values with a HC subscript refer to the normalised variables to the surprising alternation condition (i.e. equivalent to Moradi and Buxton, 2013 high contrast continuous stimulation condition). Estimates of $CMRO_2$ responses in high contrast conditions are required to estimate the scaling parameter, and this is solved by using equation (2.3) as below.

$$r_{HC} = 1 + \frac{(f_{HC} - 1)}{n_{HC}} \tag{2.3}$$

Equation (2.3) shows how $CMRO_2$ in the surprising alternation condition (r_{HC}) is estimated using the CBF (f_{HC}) response during the same condition. Moradi and Buxton, 2013 simulate various NVC ratio (n_{HC}) constants and conclude that it is trivial, and they kept the constant at 2.5 for all participants. The current study did the same (i.e. n_{HC}=2.5). Equation (2.4) below show how $CMRO_2$ (r) is estimated using the scaling parameter (M) and normalised BOLD signal change (b).

$$r = f^{0.84}(1 - \frac{(b - 1)}{M}) \tag{2.4}$$

To formally assess any differences between conditions, $CMRO_2$ data were analysed using the same non-parametric approach as for the BOLD and CBF data.

2.3.6.4 CBF:$CMRO_2$ - The n-coupling Ratio

To understand how and whether CBF and $CMRO_2$ are modulated differently depending on expectation level and attention, the n-coupling ratio was estimated. This was done by taking the ratio of CBF to $CMRO_2$. We used the mean CBF and the mean $CMRO_2$ estimate per condition and participant, and divided the former with the latter. This was computed for each ROI. This measure gives a clue as to how much CBF is modulated in relation to $CMRO_2$. For example, if the n-coupling ratio is large it means that CBF is modulated more compared to $CMRO_2$. If the ratios differ between conditions, it suggests that CBF and $CMRO_2$ are differentially modulated. This gives insights into the dynamics underlying the BOLD signal. For example, if a condition generates a very large n-coupling ratio in comparison to another, it suggests that that condition has a much larger CBF modulation. According to Buxton et al., 2014 this may signify a larger inhibitory response, as this would lead to a reduced $CMRO_2$ output whilst still requiring CBF to be recruited.

To formally assess any differences between conditions, the data were analysed using the same non-parametric approach as for the BOLD and CBF data.

2.4 Results

2.4.1 Behavioural Results

2.4.1.1 Experiment 1: Focused Attention

Responses to inverted photograph had an accuracy of 97.2% (std=0.8%).

2.4.1.2 Experiment 2: Diverted Attention

The RSVP task accuracy was 65% (std=17%). This is an acceptable performance as it is above chance level (25%) and in line with Larsson and Smith, 2011.

2.4.2 Predicted Results

Previous experiments have found that BOLD ES are evident when attention is focused (Larsson & Smith, 2011; Summerfield et al., 2008), whilst RS is present when attention is diverted (Larsson & Smith, 2011). Since no study has investigated CBF signals in response to varying statistical context, we predict that if CBF and BOLD signals couple similarly no matter the level of expectation, then the relationship should look slightly curve-linear in line with previous research (Griffeth, Simon, & Buxton, 2015) as illustrated in figure 2.7.

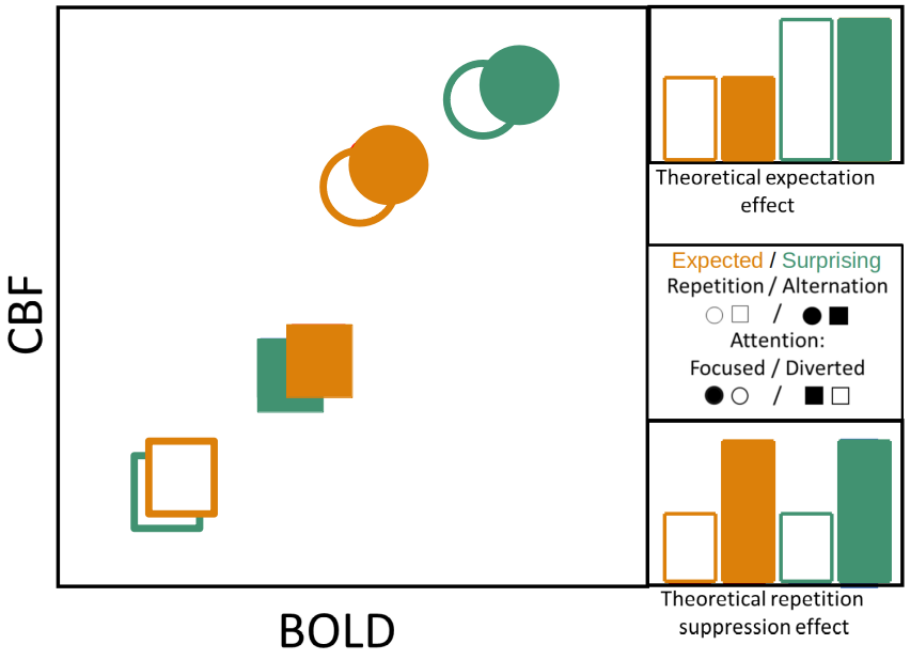

Figure 2.7: Illustration showing predicted results for the expectation experiments using calibrated BOLD. The relationship is curve-linear, as can be seen in the illustration (Griffeth, Simon, & Buxton, 2015). During focused attention (circles) we expect to see greater activation in general and we expect to see ES effects (see circles and top right panel). When attention is diverted we expect to see RS effects (see squares, and bottom right panel). Further details in text.

In this figure the circular symbols represent the focused attention experiment and the square symbols the diverted attention experiment. As can be seen, it is predicted that the focused attention experiment will, on average, generate higher percent signal change in both the CBF and BOLD signals. Moreover, within the experiments we predict that during focused attention ES will be present in both the BOLD signal (in line with previous literature) and the CBF signal. Specifically, the conditions that are surprising are predicted to generate higher percent signal change compared to the expected conditions. On the other hand, when attention is diverted it is predicted that RS will remain in both signals while ES will disappear (in line with previous literature investigating the BOLD signal). That is, conditions that are repeated will generate a lower percent signal change compared to the conditions that are alternated. For clarity, the panel to the right show theoretical ES (upper) and RS (lower) effects.

Moreover, as studies have shown that RS can occur without ES (when attention is diverted (Larsson & Smith, 2011)), but ES cannot occur without RS (as the paradigm is still RS, but varying probability of repetition), we expect to see an interaction between RS and ES if ES are present.

2.4.3 Overall Results Summary

In figure 2.8, the results from both experiments are shown. The top panel shows the first experiment where attention was focused on the stimuli and the bottom panel shows the second experiment where attention was diverted away. The left panel reflects the BOLD data in both experiments and the right panel the CBF data. The x-axes show the five ROIs and there is one cluster of four boxes per ROI – one for each condition. The first two boxes show the expected conditions – repetitions when repetitions are probable (FreqRep) and alternations when repetitions are improbable

(InfreqAlt). The second two boxes show the surprising events, namely repetitions when repetitions are Infrequent (InfreqRep) and alternations when repetitions are Frequent (FreqAlt). An interaction, or a difference between the expected and surprising conditions (i.e. surprising conditions generating higher signal change than expected conditions) would indicate expectation effects. Differences between the repetition (first and third box) and alternation (second and fourth box) trials (i.e. that repetitions generate, on average, lower signal change compared to alternations) would indicate RS effects.

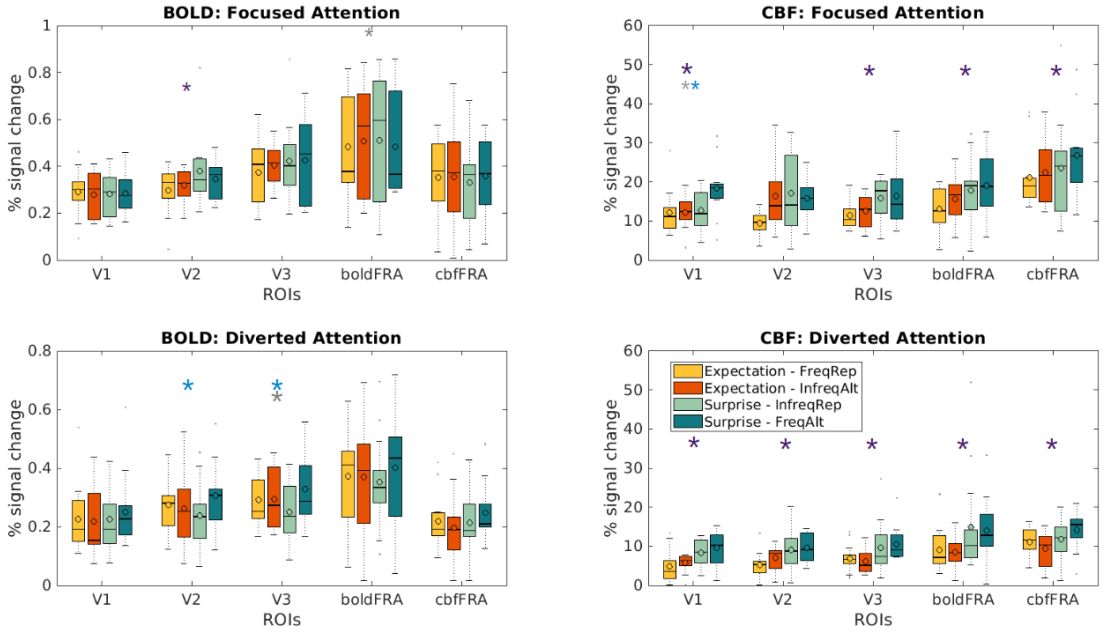

Figure 2.8: Summary of Expectation Experiments Results. These box plots show the percent signal change between the conditions in BOLD and CBF data in both experiments. The top and bottom panels show experiment 1 and 2, respectively. The left and right panels reflect the BOLD and CBF data in both experiments, respectively. Large asterisk indicates significance (p <0.05), and small asterisk indicates trends (p <0.1): blue reflect interaction effects, purple ES effects and grey RS effects. The box encapsulates the condition response's interquartile range. Whiskers include the rest of the data's range, besides outliers which are represented as dots.

As can be seen in figure 2.8 there are some effects in BOLD data. Specifically, in experiment 2 with diverted attention, V2 and V3 show interaction effects, and thus ES effects (blue asterisks). In experiment 1, there were trends towards ES effects in V2 (small purple asterisk) and RS in BOLD defined FRA (small grey asterisks). In CBF data, experiment 1 shows ES effects in V1, V3, BOLD defined FRA and CBF

defined FRA, and in experiment 2 all ROIs demonstrate this pattern. The following sections detail the findings.

2.4.4 BOLD Data Results

In the first experiment, with focused attention, the analyses show there is no evidence for interactions or main effects of ES or RS. There was a trend towards a main effect of ES in V2 ($F(1, 11) = 2.1125, p = 0.08$) and of a main effect of RS in BOLD defined FRA ($F(1, 11) = 2.2465, p = 0.0785$).

Pairwise comparisons from the permutation tests show that, in all ROIs, surprising alternations tend to generate higher signal change compared to expected alternations (FreqAlt>InfreqAlt). Moreover, in all ROIs, surprising alternations yield higher signal change compared to expected repetitions (FreqAlt>FreqRep) (further details in table 2.1).

In the second experiment, with diverted attention, analyses reveal significant interactions in V2 ($F(1, 13) = 2.4885, p = 0.023$) and V3 ($F(1, 13) = 2.633, p = 0.023$). Moreover, there is evidence for a main effect of RS in V3 ($F(1, 13) = 2.8166, p = 0.0185$).

Similar to the previous experiment, pairwise comparisons indicate that, in all ROIs, surprising alternations tend to generate higher signal change compared to expected alternations (FreqAlt>InfreqAlt). Additionally, surprising alternations yield higher signal change compared to expected repetitions (FreqAlt>FreqRep), in all ROIs (see table 2.2).

2.4.5 CBF Data Results

In experiment 1, with focused attention, the analysis from the CBF data reveal significant main effects of ES in V1 ($F(1, 11) = 2.3917, p = 0.013$), V3 ($F(1, 11) = 3.0739, p = 0.0035$), BOLD defined FRA ($F(1, 11) = 2.4286, p = 0.018$) and CBF defined FRA ($F(1, 11) = 2.0456, p = 0.034$). There was also a trend towards a significant interaction ($F(1, 11) = 2.1678, p = 0.071$) and a main effect of RS in V1 ($F(1, 11) = 2.143, p = 0.067$).

Pairwise comparison reveal the same pattern as in the BOLD data results that, in all ROIs, surprising alternations tend to generate higher signal change compared to expected alternations (FreqAlt>InfreqAlt). Additionally, surprising alternations yield higher signal change compared to expected repetitions (FreqAlt>FreqRep) (see table 2.1 for details).

In experiment 2, with diverted attention, CBF data showed significant main effects of ES in all ROIs: V1 ($F(1, 13) = 4.298, p < 0.001$), V2 ($F(1, 13) = 3.147, p = 0.0028$), V3 ($F(1, 13) = 3.1237, p = 0.0013$), BOLD defined FRA ($F(1, 13) = 2.5647, p = 0.0043$), CBF defined FRA ($F(1, 13) = 1.9418, p = 0.0089$).

Pairwise comparison reveal the same pattern as in the previous experiment – surprising alternations showed higher signal change compared to expected alternations (FreqAlt>InfreqAlt), in all ROIs. Additionally, in all ROIs, surprising alternations yield higher signal change compared to expected repetitions (FreqAlt>FreqRep) (see table 2.2 for details).

Figure 2.9 reveals a pattern demonstrating the relationship between BOLD and CBF signals across conditions in each ROI. This gives a better indication of how well the expectation conditions map onto the two signal types. Circles and squares represent experiment 1 and 2, respectively. Overall, the responses in the diverted

attention experiment are lower than the ones in the focused attention experiment, as predicted. The solid teal circle is consistently higher in magnitude which is to be expected as this is arguably the most surprising condition (as an alternation when a repetition is expected strongly violates the prediction).

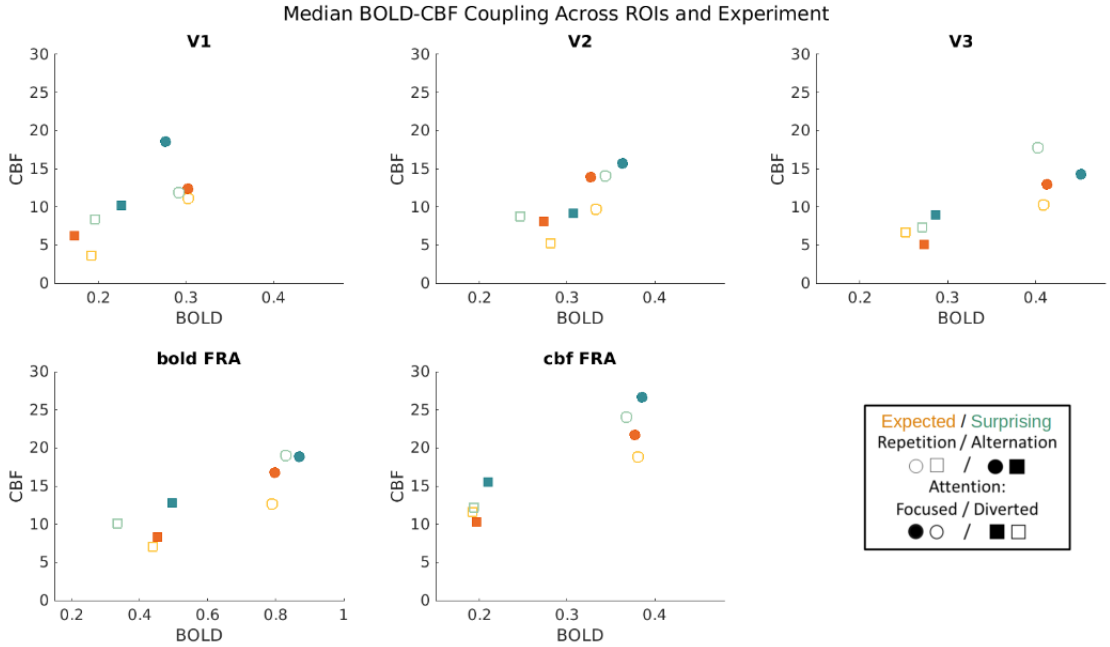

Figure 2.9: Scatter plot showing the relationship between BOLD and CBF signal change across condition in each ROI. These are median values. As can be seen in the figure legend, the circles represent experiment 1, and the squares experiment 2. The orange symbols represent expected events and the teal surprising. Open symbols reflect repetitions and closed alternations. The axes are adjusted to make the data more comparable between the ROIs and signal types, but note that BOLD defined FRA required wider x-axis.

In V1 there is no clear effect in the BOLD signal for experiment 1 and 2, although in experiment 2 there is some spread between the conditions. There are some differences supported by pairwise comparisons, specifically, surprising alternations generate higher signal change compared to expected alternations and repetitions (see table 2.1). The CBF data in figure 2.9 reveals an pattern in both the focused and diverted attention experiments. Specifically, it can be seen that the surprising responses are on average larger than the expected ones in both experiments, and this is clearer in the diverted attention experiment in which both surprising (teal squares) event responses are larger than the expected (orange squares) events. These observations are statistically supported by main effects of ES, and pairwise

comparisons, as previously mentioned.

V2 focused attention data show an expectation pattern in that the teal circles, surprise responses, are on average the highest in both signal types (BOLD and CBF). Meanwhile, the orange circles, the expected responses, are lower in response magnitude. This gives rise to a trend towards a significant ES effect in experiment 1 BOLD data. During the diverted attention experiment, in V2 the surprising events generate on average a larger signal change in CBF compared to the expected events, as reflected by the significant ES main effect. This is not as clear in the BOLD data as we can see that the alternation trials (solid symbols) are on average larger in response magnitude than the repetition trials (open symbols). This reveals an interaction effect that is statistically supported.

V3 shows us that the surprising events generate larger responses in both BOLD and CBF data in both experiments, compared to the expected events (although this is less clear for BOLD data in experiment 1). This generated a significant interaction effect in experiment 2 BOLD data, and a main ES effect in CBF data in both experiments.

BOLD defined FRA demonstrates a less clear-cut pattern in the BOLD data for both experiments. This is underscored by a trend towards a RS effect in experiment 1. However, the CBF data show that surprising events yield larger signal magnitude compared to expected events, in both experiments. This is supported by significant ES effects. Qualitatively, the pattern of activation amongst the conditions resemble the predicted pattern in figure 2.7.

Within the CBF defined ROI, CBF data reveal that surprising events generate larger percent signal change compared to expected events in both experiments. This is statistically supported by main effects of ES in both experiments. The main effect of ES can be seen amongst the circle symbols whereby the expectation responses

(orange circles) yield lower activity magnitude compared to the surprise responses (teal circles). The BOLD data show no clear pattern of differences between the conditions.

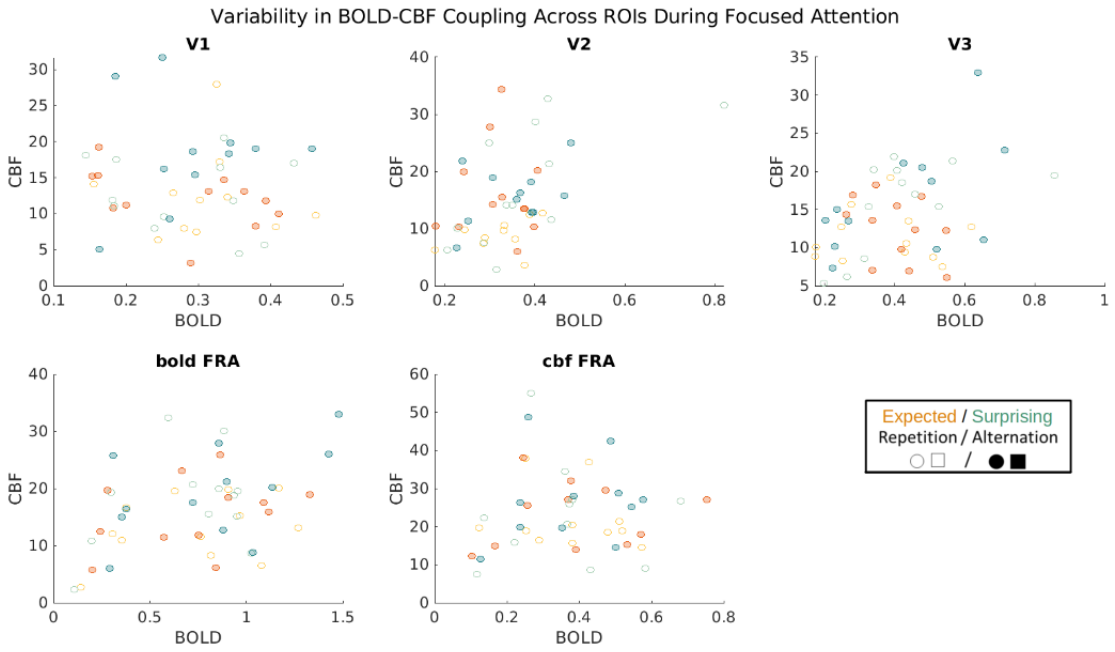

Figure 2.10: Scatter plot showing the variability of the relationship between BOLD and CBF signal change in experiment 1 with focused attention (in contrast to the mean responses shown in figure 2.9). This is plotted across condition in each ROI. These are individual data points. This plot is only for experiment 1, which is why there are only circles. The orange symbols represent expected events and the teal surprising. Open symbols reflect repetitions and closed alternations.

Note however, that the data presented in figure 2.9 reflect median responses and this variability is plotted in figures 2.10 and 2.11. To illustrate, in figure 2.10, in the first panel where data from V1 is shown, it can be seen that there is no clear difference in response in the BOLD data. In the CBF data however, one can see that the surprising conditions (teal symbols) are in general generating larger CBF signal change compared to the expected conditions (red symbols), as reflected in the figure (2.9) demonstrating the median responses.

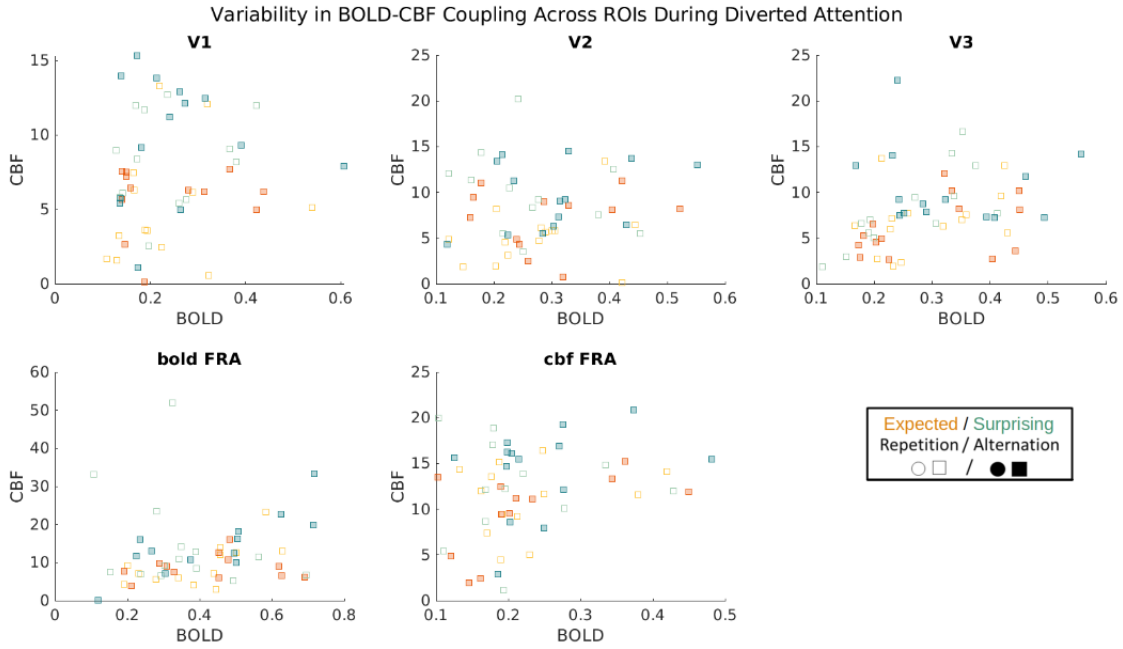

Figure 2.11: Scatter plot showing the variability of the relationship between BOLD and CBF signal change in experiment 2 with diverted attention. This is plotted across condition in each ROI. These are individual data points. The orange symbols represent expected events and the teal surprising. Open symbols reflect repetitions and closed alternations.

2.4.6 BOLD and CBF Post-hoc Pairwise Comparisons

The main experimental results have been covered in the previous sections, this part elaborates on the pairwise comparison post-hoc tests of the linear models i.e. the paired t-tests (all results are presented in table 2.1 and 2.2). These models were run on the BOLD and CBF percent signal change in response to varying levels of expectation. In experiment 1 (table 2.1), attention was focused and in experiment 2 (table 2.2), attention was diverted.

When attention was focused, BOLD data reveal differences between surprising alternations and expected alternations (FreqAlt > InfreqAlt) and repetitions (FreqAlt>FreqRep). This is consistent across ROIs.

In CBF data, the pattern differs slightly. There are differences between surprising and expected alternations in V1, V3, BOLD defined FRA and CBF defined FRA (FreqAlt>InfreqAlt). Moreover, in CBF defined FRA there is a difference between

surprising repetitions and expected alternations (InfreqRep>InfreqAlt). In V2, V3, BOLD defined FRA and CBF defined FRA there is a difference between surprising alternations and expected repetitions (FreqAlt>FreqRep).

In experiment 2, when attention was diverted, we see in the BOLD data that there were significant differences between surprising alternations and expected alternations (FreqAlt>InfreqAlt) and repetitions (FreqAlt>FreqRep), across all ROIs. This is also the case for CBF data in all ROIs (see table 2.2).

2.4.7 $CMRO_2$ Estimation Results

The analysis of the $CMRO_2$ estimates in experiment 1 shows that there is a trend towards a significant main effect of ES in V2 ($F(1,11) = 1.8842, p = 0.054$) and V3 ($F(1,11) = 2.2632, p = 0.054$).

In experiment 2, the $CMRO_2$ analyses show a significant main effect of expectation in V2 ($F(1,13) = 3.0413, p = 0.013$), a main effect of RS in V3 ($F(1,13) = 3.2757, p = 0.0015$). There were trends towards significance for an interaction in V3 ($F(1,13) = 2.2417, p = 0.0565$), and for main effects of ES in V1 ($F(1,13) = 1.7571, p = 0.065$) and CBF defined FRA ($F(1,13) = 1.6606, p = 0.065$).

2.4.8 CBF:$CMRO_2$ - n-coupling Results

The analysis of n-coupling ratio in experiment 1 shows that there were significant interaction effects in CBF defined FRA ($F(1,11) = 2.9113, p = 0.015$). There was also a significant main effect of ES in BOLD defined FRA ($F(1,11) = 2.996, p = 0.0095$). Trends towards significant main effects of ES were observed in V1 ($F(1,11) = 1.759, p = 0.07$) and V2 ($F(1,11) = 1.8638, p = 0.07$), and a main effect of RS in V3 ($F(1,11) = 1.9654, p = 0.097$).

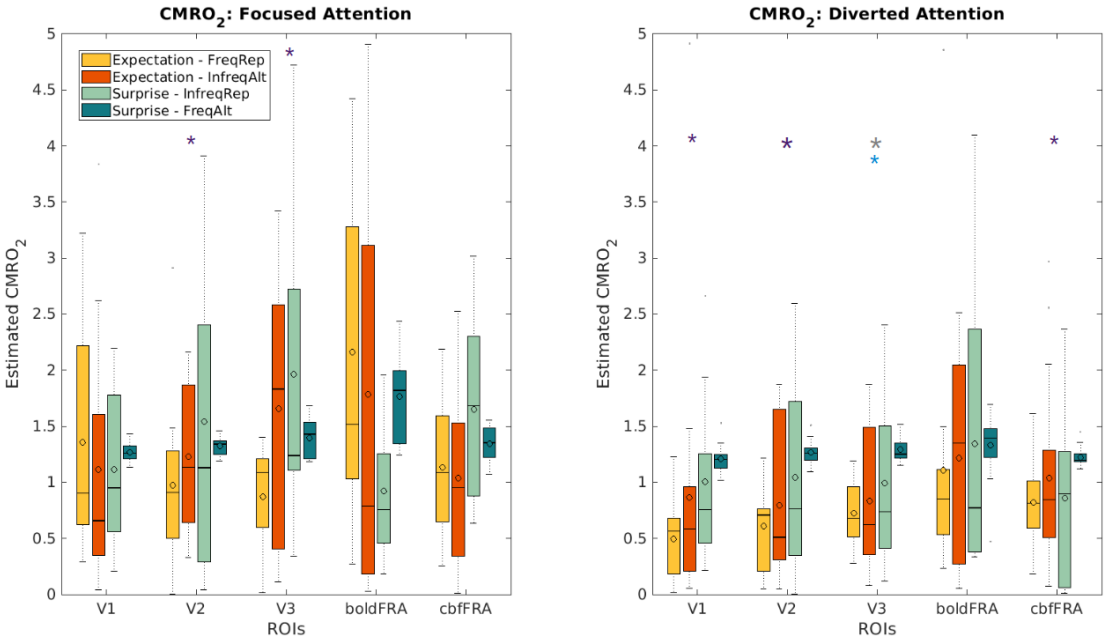

Figure 2.12: Box plot showing the estimated $CMRO_2$ and how this varies between the experiments (focused and diverted attention), and between the conditions and within each ROI. The left plot shows experiment 1 and the right plot experiment 2. Large asterisk indicates significance (p <0.05), and small asterisk indicates trends (p <0.1): blue reflect interaction effects, purple ES effects and grey RS effects. Axis are scaled to be comparable between experiments. The open dot in the middle of the box represents the condition mean, while the line represents median. The box encapsulates the condition response's interquartile range. Whiskers include the rest of the data's range, besides outliers which are represented as dots.

In experiment 2, n-coupling ratio shows a significant ES-RS interaction CBF defined FRA ($F(1, 13) = 3.7489, p = 0.002$).

2.4.9 $CMRO_2$ and n-coupling Post-hoc Pairwise Comparisons

The main experimental results have been covered in previous sections, this part elaborates on the pairwise comparisons post-hoc tests of the linear models (all results are presented in table 2.3 and (table 2.4)). These models were run on the estimated $CMRO_2$ and n-coupling ratio in response to varying levels of expectation. In experiment 1, attention was focused and in experiment 2, attention was diverted.

In experiment 1, pairwise comparisons of $CMRO_2$ data show that there a sig-

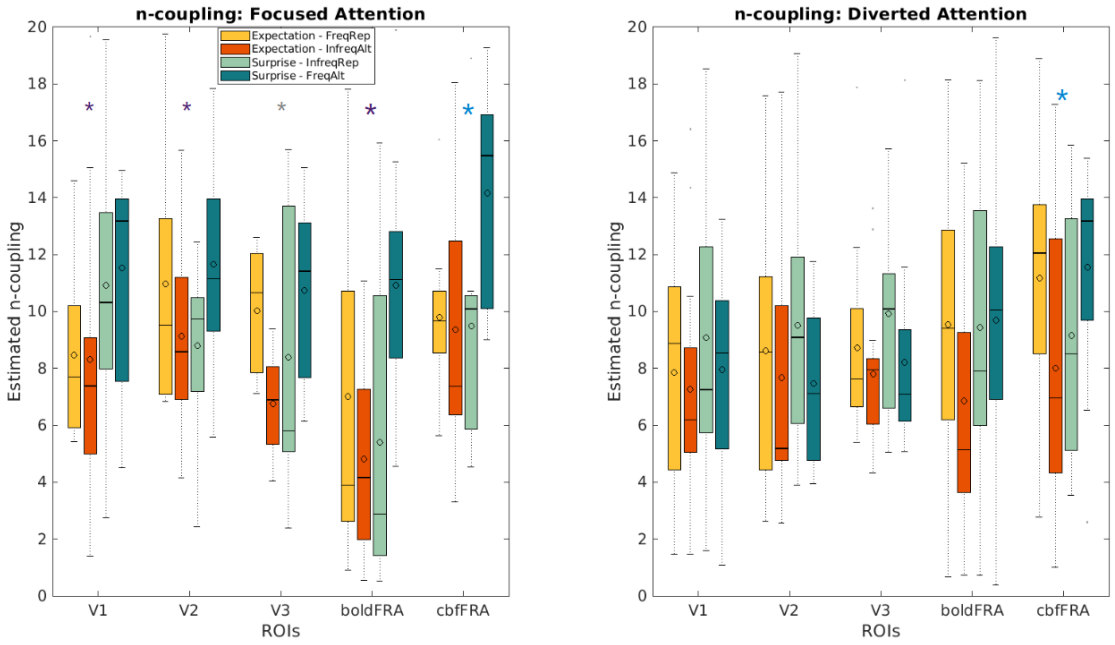

Figure 2.13: Box plot demonstrating the n-coupling ratio and how this varies with expectation within each ROI. Large asterisk indicates significance (p <0.05), and small asterisk indicates trends (p <0.1): blue reflect interaction effects, purple ES effects, and grey RS effects. The open dot in the middle of the box represents the condition mean, while the line represents median. The box encapsulates the condition response's interquartile range. Whiskers include the rest of the data's range, besides outliers which are represented as dots.

nificant difference between surprising and expected alternations in all but one ROI, namely BOLD defined FRA (FreqAlt>InfreqAlt). Moreover, all ROIs show a difference between surprising alternation and expected repetitions (FreqAlt>FreqRep) (see table 2.3 for further details).

In experiment 2, the comparisons show that there is a significant difference between surprising and expected alternations in V1 and CBF defined FRA (FreqAlt>InfreqAlt). Like in experiment 1, all ROIs show a difference between surprising alternation and expected repetitions (FreqAlt>FreqRep) (see table 2.3 for further details).

For the n-coupling data in experiment 1, the pairwise comparisons show that there is a significant difference between surprising and expected alternations in V1, V2, V3 and CBF defined FRA (FreqAlt>InfreqAlt). All ROIs show a difference between surprising alternation and expected repetitions (FreqAlt>FreqRep) (see table 2.4 for further details).

In experiment 2, the comparisons show significant differences between surprising and expected alternations in all ROIs (FreqAlt>InfreqAlt). Similarly, all ROIs show a difference between surprising alternation and expected repetitions (FreqAlt>FreqRep) (see table 2.4 for further details).

2.5 Discussion

These two experiments aimed to answer to what extent ES are attributable to haemodynamic changes and neural changes, and how neurovascular signals couple or decouple depending on expectation and attention. We find that BOLD effects do not replicate previous work (Summerfield et al., 2008) in either experiment 1 when attention is focused or experiment 2 when attention is diverted. Specifically, in experiment 1, there were only trends observed in two ROIs, namely trend towards expectation in V2 and a trend towards RS in BOLD defined FRA. Moreover, in experiment 2, there were interaction effects in V2 and V3. However, pairwise comparisons in experiment 1 indicate that there are significant differences between surprising alternations and expected repetitions, while there are no differences between surprising repetitions and expected alternations. This is somewhat in line with Larsson and Smith, 2011 as they observe larger differences between surprising alternations and expected repetitions compared to surprising repetitions and expected alternations. However, this pattern of pairwise differences remain in experiment 2, which is not in line with the findings of Larsson and Smith, 2011. Nevertheless, the fact that the effects do not emerge in the BOLD data may indicate a power issue (either in participants or trial-power, which is discussed further below) and/or a different analysis approach.

Interestingly, however, is that CBF signals reveal expectation effects in V1, V3, BOLD defined FRA and CBF defined FRA when attention is focused. Hence, the

CBF signal during focused attention are in line with previous literature better than the BOLD signal change. In experiment 2, CBF data demonstrate expectation effects in all ROIs. This is important as it suggests that BOLD and CBF signals do not necessarily map onto each other and that ES remain in CBF signals even if attention is diverted. This could mean that the ES as observed in human fMRI are in part hemodynamically driven (i.e. without accompanying neural activity). This falls in line with literature showing that hemodynamics can occur without neural activity (e.g. Lee et al., 2019; Sirotin & Das, 2009). Nonetheless, this interpretation needs to taken with caution as the BOLD data effects are not as predicted.

Moreover, when estimating neural activity in the form of $CMRO_2$ estimates, we observe a trend towards expectation effects in V1 and V2 when attention is focused, and when attention is diverted we observe a main effect of expectation in V2 and of RS in V3. Moreover, in experiment 2, there are trends towards significant expectation effects in V1 and CBF defined FRA. This shows that there are some ES present in neural activity both when attention is focused and diverted, although these effects are not strong.

Furthermore, this study also estimated the n-coupling ratio as recommended by Buxton et al., 2014. In the current study we find during focused attention that surprising events (particularly surprising alternations) generate larger n-coupling than the expected ones. This is statistically supported in BOLD defined FRA and CBF defined FRA, and there are trends towards significance in V1 and V3. This may suggest that more inhibitory activation is present during surprising event, especially the surprising alternation trials (Buxton et al., 2014). We also see during diverted attention that surprising events generate larger n-coupling ratio compared to expected conditions in CBF defined FRA. The fact that we see any significant differences in each experiment underscores that CBF and $CMRO_2$ couple differentially depending on expectation. Furthermore, the fact that we see some differing patterns emerging

between the two experiments suggest that attention further affects this coupling. This is important as it further underscores that the signals modulating the BOLD signal differentially couple depending on expectation, and attention. Although, it is important to not interpret the ROIs that do not show an effect in experiment 2.

Buxton et al., 2014 suggest that the n-coupling ratio could describe the inhibitory and excitatory dynamics occurring at a neural level. Specifically, they propose that as studies have shown that inhibitory activity lead to reduced $CMRO_2$ yet still recruits CBF, that a large n-coupling reflects a situation of high inhibitory activation. Moreover, that a small n-coupling may suggest that there is less inhibition occurring (Buxton et al., 2014). This would suggest, according to Buxton et al., 2014, that the surprising events are associated with higher inhibitory activity. However, in most of these cases, it can be seen that $CMRO_2$ estimates are in fact larger in comparison to the other trials and conditions. That is, when n-coupling is high, often so is $CMRO_2$. This may indicate that CBF is dis-proportionally modulated in these conditions as the ratio is still large. In other words, the current study does not observe evidence of increased inhibition in terms of $CMRO_2$ estimates, per se. However, this is not evidencing that inhibitory activity does not increase, as we have not simultaneously measured GABA. One could argue that there may be an increased inhibitory response to surprising conditions, and this is what is causing the huge modulation of CBF in comparison to $CMRO_2$. It is impossible to tell from this study alone.

2.5.1 Limitations and Future Directions

This study differed from previous studies (Larsson & Smith, 2011; Summerfield et al., 2008) in three important ways: 1) the number of trials were lower, 2) the analysis approach was different, and 3) the ITIs were longer. The first difference may have

resulted in the BOLD data not showing any clear effects and future studies should consider increasing the number of trials. In the current study we used a condition with equal probability of repetition (see the methodology section) to use as a control condition. However, as this had even less trial power it could not be used. This is why experiment 2 did not have this condition and we opted for one extra run of high and low repetition probability.

Alongside this, it is important to underscore the size of the sample. Experiment 1 and 2 had 12 and 15 data-sets, respectively. One could argue that the reason the first experiment did not replicate the BOLD results may be due to too few participants. Although Larsson and Smith, 2011 had fewer participants (N=8), the current experiment was additionally affected by lower trial-power as discussed above and longer ITIs as will be discussed. Therefore, future studies would benefit from increasing the sample size, particularly if they use the same parameters as the current study.

Moreover, due to the low sample size, care had to be taken when choosing inferential statistics. A small sample size decreases the power of an inferential test because it is more difficult to detect a true effect (especially if the predicted effect is small). Previous ES literature utilised t-tests and a two-by-two design (Summerfield et al., 2008) and paired t-tests (Larsson & Smith, 2011). Both of these approaches are parametric and rely on certain assumptions to be reliable. In both cases, it is important that the data is normally distributed. In the two-by-two design, it additionally necessitates that the groups have equal variance. This information is lacking from both studies, and therefore it can only be assumed that all assumptions for the parametric tests were upheld. However, given the low sample size in each (N=16 in Summerfield et al., 2008 and N=8 in Larsson and Smith, 2011), there is a risk that neither normality or equal variance assumptions were met (e.g. Kim & Park, 2019). This means that if there were violations to the tests' assumptions, then the results

may not be valid. Hence, the current study chose a non-parametric approach to remain robust against these violations, and this may be a reason for why we failed to replicate Larsson and Smith, 2011 and Summerfield et al., 2008. Moreover, both studies conducted more than one test, and there is no report of how or whether the results were adjusted to account for multiple comparisons. This becomes an issue as the rate of false positives increase with number of tests. Therefore, the current study made these multiple comparison corrections to avoid false positives, and this may also have contributed to the differing results from previous studies.

In addition to these issues, the longer ITIs could also have had consequences. The rationale for this was to make less assumptions about the additivity of CBF signals and the impulse response function shape. One consequence is that the experiment had to sacrifice trial number power, and another consequence may be that the additional ITI may weaken the effect of one trial following another. In previous studies where the trials followed each other in relatively close succession, the effect of the overall statistical context may have been stronger (potentially due to memory effects or ability for participants to pay attention). It may be useful to replicate this experiment with shorter ITI (but sacrifice fewer IRF shape assumptions) to assess if ITI length has a strong enough effect. In fact, this opens yet another opportunity for exploration – a fuller characterisation of the impulse response function of the BOLD signal during expectation manipulation and a characterisation of CBF signals under the same conditions. This can also be done for attentional differences.

2.5.1.1 Comment on Lack of ROI Overlap

A strange observation was that the face localiser-based signals from BOLD and CBF did not always spatially overlap. This was surprising to us as we predicted the CBF activity to be centred within the BOLD activity – based on literature comparing the specificity of the two signals. One reason for this may be that the signal types

are biased towards different physiological processes. For example, CBF is biased towards microvasculature (e.g. Huber et al., 2014) while the BOLD signal may be biased towards CBV changes in draining veins (Buxton, 2009). This may lead to the CBF signal capturing activity in the mid-cortical layers whilst the BOLD signal is drawn towards venous activity in the superficial layers as demonstrated by Goense et al., 2012.

In contrast, it may just mean that as the signals capture slightly different aspects of activation pattern and are slightly biased towards different physiological processes. Hence, the experiment has measured response patterns of two different signal types to an identical experimental paradigm. As mentioned in the previous section, some studies suggest that the BOLD and CBF signals may be well-suited for capturing different aspects of neuronal activity, and this may explain the lack of overlap in bold and CBF defined FRAs

2.5.1.2 Ecological Validity: Dynamic vs Static Stimuli

An issue that arise when studying fundamental visual processes is whether the observations carry ecological validity – are these observations in the lab translatable to the real world? The stimulus choice in the current studies differ from previous literature (except for Larsson & Smith, 2011). Specifically, that the face stimuli used here were better controlled for assessing RS and ES effects of face identity in contrast to face image. This is important as in the real world, humans process identities of faces that are dynamic and not static images of faces. Previous studies have used identical images of the same face and this means that there is a higher likelihood of inherited RS effects from lower visual areas, meaning that it does not measure how the brain processes face identity per se. This means that those experiments can draw conclusions about *image* effects and not effects relating to *identity*. This may be a reason for the current study not observing as strong effects as previous work,

despite being better controlled. Summerfield et al., 2008 replicated their own study while varying the image sizes and found similar results. Specifically, they reduced the adapter or probe image by 15% in half of the trials. One could however argue that although they varied the size of the face image, the image is still identical just slightly smaller, and therefore there is still a chance of inherited RS. Therefore, the result cannot be concluded to fully pertain to face identity.

Nevertheless, despite this control that the current study exerts, it does not circumvent the fact that faces in real world move and change constantly. Therefore, to increase the field's ecological validity an important advance would be to use dynamic faces. Studies have shown that static and dynamic faces are processed in differently. For example, one study shows that FFA and OFA respond similarly to dynamic and static faces, while posterior superior temporal sulcus (STS) responded a lot more to dynamic compared to static faces, while anterior STS responded only to dynamic faces (Pitcher, Dilks, Saxe, Triantafyllou, & Kanwisher, 2011). Moreover, by disrupting OFA with TMS when presenting static and dynamic faces led to less responses in ipsilateral FFA to both types of stimuli. It also led to reductions in activity in the ipsilateral posterior STS but only for static images (Pitcher, Duchaine, & Walsh, 2014). When the authors disrupted STS instead, this led to no response change to static faces while responses to dynamic faces reduced. In addition, Fox, Iaria, and Barton, 2009 demonstrate that dynamic face stimuli generate more robust responses compared to static faces. This underscores how these stimuli could be a better choice when investigating processes such as expectation as these stimuli may better capture how neural processing works in the real world.

Considering this, to understand face identity processing, one could design an experiment that shows short video clips of faces that are neutral but may be filmed from different angles and zooms and lighting. Specifically, the video clips can match in identity or not whilst the low-level features are varied. If FFA, STS, and OFA

are tuned for faces and face identities then this experimental set-up should confirm this – but with increased validity. Perhaps this would be applicable for studies investigating other high-level stimuli also – such as showing objects or scenes that are dynamic. This paradigm could also be used to understand expectation effects in that we could manipulate the statistical context in which the face identities are repeated or not. It would be interesting to do this set-up for objects and/or scenes and see if ES may be more detectable when stimuli resemble the external world more.

2.5.2 Summary

In summary, these two presented studies suggest that ES may be more haemodynamically driven than previously thought, as expectation effects are consistently demonstrated in CBF signals independent of attentional manipulation. This suggests that the BOLD signal alone does not adequately capture signal changes in this type of paradigm. Additionally, the fact that we observe coupling differences (in terms of n-coupling) is evidence that NVC varies with expectation, and attention may modulate this. Moreover, the differential response pattern between BOLD and CBF signals may further support studies showing that CBF signals are more sensitive to sustained changes such as expectation and learning.

These findings are important as they highlight the issue with using only the BOLD signal when studying fine-grained brain responses, such as expectation and attention. Especially as we find that ES may be in part hemodynamic it underscores the importance of being cautious when drawing conclusions about brain dynamics and mechanisms in experiments with similar design and protocol.

Table 2.1: BOLD and CBF signal pairwise comparisons in experiment 1 when attention was focused. This table contains the results from post-hoc pairwise comparisons of the expectation experiments. The first part of the table contains the results from the BOLD data, and the second part the CBF data. In the columns are the t-statistic and p-values from the pairwise condition comparisons, per ROI. The comparisons are grouped into RS and ES comparisons. RS refers to when the comparison is between repetitions and alternations. ES refers to when comparisons are between frequent and infrequent probability of repetitions. All comparisons are FDR corrected.

BOLD data

	RS				ES			
ROI	FreqAlt-FreqRep		InfreqRep-InfreqAlt		InfreqRep-FreqRep		FreqAlt-InfreqAlt	
	t_{11}	p-val	t_{11}	p-val	t_{11}	p-val	t_{11}	p-val
V1	14.326	<0.001	-14.571	1	-14.215	1	14.46	<0.001
V2	17.29	<0.001	-15.77	1	-15.39	1	13.87	<0.001
V3	22.7	<0.001	-20.85	1	-22.07	1	22.211	<0.001
BOLD FRA	31.55	<0.001	-29.18	1	-32.8	1	30.45	<0.001
CBF FRA	22.71	<0.001	-22.457	1	-23.8	1	23.547	<0.001

CBF data

	RS				ES			
ROI	FreqAlt-FreqRep		InfreqRep-InfreqAlt		InfreqRep-FreqRep		FreqAlt-InfreqAlt	
	t_{11}	p-val	t_{11}	p-val	t_{11}	p-val	t_{11}	p-val
V1	-9.82	1	-1.867	0.93	-3.31	0.99	6.14	<0.001
V2	3.38	<0.001	-7.87	1	-9.82	1	1.8	0.081
V3	11.34	<0.001	-10.26	1	-12.15	1	6.35	<0.001
BOLD FRA	13.17	<0.001	-15.44	1	-17.65	1	9.23	<0.001
CBF FRA	18.21	<0.001	10	<0.001	-6.35	1	14.9	<0.001

Table 2.2: BOLD and CBF signal pairwise comparisons in experiment 2 when attention was diverted. This table contains the results from post-hoc pairwise comparisons of the expectation experiments. The first part of the table contains the results from the BOLD data, and the second part the CBF data. In the columns are the t-statistic and p-values from the pairwise condition comparisons, per ROI. The comparisons are grouped into RS and ES comparisons. RS refers to when the comparison is between repetitions and alternations. ES refers to when comparisons are between frequent and infrequent probability of repetitions. All comparisons are FDR corrected.

BOLD data

	RS				ES			
ROI	FreqAlt-FreqRep		InfreqRep-InfreqAlt		InfreqRep-FreqRep		FreqAlt-InfreqAlt	
	t_{13}	p-val	t_{13}	p-val	t_{13}	p-val	t_{13}	p-val
V1	19.2	<0.001	-17.88	1	-18.9	1	17.53	<0.001
V2	20.96	<0.001	-19.3	1	-22.2	1	20.6	<0.001
V3	24.76	<0.001	-22.3	1	-26.78	1	24.8	<0.001
BOLD FRA	19.34	<0.001	-18.3	1	-19.89	1	18.8	<0.001
CBF FRA	12.447	<0.001	-11.41	1	-11.66	1	10.6	<0.001

CBF data

	RS				ES			
ROI	FreqAlt-FreqRep		InfreqRep-InfreqAlt		InfreqRep-FreqRep		FreqAlt-InfreqAlt	
	t_{13}	p-val	t_{13}	p-val	t_{13}	p-val	t_{13}	p-val
V1	13.2	<0.001	-8.77	1	-10.75	1	6.33	<0.001
V2	11.6	<0.001	-8.2	1	-9.97	1	6.57	<0.001
V3	10.79	<0.001	-8.37	1	-8.23	1	5.81	<0.001
BOLD FRA	8.28	<0.001	-6.54	1	-5.92	1	4.18	<0.001
CBF FRA	6.78	<0.001	-5.92	1	-4.54	1	3.68	0.002

Table 2.3: Pairwise comparisons of $CMRO_2$ estimates. In the columns are the t-statistic and p-values from the pairwise condition comparisons, per ROI. The comparisons are grouped into RS and ES comparisons. RS refers to when the comparison is between repetitions and alternations. ES refers to when comparisons are between frequent and infrequent probability of repetitions. All comparisons are FDR corrected.

Experiment 1: Focused Attention

	RS				ES			
ROI	FreqAlt-FreqRep		InfreqRep-InfreqAlt		InfreqRep-FreqRep		FreqAlt-InfreqAlt	
	t_{11}	p-val	t_{11}	p-val	t_{11}	p-val	t_{11}	p-val
V1	4.44	0.0013	-4	0.99	-4.66	0.99	4.23	0.007
V2	3.93	0.0013	-3.13	0.99	-1.678	0.99	0.88	0.33
V3	3.39	0.005	-0.91	0.99	-2.2	0.99	-0.28	0.59
BOLD FRA	3.1	0.005	-3.4	0.99	-1.3	0.99	1.63	0.18
CBF FRA	2.678	0.02	-1.78	0.99	-3.78	0.99	2.88	0.0.31

Experiment 2: Diverted Attention

	RS				ES			
ROI	FreqAlt-FreqRep		InfreqRep-InfreqAlt		InfreqRep-FreqRep		FreqAlt-InfreqAlt	
	t_{13}	p-val	t_{13}	p-val	t_{13}	p-val	t_{13}	p-val
V1	6.381	<0.001	-5.123	1	-4.8	1	3.58	<0.001
V2	9.46	<0.001	-5.79	1	-8.28	1	4.61	<0.001
V3	3.97	<0.001	-3.55	1	-8.78	1	5.4	<0.001
BOLD FRA	2.61	0.023	-1.47	1	-2.16	1	1.02	0.25
CBF FRA	3.75	<0.001	-3.13	1	-1.71	1	1.1	0.25

Table 2.4: Pairwise comparisons of n-coupling estimates. In the columns are the t-statistic and p-values from the pairwise condition comparisons, per ROI. The comparisons are grouped into RS and ES comparisons. RS refers to when the comparison is between repetitions and alternations. ES refers to when comparisons are between frequent and infrequent probability of repetitions. All comparisons are FDR corrected.

Experiment 1: Focused Attention

	RS				ES			
ROI	FreqAlt-FreqRep		InfreqRep-InfreqAlt		InfreqRep-FreqRep		FreqAlt-InfreqAlt	
	t_{11}	p-val	t_{11}	p-val	t_{11}	p-val	t_{11}	p-val
V1	6.99	<0.001	-4.64	0.99	-6.5	1	4.14	0.005
V2	6.4	<0.001	-3.9	0.99	-5.89	1	3.38	0.007
V3	3.78	0.003	-2.1	0.99	-5.26	1	3.56	0.005
BOLD FRA	6.9	<0.001	-3.34	0.99	-5.62	1	2.05	0.055
CBF FRA	5.19	<0.001	-3.1	0.99	-6.1	1	4	0.002

Experiment 2: Diverted Attention

	RS				ES			
ROI	FreqAlt-FreqRep		InfreqRep-InfreqAlt		InfreqRep-FreqRep		FreqAlt-InfreqAlt	
	t_{13}	p-val	t_{13}	p-val	t_{13}	p-val	t_{13}	p-val
V1	8.79	<0.001	-9.37	1	-7.59	1	8.17	<0.001
V2	9.89	<0.001	-10.8	1	-8.42	1	9.37	<0.001
V3	11.8	<0.001	-12.24	1	-9.85	1	10.29	<0.001
BOLD FRA	8.32	<0.001	-7.6	1	-7.5	1	6.76	<0.001
CBF FRA	9.69	<0.001	-9.87	1	-10.59	1	10.77	<0.001

Chapter 3

Chapter Three: The Relationship Between GABA, CBF, and Positive and Negative BOLD

3.1 Overview

In this experiment and chapter, I explored the relationship between different neuroimaging signals that are used for understanding neural dynamics: GABA, CBF, and positive and negative BOLD. The literature is mixed when it comes to characterising how positive and negative BOLD responses associate with CBF and GABA. To our knowledge, no study has simultaneously measured BOLD, CBF and GABA, and therefore, we set out to bridge that gap. After estimating GABA concentrations using spectroscopic imaging, we used BOLD responses to meridian mapping stimuli (checkerboards in bowtie formations presented vertically and horizontally) to define negatively and positively responding voxels. From these voxels we extracted CBF responses. We found a positive correlation between BOLD and CBF in both posi-

tively and negatively responding voxels in V1, and in V3 for positively responding voxels. Furthermore, we found a trend towards a significant positive relationship between n-coupling and GABA, suggesting that CBF and $CMRO_2$ differentially couple as GABA levels vary. In addition to this, we found significant differences between $CMRO_2$ levels in positively and negatively responding voxels.

3.2 Introduction

In order to draw appropriate conclusions about fMRI research it is important that we understand how the underlying neural interactions and dynamics work together. Moreover, how neural activity, neurotransmission, and hemodynamics interact to elicit the BOLD signal is not fully understood. The current thesis has so far investigated how NVC couples or decouples depending on expectation and attention. Another fundamental question is how NVC may vary depending on whether the BOLD response is positive or negative, and the local GABA concentration.

This is important as GABA may indicate levels of inhibition in the measured region. GABA concentrations and the BOLD signal have been demonstrated to be negatively associated (Donahue et al., 2010; Muthukumaraswamy, Edden, Jones, Swettenham, & Singh, 2009; Muthukumaraswamy et al., 2012), meaning that the magnitude of the BOLD signal is less when GABA is high. Importantly, increased GABA levels (from inhibitory GABA receptors) correlate with reduced BOLD magnitude in mice during somatosensory stimulation (Chen & Zhou, 2014). This is, however, distinct from GABA and *negative* BOLD being associated. Nevertheless, GABA concentrations have been shown to negatively correlate with the magnitude of negative BOLD responses in the cingulate cortex (Hu, Chen, Gu, & Yang, 2013; Northoff et al., 2007). This is in line with predictions that increased inhibition results in more oxygen metabolism and as such yields a smaller positive BOLD

response or a strengthened negative BOLD response (Logothetis & Wandell, 2004).

Inhibitory activity will, in general, lead to a net decrease in energy consumption because inhibition of excitatory activity will decrease the overall output (e.g. Attwell & Laughlin, 2001). However, it is important to underscore that increased inhibition is still an active process and will generate higher $CMRO_2$ consumption compared to no changes in inhibition as these processes also require energy. Although, it has been shown that active inhibition is related to local decreases in $CMRO_2$ and CBF (Shmuel et al., 2002). Moreover, this active inhibition has been linked with negative BOLD signals (Shmuel et al., 2002) and could be a result of a change in CBF and $CMRO_2$ modulation (e.g. Mullinger, Mayhew, Bagshaw, Bowtell, & Francis, 2014). Specifically, if $CMRO_2$ change increases relative to CBF or if CBF changes decrease relative to $CMRO_2$, then this could generate a negative BOLD response. Particularly, if a region has a low capillary density and as such has a smaller CBF capacity (Harrison et al., 2002).

The relationship between negative BOLD and CBF is clearer as evidence is corroborating that negative BOLD associated with CBF decreases (Goense et al., 2012; Mullinger et al., 2014). However, the relationship between GABA and CBF is unclear and findings are mixed. Some studies find that GABA and CBF show a positive relationship (Donahue et al., 2014; Muthukumaraswamy et al., 2009; Muthukumaraswamy et al., 2012) suggesting that more GABA yields greater inhibition and as such a greater need for oxygenated blood. However, some studies fail to replicate this (Muthukumaraswamy et al., 2012), and others have found that GABA reduces response amplitudes in CBF and $CMRO_2$, at least in the cerebellum (Caesar, Offenhauser, & Lauritzen, 2008). Moreover, Shmuel et al., 2002 show that decreases in $CMRO_2$, putatively from increased inhibition, is associated with decreases in CBF. Hence, it is important to simultaneously assess the relationship between GABA, CBF, and BOLD responses.

To date, no study has directly investigated the relationship between local GABA concentrations, CBF, and positive and negative BOLD. This study aims to bridge that gap. We induce positive and negative BOLD responses by using meridian mapping through flickering checkerboards in bowtie formation. These are presented in blocks of vertical and horizontal orientations. This way the study can assess positive BOLD changes in the stimulated retinotopic regions, and negative BOLD in cortical regions responding to adjacent unstimulated parts of the visual field, in the early visual areas.

We predicted that CBF would correlate positively with positive BOLD because the impulse response function of BOLD depends on disproportionately increasing oxygenated blood recruited through increased CBF. CBF and negative BOLD would have a less positive, or negative, correlation because increased inhibition generates more $CMRO_2$ which would reduce the BOLD signal. Hence, we predicted that higher GABA concentration would be associated with stronger negative BOLD responses. Furthermore, the relationship between GABA and positive BOLD responses was predicted to be negative because higher GABA concentrations suggest more inhibition and as such $CMRO_2$ activity may produce a weakened BOLD response.

This study found a positive correlation between BOLD and CBF for positive and negative BOLD responses in V1, and in V3 for positively responding voxels, as predicted. Moreover, we observed a negative association between GABA and positive BOLD responses in V1, however this was not statistically supported. Furthermore, we found a trend towards a significant positive relationship between n-coupling and GABA, suggesting that CBF and $CMRO_2$ couple differentially with varying GABA levels. Additionally, we found that positively responding voxels use significantly more energy (in terms of $CMRO_2$) compared to negatively responding voxels, supporting literature showing that excitatory activation uses more energy than inhibitory activation (e.g. Attwell & Laughlin, 2001).

3.3 Methodology

3.3.1 Participants

Fourteen participants (F=10; mean age=26.3 years old) with normal or corrected-to-normal vision partook. The procedures were in accordance with the Psychology Department Ethics Committee at Royal Holloway University of London, and the participants' written informed consent was obtained. Two participants' data-sets were discarded due to data corruption, and one participant's GABA estimate was discarded for the same reason.

3.3.2 Stimuli and Design

Stimuli consisted of two horizontal or vertical checkerboard wedges (subtending 22.5° visual angle), radially arranged in opposite visual quadrants, forming a bow-tie shape (see figure 3.1). Each wedge consisted of two radial strands of black and white checks moving in opposite directions (either outwards or inwards) along the eccentricity dimension, with the direction of movement changing randomly. During each experimental run, the horizontal and vertical bowtie stimuli alternated as follows: a blank screen was shown for 32s, followed by a bowtie stimulus at one orientation for 32s, followed by a 32 second baseline, after which the other orientation was displayed for 32 seconds. This cycle was repeated twice during each run. Each participant completed two runs, with the initial stimulus orientation counter-balanced between runs. The initial stimulus orientation was counter-balanced across participants.

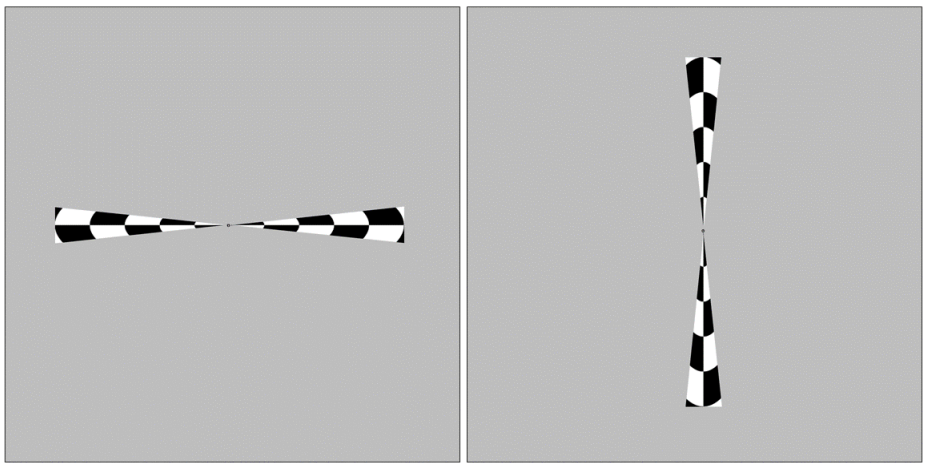

Figure 3.1: Illustration of bowtie stimulus in a horizontal and vertical orientation.

3.3.3 MRI acquisition

3.3.3.1 Anatomical Acquisition

MRI and spectroscopy (MRS) data were collected using a Siemens 3T TRIO system (Erlangen, Germany; 32-channel head-coil). A whole-brain anatomical scan was obtained for each participant for alignment and visualisation of data (MPRAGE sequence; 1mm isotropic; 160 slices; TR: 1830ms; TE: 3.03ms; TI: 1100ms; FA: 11°; GRAPPA acceleration of 2; echo space: 8.9ms; 4:52 minutes).

Additionally, a T2 weighted anatomical was acquired to assist with MRS voxel placement (TR: 3490ms; TE: 93ms; 20 slices; GRAPPA acceleration of 2; echo space: 9.3ms). It was collected in three planes (sagittal, transverse, and coronal, with in-place resolution of 0.8x0.8x3mm).

3.3.3.2 Functional Acquisition

Functional data were obtained using a standard Siemens pulsed ASL sequence (PICORE; 3mm isotropic; 13 slices; axial acquisition; TR: 2000ms; TE: 15ms; IT1:

700ms; IT2: 1401.6ms; Saturation stop time: 1200ms; FA: 90°; GRAPPA acceleration factor of 2; gap: 22.1mm; echo space: 0.53ms). 144 volumes per run were acquired in each of the two runs.

To acquire CBF estimates, the pulsed ASL sequence alternates tagged and control volumes in an interleaved fashion. CBF responses were estimated by subtracting the control from the tag volume, while BOLD responses were obtained by averaging the tag and control volumes. The procedure was the same as in the previous chapter.

3.3.3.3 Spectroscopy

To estimate GABA levels, we used the methods of Edden, Puts, Harris, Barker, and Evans, 2014, as described in Cook, Hammett, and Larsson, 2016. With the aid of the T2-weighted anatomical scans the MRS voxel was placed over the calcarine sulcus encompassing primary visual cortex, aiming to avoid as much CSF as possible (see figure 3.2). MRS data were obtained using the MEGAPRESS sequence (voxel: 30x35x25mm; TR: 2000ms; TE: 68ms; FA: 90 degrees). To obtain GABA estimates and separate its signal from the spectra, an editing pulse of 1.9ppm was applied. For comparison, a reference scan without an editing pulse was acquired.

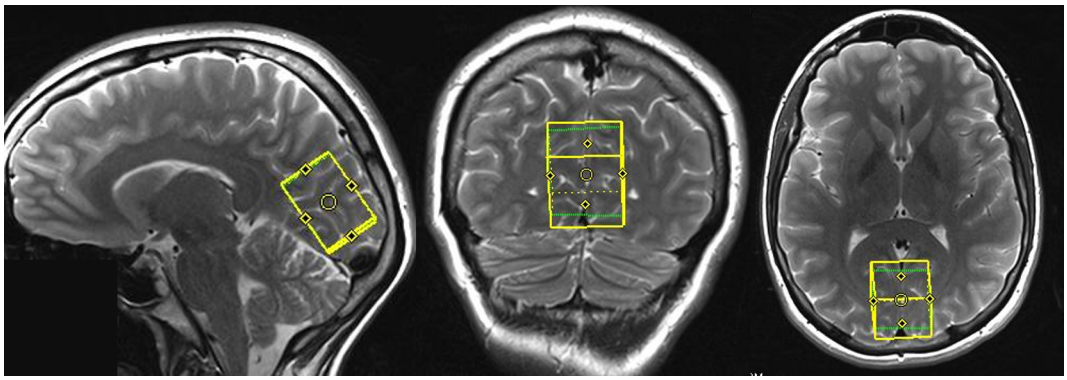

Figure 3.2: Figure showing an example of how and where the spectroscopy voxel were positioned in the occiputal region.

For each participant we acquired two GABA and corresponding reference scans,

where GABA was always the first scan. Acquisition took 30 minutes.

3.3.4 Pre-processing

Pre-processing of MRI data (motion correction, slice time correction, between run alignment) was carried out as described for previous chapters.

3.3.5 GABA Estimation

The Gannet toolbox (Edden et al., 2014) was used to analyse the MRS data. Estimates were obtained by taking the pairwise differences between the scan with the editing pulse and the subsequent reference scan. GABA and creatine signals overlap, which is why the 1.9ppm editing pulse was needed to separate GABA from creatine at 3.0ppm. The toolbox offers two GABA estimates – one relative to water and one relative to creatine. Following Cook et al., 2016 we used the estimate of GABA relative to water, which has higher SNR and is not confounded by individual variability in creatine concentration (Puts & Edden, 2012). The two GABA concentration estimates acquired in the same session were averaged, so that there was one mean estimate per participant.

3.3.6 Analysis Approach

ROIs were estimated from retinotopic mapping that were acquired from other sessions (previous chapters). To find the voxels responding to the experimental stimuli, we first performed a voxel-wise least-squares regression analysis (as described in the previous chapter) within each ROI. We created two response models – one each for responding to vertical or horizontal bowties. The voxels were selected based on how

well they responded to the bowtie stimuli. Specifically, a voxel's BOLD data were classified as positive or negative according to the following criteria: if the first 16 seconds (standard length of hemodynamic response) of a voxel's timecourse had an area under the curve that was positive, then it was classified as a positively responding voxel, and if the area under the curve was negative, then it was classified as a negatively responding voxel. Each voxel's percent signal change response mean was used for the analysis.

As this was done for both positively and negatively responding voxels it yielded two separate datasets. We studied the BOLD and CBF responses of these two datasets. To assess the relationship between BOLD and CBF in positively and negatively responding voxels within each ROI, we calculated the mean response per voxel and then correlated the BOLD and CBF signal change. To get an approximation of NVC we also used the BOLD signal change to predict CBF signal change using regression analyses. Specifically, we ran six regression models: one for positively responding voxels and one for negatively responding ones, and we did this for each of the three ROIs.

All results (correlation and difference measures) underwent False Discovery Rate (FDR) adjustments within data-sets (positively and negatively responding voxels) to safe-guard against false positives due to multiple comparisons.

All analyses were done in MATLAB 2020a (MATLAB, 2020).

3.3.7 $CMRO_2$ Estimation

We chose to use the same $CMRO_2$ estimation model as in previous experimental chapters since it is optimised for adaptation, or prolonged exposure, paradigms. Although, one could argue that the flickering checkerboard stimuli are stimulus types

that are presented to generate the highest possible neural activation. Nonetheless, considering the design of the current experiment is a blocked design with 32 second presentation of checkerboards, it seems reasonable to employ a $CMRO_2$ estimation model that is designed to best work for designs with prolonged exposure of a stimulus.

$$\Delta b = M(1 - f^{\alpha-\beta} r^{\beta}) \tag{3.1}$$

As per the previous chapter, Δb, f, and r refer to normalised BOLD, CBF, and $CMRO_2$ signal change, respectively (Griffeth & Buxton, 2011; Moradi & Buxton, 2013). Alpha (α) and beta (β) are the empirically estimated constants and are equal to 0.16 and 1, respectively (Moradi & Buxton, 2013). The only notable difference lies in what condition was deemed equivalent to the "high contrast" condition used by Moradi and Buxton, 2013: in their study the authors used the prolonged high contrast checkerboard stimulus presentation as their high contrast condition. This is similar to the current experiment's presentation of bowties – therefore the chosen equivalent condition is the average BOLD and CBF responses to the bowties, or in other words, the positively responding voxels. This was done per participant and ROI.

In other words, the values with a HC subscript in equation 3.2 refer to the average response to the bowtie checkerboards.

$$M = \frac{(b_{HC} - 1)}{(1 - f_{HC}^{\alpha-\beta}\ r_{HC}^{\beta})} \tag{3.2}$$

The scaling parameter (M) is then used to approximate $CMRO_2$, or r, as per equation 3.3 below.

$$r = f^{0.84}(1 - \frac{(b-1)}{M}) \tag{3.3}$$

In equation 3.2, the denominator contains a high contrast $CMRO_2$ response, and this was estimated using equation 3.4 below. This equation has an n_{HC} coupling ratio in its denominator and it is kept at 2.5 as in the previous chapter (Moradi & Buxton, 2013).

$$r_{HC} = 1 + \frac{(f_{HC} - 1)}{n_{HC}} \tag{3.4}$$

3.3.8 NVC Estimates: Slopes and n-coupling

To gain an understanding of CBF and BOLD coupling, we estimated an NVC slope per participant. This was done by fitting a regression line between BOLD and CBF responses for each participant. This slope is thought to reflect the coupling of BOLD and CBF. Then we correlate all participants' NVC slopes with their GABA data.

To get insights into whether CBF and $CMRO_2$ are differentially modulated depending on whether the BOLD signal response is positive or negative, we estimated the n-coupling ratio. This is done the same way as in the previous chapter, namely each participants' mean CBF score is divided by each participants' mean $CMRO_2$ score per ROI. This was done for both positively and negatively responding voxels.

3.4 Results

3.4.1 BOLD and CBF Relationships

Firstly, all the voxels from BOLD and CBF data are plotted to descriptively assess whether the voxel extraction was successful and whether the data seem reasonable. As can be seen in figure 3.3, each subplot represent an ROI and within the ROIs the

best responding voxels are plotted from both positively and negatively responding voxels. The colours correspond to the variance explained (R^2) of each voxel, where yellow means high variance explained and blue low variance explained. At first glance, it looks as though BOLD and CBF data relate well, where more strongly responding positive or negative voxels tend to do so within both data-sets. This pattern is further supported by the higher variance explained values – although this is more apparent in the positively responding voxels compared to the negatively responding voxels.

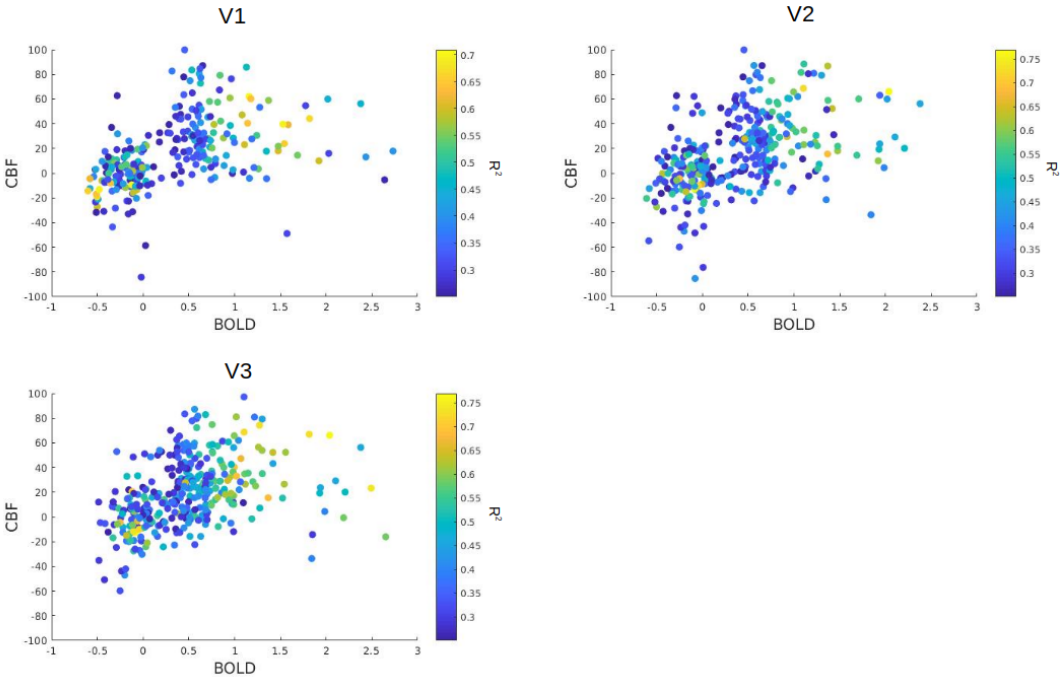

Figure 3.3: Scatter plot demonstrating the relationship between BOLD and CBF signal change across voxels that had a variance explained of above 25% in each ROI. The x-axis show BOLD percent signal change and the y-axis CBF percent signal change. Voxels are colour-coded based on their R^2 value, and the colour-bar to the right show the corresponding variance explained to colour.

Given that the data look reasonable, we continue to assess the relationships between BOLD and CBF data for positively and negatively responding voxels in each ROI.

When separately plotting CBF and BOLD data from positively responding voxels we observe a slight positive relationship in V1 and V3 and this relationship is

confirmed through a correlation analysis (see figure 3.4, upper panels). We pooled all voxels from participants so as to observe the voxel variability. In the correlation analysis we observe that there is a weak positive relationship between BOLD and CBF signal change in V1 ($N = 686, r = 0.115, p = 0.02$, where N equals to total number of voxels in that ROI) and V3 ($N = 708, r = 0.186, p < 0.001$). There is no significant association in V2 ($N = 694, r = 0.0418, p = 0.63$). This suggests that there is some relationship between BOLD and CBF signals amongst positively responding voxels in some early visual areas. In other words, in V1 and V3, the more positive the BOLD response, the more positive the CBF response.

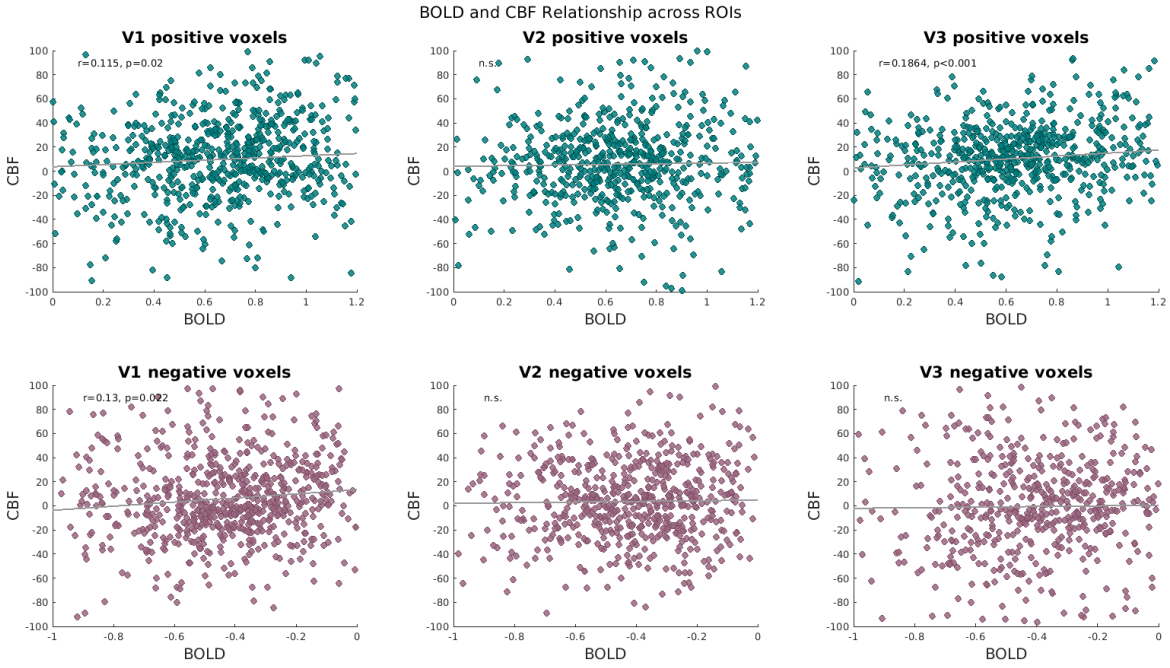

Figure 3.4: Scatter plot demonstrating the relationship between BOLD and CBF signal change in positively responding voxels (upper panels) and negatively responding voxels (lower panels), across ROIs (left panels reflecting V1, middle panels V2, and right most panels V3). Data points reflect voxel mean and the voxels are pooled from all participants. The line of best fit is a fitted least square line. Note that the axes are scaled in order to allow comparisons across data-sets and ROIs, but all voxels are included in the correlation analysis.

For negatively responding voxels we observe a positive relationship between BOLD and CBF signal change in V1 (see figure 3.4, lower panels). Correlation analyses reveal that there is a weak positive relationship between BOLD and CBF

signal change in V1 ($N = 761, r = 0.13, p = 0.02$). No relationships were found in and V2 ($N = 667, r = 0.02, p = 0.79$) and V3 ($N = 735, r = 0.019, p = 0.79$).

Since the large number of voxels included in the correlation analysis could lead to meaningless significant results, Bayes factors were calculated to assess likelihood of significance. If a Bayes factor exceeds 100 it suggests that there is overwhelming evidence for the alternative hypothesis - in this case, an existence of a relationship. Bayes factor of between 3 and 10 indicates moderate evidence for the alternative hypothesis. Moreover, a factor of between 0.01 and 0.333 suggests very strong evidence for the null hypothesis - in this case, no relationship between the data. Calculated factors for positively responding voxels were 2.3×10^{10} in V1, 730 in V2, and 9.3×10^{15} in V3. This suggests that there is overwhelming evidence for a significant correlation in all ROIs. For negatively responding voxels, the factors were 3.7×10^{5} for V1, 7.3 for V2, and 0.02 for V3. Thus, there is overwhelming evidence for a significant correlation in V1, moderate evidence of a correlation in V2, and very strong evidence for no correlation in V3.

These results corroborate previous literature finding evidence for a relationship between BOLD and CBF during positive and negative responses, hence we can go ahead with analysing the data further. Figure (3.5) shows the relationship between the mean percent signal change responses of the BOLD and CBF data. These analyses revealed no significant associations, which may be explained by a reduction in power as a result of the averaging process.

3.4.2 GABA and BOLD Relationships

In order to answer the question whether positive and negative BOLD vary with GABA concentrations we correlated each participant's mean positive BOLD response, and the negative BOLD response per ROI with their average GABA con-

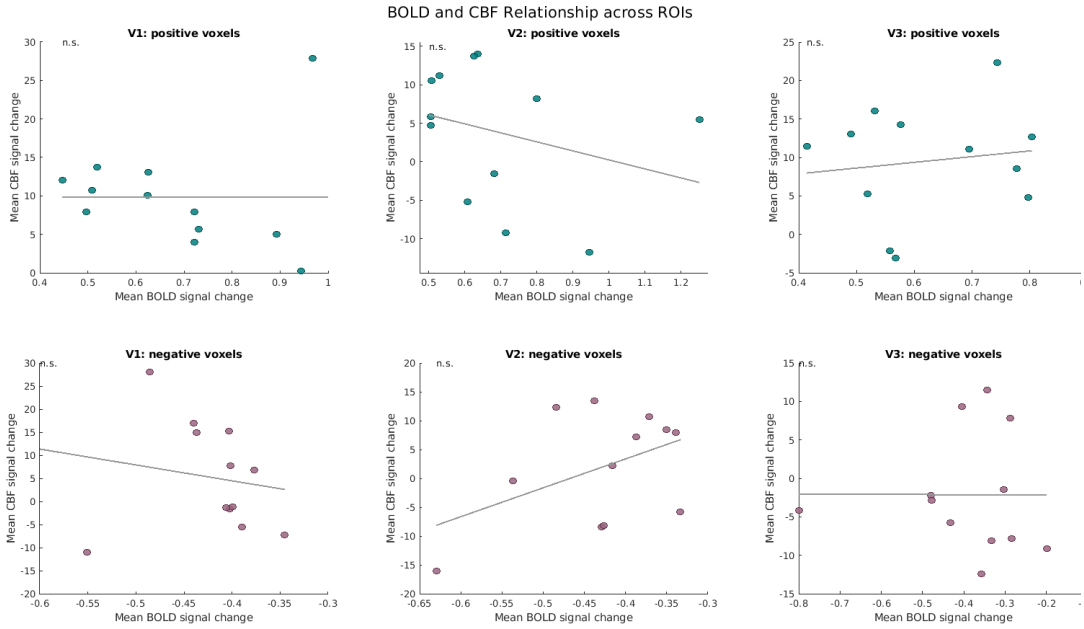

Figure 3.5: Scatter plot with fitted least square line showing the association between positive (upper panels) and negative (lower panels) BOLD and CBF responses, per ROI (left panels reflecting V1, middle reflecting V2, and right most panel reflecting V3). This analysis showed no significant association between the signals in any ROI for either positive responses (V1 (-0.0015, p=1), V2 (r=-0.3, p=68), V3 (r=0.14, p=0.79)) or negative responses (V1 (r=-0.16, p=0.79), V2 (r=0.45, p=0.62) or V3 (r=-0.002, p=0.99)).

centration. There were no significant correlations between GABA and BOLD in either positively or negatively responding voxels.

3.4.3 GABA and CBF Relationships

Thereafter, to answer the question whether positive and negative CBF vary with GABA concentrations we correlated each participant's mean positive CBF response, and the negative CBF response per ROI with their average GABA concentration. There were no associations found between GABA and positive and negative CBF responses (see figure 3.7).

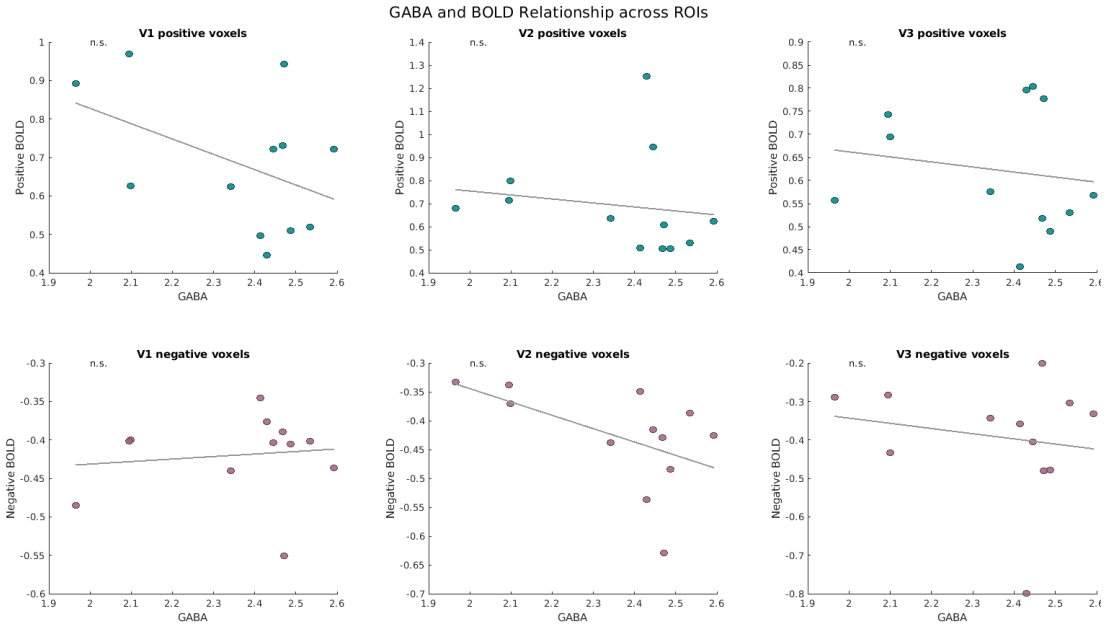

Figure 3.6: Scatter plot with fitted least square line showing the association between positive (upper panels) and negative (lower panels) BOLD responses and GABA, per ROI (left panels reflecting V1, middle reflecting V2, and right most panel reflecting V3). No associations were found between positively responding voxels in any ROI (V1 (r=-0.44, p=0.58), V2 (r=-0.156, p=0.79), V3(r=-0.16, p=0.79)). The same held for negatively responding voxels (V1 (r=0.12, p=0.79), V2 (r=-0.526, p=0.55) and V3 (r=-0.17, p=0.79)).

3.4.4 GABA and $CMRO_2$ Relationships

When correlating GABA concentration and $CMRO_2$ estimates there is no relationship between the data in either positively nor negatively responding voxels (see figure 3.8).

3.4.5 Positive and Negative $CMRO_2$ Differences

Figure 3.8 further indicates that positively responding voxels seem to have an overall higher $CMRO_2$ value compared to negatively responding voxels, in V1 and V3. This indicates that more energy is required to produce a positive BOLD response compared to a negative one. To assess this difference and avoid the problem of low sample sizes, all voxels per ROI were used instead of the averaged response per

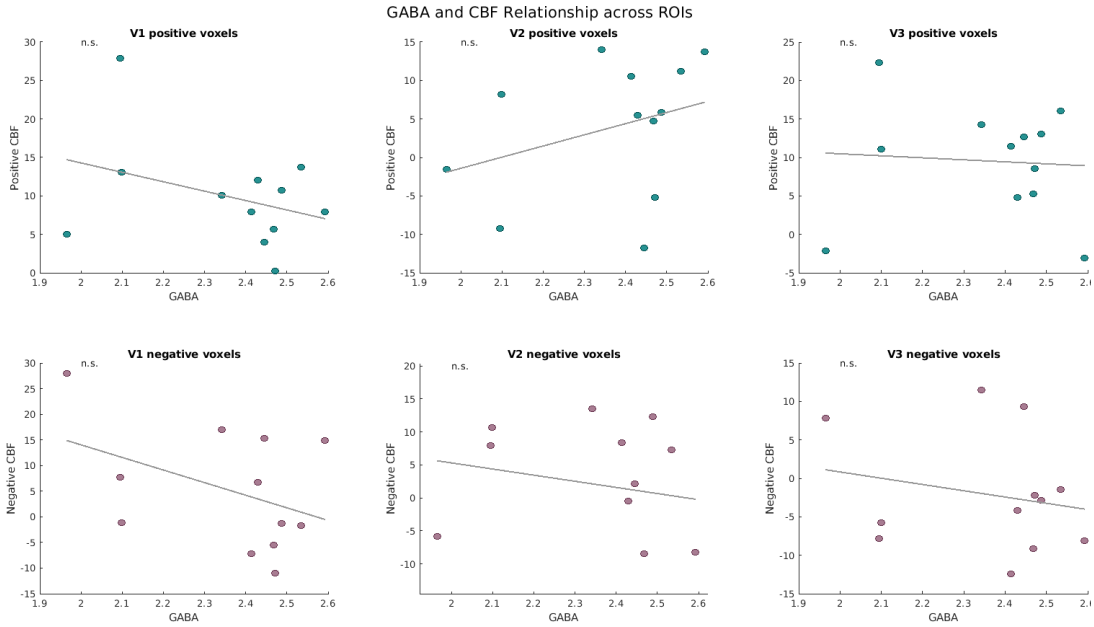

Figure 3.7: Scatter plot with fitted least square line showing the association between positive (upper panels) and negative (lower panels) CBF responses and GABA, per ROI (left panels reflecting V1, middle reflecting V2, and right most panel reflecting V3). There were no associations between positive responses and GABA in any ROI (V1 (r=-0.35, p=0.63), V2 (r=0.33, p=0.63), V3 (r=-0.071, p=0.91)). There were also no associations between negative responses and GABA in any ROI (V1 (r=-0.41, p=0.63), V2 (r=-0.19, p=0.79), V3 (r=-0.21, p=0.79)).

participant. The observed difference is confirmed to be significant in V1 ($t_{913.9} = 5.3, p < 0.001$) and V3 ($t_{985.4} = 7.37, p < 0.001$). There was no difference in V2 ($t_{800.5} = 1.55, p = 0.12$). As there are different numbers of voxels in positive and negative responding voxels, the test assumed the variances were unequal between the groups. In V1 the positively responding voxels ($SD = 62.8$) varied less than the negatively responding voxels ($SD = 143.5$). In V3 the variances were more similar, but nevertheless differed (positive voxels $SD = 14.23$, negative voxels $SD = 20.2$). In V2 the standard deviations were as follows: positive voxels $SD = 26.3$, negative voxels $SD = 64.34$.

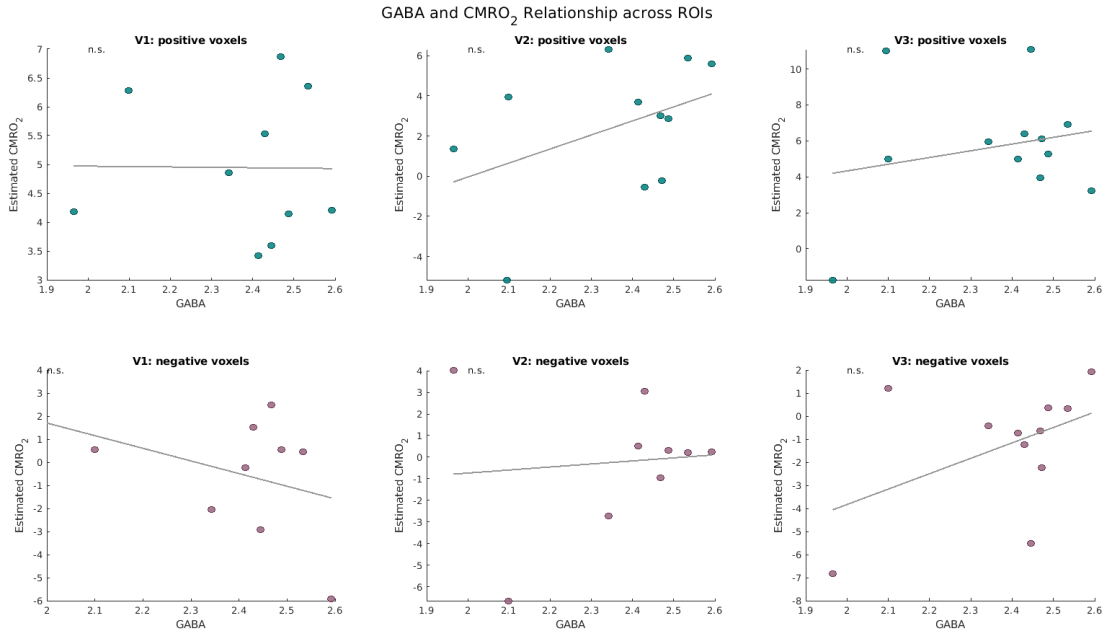

Figure 3.8: Scatter plot showing the relationship between GABA and estimated $CMRO_2$ and fitted least square line. Data points reflect each participant's mean GABA and $CMRO_2$ estimate. The panels reflect positively responding voxels (upper panels) and negatively responding voxels (lower panels), across ROIs (left panels reflecting V1, middle panels V2, and right most panels V3). There were no associations between the data in any ROI. Positively responding voxels: V1 (r=-0.01, p=1), V2 (r=0.423, p=0.59) and V3 (r=0.22, p=0.74). Negatively responding voxels: V1 (r=-0.3, p=0.79), V2 (r=0.01, p=0.85) and V3 (r=0.47, p=0.62)

3.4.6 GABA and Coupling Relationships

When estimating NVC (BOLD-CBF slopes per participant) there were no significant associations when correlating this with GABA in any ROI in either positively or negatively responding voxels (see figure 3.9).

When correlating GABA with the estimated n-coupling ratio (i.e. ratio of fractional change of CBF and $CMRO_2$), there is a trend towards a significant correlation between GABA and n-coupling in V1's positively responding voxels ($r = 0.72, p = 0.056$) (see figure 3.10). This indicates that the higher the GABA concentration, the larger the modulation difference of CBF and $CMRO_2$ in V1 for positively responding voxels. There were no other significant correlations or trends towards any relationship.

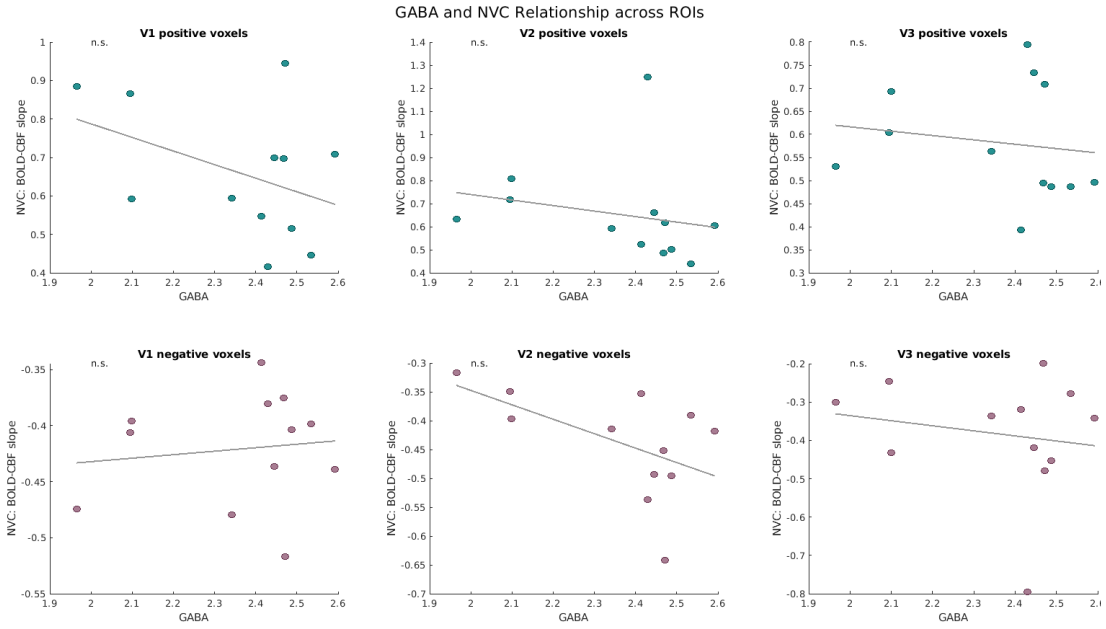

Figure 3.9: Scatter plot showing the relationship between GABA concentration estimates and NVC in terms of BOLD-CBF slopes and fitted least square line. The panels reflect positively responding voxels (upper panels) and negatively responding voxels (lower panels), across ROIs (left panels reflecting V1, middle panels V2, and right most panels V3). No associations were found in positively responding voxels: V1 (r=-0.41, p=0.58) V2 (r=-0.22, p=0.74), V3 (r=-0.15, p=0.79), or negatively responding voxels: V1 (r=0.12,p=0.79), V2 (r=-0.54 ,p=0.55), V3 (r=-0.17, p=0.79).

3.5 Discussion

3.5.1 Summary of Results

The study found a positive correlation between BOLD and CBF for positive and negative BOLD responses in V1, and in V3 for positively responding voxels. Considering that the BOLD signal is a combination of CBF, CBV, $CMRO_2$, and the interactions of these, it is not a surprise that these signals correlate. Nevertheless, it underscores that the experiment worked and it is in line with previous studies (e.g. Goense et al., 2012; Mullinger et al., 2014). Furthermore, in line with previous literature (e.g. Donahue et al., 2010; Muthukumaraswamy et al., 2012), we observed a negative association between GABA and positive BOLD responses in V1, however

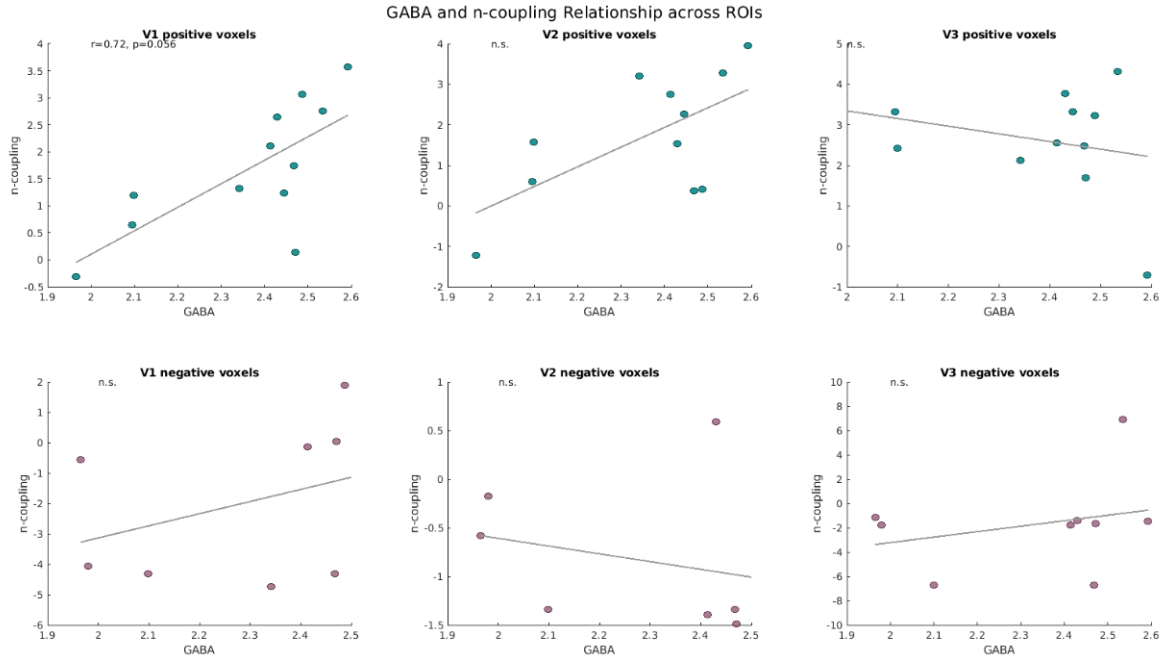

Figure 3.10: Scatter plot showing the relationship between GABA concentration n-coupling ratio. The line is a fitted least squares line. The panels reflect positively responding voxels (upper panels) and negatively responding voxels (lower panels), across ROIs (left panels reflecting V1, middle panels V2, and right most panels V3). A trend towards a correlation was found in V1 positively responding voxels (r=0.72, p=0.056). No other associations were found in positively responding voxels: V2 (r=0.635, p=0.19), V3 (r=-0.23, p=0.74), or negatively responding voxels: V1 (r=0.35,p=0.79), V2 (r=-024,p=0.79), V3 (r=0.3 ,p=0.79).

this was not statistically significant.

Moreover, when plotting GABA against $CMRO_2$, there seemed to be differential $CMRO_2$ levels recruited between positively and negatively responding voxels. This difference was confirmed showing that positively responding voxels use significantly more energy (in terms of $CMRO_2$) compared to negatively responding voxels, supporting literature showing that excitatory activation uses more energy than inhibitory activation (e.g. Attwell & Laughlin, 2001).

3.5.2 Inhibition and n-coupling

Furthermore, we found a trend towards a positive relationship between n-coupling estimates and GABA in positively responding V1 voxels (and a non-significant pat-

tern in the same direction in V2). This suggests, albeit speculatively, that as GABA increases, the modulations of CBF and $CMRO_2$ increasingly differ, indicating increasing decoupling. This is in line with the prediction of Buxton et al., 2014, whereby they suggest that the n-coupling ratio may give insights into inhibitory and excitatory interplay. Specifically, they suggest that large n-coupling may be indicative of increased inhibitory activation: inhibition would decrease $CMRO_2$ activity whilst CBF may remain unchanged, resulting in a larger ratio. The current study is qualitatively consistent with this as we observe the ratio to increase with higher GABA concentrations.

3.5.3 GABA and Efficiency

Although the current study did not find statistical evidence for the relationship between GABA, BOLD and CBF in positively and negatively responding voxels, it is worth commenting on some general trends that may benefit from further investigation. Because GABA is only estimated in V1, it makes sense to only comment on qualitative observations in this ROI, as concentrations of GABA may be different in extrastriate cortices. In addition to this, the stimulus choice of flicker checkerboards is likely to consistently stimulate V1.

When looking at the relationship between GABA and CBF, there is a qualitative negative relationship between the signals in V1. This is also the case between GABA and BOLD in positively responding voxels (in line with e.g. Lauritzen, Mathiesen, Schaefer, and Thomsen, 2012 and Muthukumaraswamy et al., 2012), and between GABA and $CMRO_2$ in negatively responding voxels. There is no apparent relationship between GABA and BOLD in negatively responding voxels nor between GABA and $CMRO_2$ in positively responding voxels. In other words, in V1 where there is a qualitative relationship observed, it is negative. Purely speculatively, this

may indicate that increased GABA is sometimes related to decreased BOLD, CBF, and $CMRO_2$ in V1.

This may benefit from further study, especially as previous work has shown a relationship between GABA concentrations and visual perceptual task performance. That is high GABA concentrations are associated with high performance in visual intelligence and contrast discrimination tasks (Cook et al., 2016; Hammett et al., submitted). It has been suggested that the mechanism for perceptual task improvement is linked to GABA acting to reduce cortical noise (i.e. increases cortical signal to noise ratio) (Ozeki, Finn, Schaffer, Miller, & Ferster, 2009). A recent study (Hammett et al., submitted) uses a recurrent network model to show that GABA effectively decreases how much neurons respond to stimuli - GABA seems to gate information. Additionally, the model shows that GABA reduces cortical noise. Specifically, using the recurrent network model of Wilson and Cowan, 1972, the authors find that GABA best approximates the parameter describing the inhibitory input to excitatory neural populations. In other words, GABA mediates inhibition. This is interesting as GABA seems to increase perceptual sensitivity, whilst decreasing neural sensitivity. This is in line with literature relating GABA, inhibition, and perceptual processes.

The current study cautiously offer qualitative observations that may give insights into these putative mechanisms, as we find that high GABA concentrations are related to decreases in BOLD, CBF, and $CMRO_2$ signals. However, this needs to be further studied with a larger sample size...

In summary, the study demonstrates that BOLD responses correlate with CBF in positively and negatively responding voxels in V1, and in V3 for positively responding voxels. Moreover, the study observes a trend towards a significant positive relationship between GABA and n-coupling, which may suggest that NVC varies with levels of inhibition (corroborating the hypothesis of Buxton et al., 2014). In

addition to this, differences between $CMRO_2$ recruitment in positively and negatively responding voxels were observed in V1 and V3, which is in line with previous literature (Attwell & Laughlin, 2001).

Chapter 4

Chapter Four: Repetition Suppression of Visual Duration

4.1 Overview

This chapter differs from the other chapters in that it uses solely the BOLD signal to probe duration preferences in visual and parietal areas. I adapted a vMMN EEG study into a fMRI RS experiment and attempted to replicate the findings. No evidence of RS effects of duration was found; however, I observe that there is an effect of total duration (i.e. the longer the duration, the larger the percent signal change), although this diminishes with multiple correction adjustments. Moreover, I discuss how stimulus choice and choice of attentional control may make a difference when comparing the current fMRI study with another fMRI study probing the same question. Furthermore, I discuss the differences and similarities between how repetition suppression and visual oddball paradigms, as well as the differences and similarities between using EEG and fMRI to study cortical processing of visual duration.

4.2 Introduction

How is time perception achieved? The fundamental questions are how and where time perception is processed. There are, roughly speaking, two main schools of thought regarding the neural mechanisms of how time and duration processing is achieved: time perception is achieved globally or locally (Coull, Cheng, & Meck, 2011; Grondin, 2010; Ivry & Schlerf, 2008; Van Rijn, Gu, & Meck, 2014). The former posits a centralised pace-keeper that may send signals at particular intervals with which it can assess duration of incoming events. The latter suggests that duration encoding occurs locally in specialised regions, for example, in early visual or auditory areas.

One hypothesis that has recently piqued the interest of the field is the idea of duration channels (Heron et al., 2011; Muller & Nobre, 2014; Murai, Whitaker, & Yotsumoto, 2016) - i.e. overlapping populations of neurons that have a preference for a particular duration range. This is an attractive mechanism as evidence for other feature channels have been uncovered in sensory modalities. For example, primary auditory pathway show pitch preference (e.g. De Martino et al., 2013), and primary visual cortex, V1, reveal orientation channels(e.g. Tong, Harrison, Dewey, & Kamitani, 2012). However, they have their own specialised regions for processing their relevant information. Considering the importance of time processing we get to the heart of the issue – is there a specialised central region for time encoding, or are there time processors in each sensory region?

Adaptation paradigms have been utilized to probe the presence of duration selectivity. Results from behavioural studies have been inconsistent. For example, Heron et al., 2011 used visual or auditory stimuli to adapt to a range of durations, and thereafter presented a reference stimulus of a fixed duration in the modality opposite to the adapted (e.g. if adapted to visual, the reference stimulus was audi-

tory). Then they presented a test stimulus in the modality adapted to for the same duration as the reference stimulus. The participants were asked to compare the reference and test durations and judge whether the test duration was longer or shorter than the reference duration. They observed that with adaptation to stimulus durations shorter than the reference and test durations, participants reported the test duration as longer than the reference, whereas when the adaptation duration was longer, participant reported that the test duration was shorter than the reference. They interpret this as evidence for the existence of duration channels.

A study using a similar set-up found different results. Curran, Benton, Harris, Hibbard, and Beattie, 2016 found that participants estimated a test duration as shorter, regardless of the duration being adapted to was longer or shorter than the test duration. The methods have some fundamental differences, where for example Curran et al., 2016 only use visual stimulation and their stimuli are unidirectionally moving dots, while Heron et al., 2011 utilized visual Gabor patches and auditory tones. Additionally, Curran et al., 2016 use a 600ms test stimulus, while Heron et al., 2011 test and reference stimuli were 320ms. Their basic approach to duration is similar and therefore one would expect the results to corroborate.

An important question that these studies do not consider, is whether duration is an automatic process, and hence occurs without attentional engagement with the stimulus. This is difficult to assess behaviourally, and therefore neuroimaging is more appropriate. Hayashi et al., 2015 investigated RS of duration using fMRI. They showed a reference shape (circle or square) for either 400 or 600ms, and a test shape (circle or square) for 167, 283, 400, 533 or 650ms and 250, 433, 600, 783 or 967ms respectively. The participant was asked to indicate when the duration of the test shape was identical to the reference shape. Additionally, to control for attentional effects they also added a task based on the shape identity requiring the participants to judge whether the test shape was the same as the reference shape. In

the right inferior parietal lobule (IPL), they found that when the test stimulus had the same duration as the adapter stimulus, percent signal change was significantly decreased compared to when the test stimulus was different. This suggests RS effects of duration in this region, and the effect was observed for both the shorter and longer duration. Furthermore, they show that RS of duration is present regardless of task, in other words, the effects were evident whether the participant was explicitly engaging in estimating duration, or shape. They interpret this as duration being automatically processed.

On the other hand, Chen, Huang, Luo, Peng, and Liu, 2010 used a cross-modal design, where participants were presented with both auditory and visual oddball tasks and asked to attend and respond to one or the other. Auditory MMN was found to not be significantly different when attending to auditory or visual stimuli, while visual MMN was significantly modulated by attention. In other words, although there were MMN effects in both modalities, only visual MMN showed significant effects of attention. Thus, the authors conclude that auditory MMN is an automatic process as attention does not affect its' signal, while visual MMN is not automatic.

Many of the studies reporting duration selectivity ask participants to explicitly estimate or engage with the stimulus, which raises the question if the results reflect duration selectivity or whether the results reflect judgement or estimations regarding stimulus duration. For example, in the experiment by Hayashi et al., 2015 although the participants were focusing on the shape of the stimulus rather than the duration, the two features are not independent. Therefore, one could argue that it is problematic to conclude that the stimulus duration was not monitored during the shape discrimination task, as the previous task was to estimate durations.

However, the study by Chen et al., 2010 asked participants to attend to durations in either the visual or auditory modality, which again raises the question how effectively participants can ignore the stimuli in the non-relevant modality. In

fact, it has been suggested that as the visual system is a more dominating sensory system than the auditory, it is problematic to devise cross-modal attentional tasks. Specifically, visual tasks can be utilised to divert attention away from auditory stimuli, but not vice versa – visual tasks are also needed to divert attention away from visual stimuli (Chen & Zhou, 2014; Stefanics, Kremláček, & Czigler, 2014). Hence, a way to solve the issue of whether visual duration processing is automatic is to measure vMMN while asking participants to engage in an orthogonal visual task. This was addressed by Durant et al., 2018 using EEG. They found that there were differences in event related potentials (ERPs) at occipital and posterior-occipital electrodes in response to same and different duration pairing within the same total duration. This suggest that duration differences are automatically encoded in early visual areas. Therefore, this provides evidence that (at least some) visual MMN effects are processed independently of attention.

Hence, while previous fMRI studies found evidence for automatic duration processing in parietal areas, some EEG studies, in contrast, show inconsistent results whether duration processing is attention-dependent or automatic. To resolve this inconsistency the current study sought to replicate the EEG study by Durant et al., 2018 modified into an RS fMRI paradigm. This will additionally offer better localisation of the effects.

By presenting pairs of duration stimuli, where the second stimulus duration is either the same or different from the first, we wanted to assess if duration repetition results in decreased BOLD signal change, compared to duration alteration. Moreover, by engaging participants with a demanding orthogonal visual task, we aimed to test whether these effects were evident while attention was diverted away. The aim was to determine whether visual duration encoding was still present in rIPL when attention was diverted - thus corroborating the results of Hayashi et al., 2015 – and/or if duration-specific RS effects were found in visual areas, thereby corrob-

orating the results of Durant et al., 2018. As the stimuli comprise of moving dots, we expected to see stronger V1 and V5 responses compared to other areas.

We found that there was no evidence for RS effects of duration in neither visual nor parietal areas. Although we found an effect of total duration (i.e. differences between short, medium, and long durations) in V1, this effect disappeared once corrected for multiple tests.

4.3 Methodology

4.3.1 Participants

10 participants (f=7, mean age=26.7) took part in the experiments. Written consent was obtained from all. The procedures adhered to the ethical guidelines of the Psychology Department Ethics Committee at Royal Holloway University of London. All participants had normal or corrected-to-normal vision. One participant's dataset was excluded due to excessive head motion.

4.3.2 Stimuli and Design

4.3.2.1 Duration Stimuli

The stimuli were generated using Cogent Team, 2011 in MATLAB, and projected with a refresh rate of 60 Hz onto a screen (1024 x 768 pixel resolution and about 30° visual angle) located at the head of the bore, 85 cm from participants.

The stimuli (figure 4.1, top right) were comprised of 200 white dots with a size of 0.0892 x 0.0892° visual angle (5x5 pixels; luminance of 52 cd/m^2) randomly dis-

tributed within in a circle subtending a visual angle of 16 degrees, with a blue fixation square in the centre and presented against a uniform grey background (luminance of 13 cd/m^2).

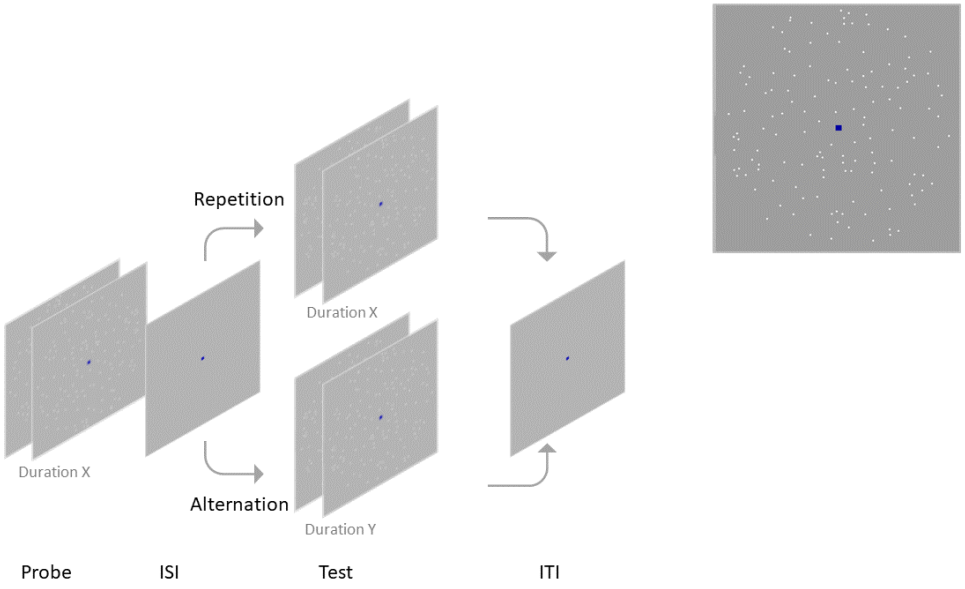

Figure 4.1: Stimulus and Protocol. Top right of the figure shows an example of single stimulus frame. The bottom left of the figure shows experimental protocol. The dot motion stimulus appeared for a certain probe duration (see figure 4.2, and in text), followed by a static gap of 150ms, and then followed by a test stimulus for a duration that was either identical or different from that of the probe. Thereafter, the next pair was presented following an inter-trial interval (ITI) of variable durations (see text for details).

At the beginning of each run, the dots were placed at random positions within the stimulus aperture. The position of the dots changed from frame to frame, giving the appearance of movement, although there was no net global motion or trajectory information in the stimulus. This was achieved by rotating the dot pattern by a random angle on each frame. Within each run the dot pattern remained constant, changing only in orientation. New dot patterns were generated for each run. Within each trial, the dot patterns were shown in two sequential intervals of variable duration separated by a fixed duration gap during which the dots were static. The static dots were also present between events, as this reduced the contrast changes brought on by on-off stimulus presentation.

There were three different total durations, and six different duration pairings: short durations of 517ms (6 + 16 frames or 100 + 267ms, and 11 + 11 frames or 183 + 183ms), medium duration of 684ms (16 + 16 frames or 267 + 267ms), and long durations of 850ms (16 + 26 frames or 267 + 433ms, and 21 + 21 frames or 350 + 350ms, and 26 + 16 frames or 433 + 267ms). The static dot gap was always 150ms or 9 frames (see figure 4.2).

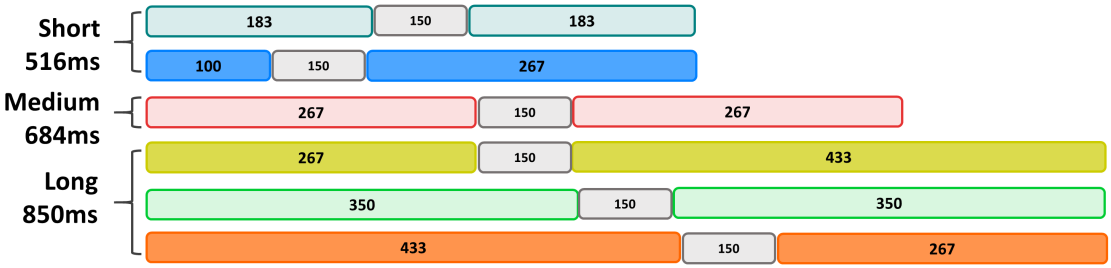

Figure 4.2: Illustration of Stimulus Durations and Pairings. Stimulus duration pairings for each duration condition. All expressed in ms. Total durations found to left of figure.

We used a repetition suppression paradigm to probe duration selectivity, looking for response reductions to sequential pairs of identical duration, compared to pairs with unequal stimulus duration but the same total duration (see figure 4.2 for illustration).

An event-related design was utilised for the duration experiment runs. Inter-stimulus intervals (ISI) were jittered using randomly obtained timings from a Poisson distribution of a mean of 8s. The ISI was adjusted so that stimulus onset was time-locked to the acquisition of each BOLD volume. The duration experiment consisted of six runs where within each, the six conditions were repeated six times, resulting in 36 trials per run, and thus 36 repetitions of each condition across the whole experiment.

4.3.2.2 Retinotopic Mapping Stimuli

Retinotopic visual areas were mapped using standard phase-encoded mapping stimuli consisting of a high-contrast checker-board wedge subtending 22.5° visual angle that rotated around the centre of fixation. Each wedge consisted of two radial strands of checks that moved either outwards or inwards along the eccentricity dimension. Each run included six cycles of a full rotation of the wedge stimuli moving in a single direction (clockwise or counter-clockwise). Each cycle took 26s and wedge stimuli were presented in two blocks of three cycles each. Before, between, and after the blocks there was a 26s baseline during which only a blank screen was shown. Two scans were obtained for retinotopic mapping, one scan with the wedge rotating clockwise and the other counter-clockwise.

4.3.3 Procedure and Task

Anatomical scans were acquired first, and thereafter the two retinotopic mapping runs were obtained followed by the six experimental runs.

For both the main (duration) experiment and retinotopic mapping, attention was diverted and controlled by having the participants engaging in a demanding attention task, where they had to detect luminance changes in the fixation square. Participants indicated by pressing one of two buttons (using the Lumitouch button-box) if the luminance of the central fixation target increased or decreased, with the magnitude of luminance changes controlled by a 1-up, 1-down staircase procedure to ensure sufficient task difficulty.

4.3.4 MRI Acquisition

MRI data were collected using a Siemens 3T TRIO system (Erlangen, Germany), with a 32-channel head coil. Behavioural data were obtained through button-presses using a MR-compatible Lumitouch button-box.

4.3.4.1 Anatomical Acquisition

A T1 weighted anatomical volume of 1mm isotropic resolution (T1w; TR: 1830ms; TE: 3.03ms; 160 slices per volume; TI: 1100ms; FA: 11°; echo space: 8.9; Single shot) was acquired for localisation and visualisation of functional data.

4.3.4.2 Functional Acquisition

For the functional runs, multiband functional axial acquisition was used acquiring 36 slices, yielding a resolution of 3mm isotropic (TR: 800ms; TE: 36.8ms; FA; 30°; 192x192 FoV; multiband acceleration factor of 4; bandwidth 1220). For the experimental runs, a total of 450 volumes per run were obtained resulting in a run-time of 360 seconds, and 288 volumes per run for retinotopic scans resulting in scan-time of 230 seconds. A multiband sequence was used to gain a higher temporal resolution of the data. We chose the multiband acceleration factor of 4 based on empirical evidence demonstrating that increasing from a factor of 2 to 4 results in negligible loss of signal to noise ratio, while still increasing sensitivity (Preibisch, Bührer, Riedl, et al., 2015).

Between-scan alignment and motion correction were done using the mcflirt tool (Jenkinson et al., 2002). Slice timing, linear de-trending and high-pass filtering (using a cut-off of 0.022Hz) was applied using in-house software written in MATLAB. Surfaces, used for visualisation and identifying visual areas, of each participant's

cortex were reconstructed from the anatomical MR image using SurfRelax (Larsson, 2001).

4.3.5 Analysis

All analyses were done in MATLAB 2020a (MATLAB, 2020).

4.3.5.1 Identification of Visual Area ROIs

As in the previous chapters, each participant's retinotopic data (maps of phase and coherence) were projected onto a reconstructed flat-map of their occipital area. Identification and drawing of area V1, V2, V3, hV4, LO1, LO2, V3A/B were done manually based on the acquired maps (Larsson & Heeger, 2006), and ROIs from left and right hemisphere were combined.

In contrast to previous chapters, this study also identified area V5/MT. This region was localised by conducting a voxelwise deconvolution analysis of the whole brain (see below), to identify areas responding to visual motion (given that experimental stimuli were moving dots).

For each voxel, the response effect size (operationally defined as the coefficient of determination R2 of the deconvolution model fit) was visualised on the cortical flat map and area V5/MT identified as a cluster of peak activity adjacent and anterior to LO2 (Huk & Heeger, 2002; Larsson & Heeger, 2006). Visually responsive clusters of voxels in parietal cortex were also identified by a similar procedure. However, very few participant's parietal areas showed responsiveness to the stimuli and were therefore not further investigated. For one participant, LO1 and LO2 could not be identified.

4.3.5.2 Duration Experiment

A general linear model (GLM) was fit to the mean time series for each ROI using a canonical double-gamma HRF convolved with the timecourse of stimulus onset for each condition (see figure 4.3 panel A for illustration). Each trial (duration pair) was treated as a single event (i.e. the actual stimulus duration lengths were not modelled). RS effects were assessed by comparing the beta estimates for conditions with duration pairs that had the same total durations, to test whether the identical duration pairs showed a reduction in activity compared to the non-identical pair(s). This was tested using one-way repeated measures ANOVA in MATLAB (MATLAB, 2020). Thereafter, we applied FDR adjustments for multiple comparisons within and across tests.

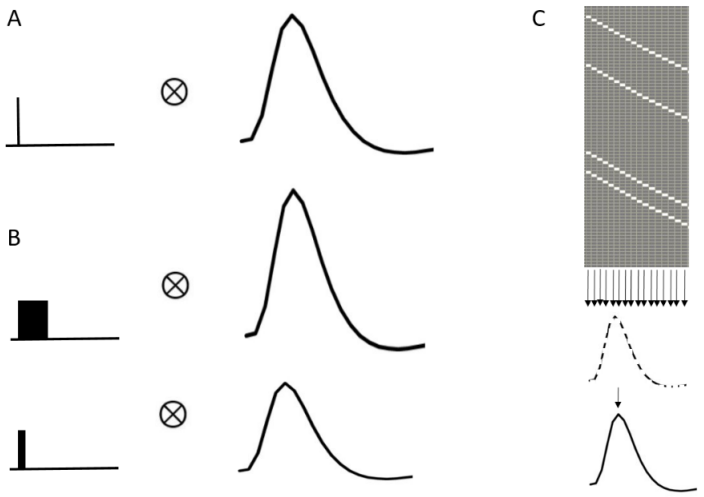

Figure 4.3: Illustration of analysis approaches. A) standard HRF fitted GLM, where a design matrix consisting of delta functions marking stimulus onset was convolved with a canonical HRF. B) simulated data was achieved in a similar way, with the important difference that the standard HRF was convolved with boxcar signals that reflected the duration conditions. Hence, the simulated data have different evoked responses where longer durations result in large percent signal change. C) deconvolution results generating estimated impulse response function (IRF) of each condition's evoked responses. For each condition, each time-point was combined and fitted with a GLM generating response magnitudes at each time-point.

4.3.5.3 Estimation of Response Time Courses

Since the nature of the experiment investigated small temporal differences, we hypothesised that there may have been small differences in the shape of the HRF, rather than just the amplitudes. Therefore, as in line with the previous chapters, we also performed a deconvolution analysis in order to avoid making HRF-shape assumptions (Burock & Dale, 2000) (see figure 4.3 panel C for illustration). For this experiment we created a design matrix consisting of 20 columns (time-points) per condition, where the first column indicated the start of each trial in that condition and subsequent columns each subsequent time-point. This resulted in 121 columns (1+20*6), where the first represents the mean response. Thereafter, a standard GLM was used to estimate response magnitude at each time point following stimulus onset (Burock & Dale, 2000). Any differences between the durations within each ROI were assessed with a one-way repeated measures ANOVA.

4.3.5.4 Simulation of Response Time Courses

To further investigate the effect of total duration on percent BOLD signal change, we simulated stimulus-evoked responses by convolving the canonical HRF with the actual stimulus duration lengths used in the experiments (see figure 4.3, panel B). Specifically, instead of using a delta function to fit an HRF, we generated time-continuous boxcar signals corresponding to number of frames in each condition and convolved with a standard HRF. This procedure generated a prediction of response magnitudes under the assumption that responses simply reflected total stimulus duration (i.e. without any repetition suppression indicating duration selectivity).

By comparing these predictions with the measured data, we were able to assess whether the measured responses deviated from these predictions (suggesting responses did not solely reflect the overall duration of stimuli). To compare the

relative changes in responses to duration, we compared the simulated data with a) the average short, medium, and long beta estimates obtained from the GLM analysis, and b) the average area under the curve from short, medium, and long BOLD responses from the deconvolution analysis. We compared betas and area under curves, as the betas from the HRF fitted GLM are proportional to its area under the curve. It was hypothesised that if the increase in percent signal change in the measured data deviated significantly from the simulated, then there may be evidence for duration encoding.

4.4 Results

4.4.1 Behavioural Measures

The behavioural task showed a mean 51.8% accuracy (std=0.04). This could suggest either that the task was sufficiently difficult to ensure attentional diversion, or the participants made random guesses. It is difficult to deduce this from the behavioural data, however qualitative checks post scanning suggests that the participants engaged with the task and did not perceive the simultaneous duration changes.

4.4.2 RS Effects

4.4.2.1 Regular GLM with Fitted HRF

Figure 4.4 suggests that there may be RS effects in the short durations in V1. The result from the repeated measures ANOVA on HRF data shows there is an effect of duration in V1 ($F(5, 48) = 2.557, p = 0.04$), although after FDR adjustments

this effect disappears ($F(5, 48) = 2.557, p = 0.54$). Hence, there is no evidence of duration nor RS effects in V1. It may be that the effect of duration was not detected due to a lack of statistical power due to too few trials. Given that in figure 4.4 there seems to be differences between longer and shorter durations, it warrants further investigations (see below).

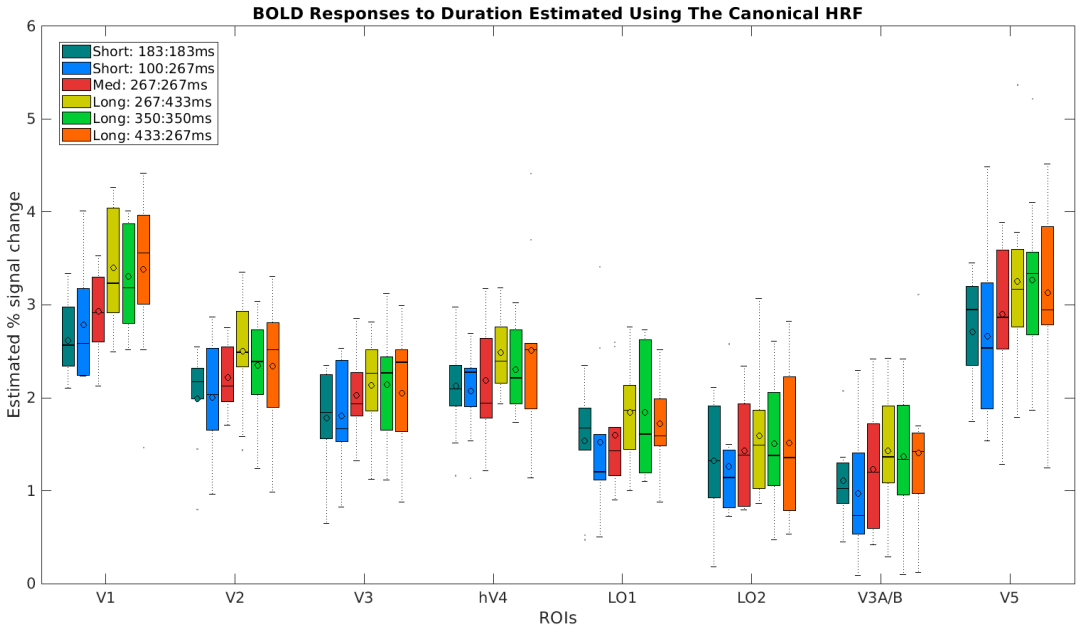

Figure 4.4: Canonical HRF: percent signal change across condition and ROI. The figure show estimated percent signal change on the y-axis and ROI on the x-axis. Each ROI has a cluster of boxes indicating the median response (line) as well as mean response (open circle). The box encapsulates the response's interquartile range (see inset for details and colour key). Whiskers include the rest of the data's range, besides outliers which are represented as dots.

4.4.2.2 Estimated Responses Using the Area Under the Impulse Response Function Curve

To avoid making assumptions about the impulse response curve, we also assessed percent signal change estimates using area under the curve resulting from the deconvolution analysis. An example of impulse response function (IRF) curves are shown in figure 4.5, which shows V1 mean response curves.

Figure 4.6 suggests that there may be some effects of RS within short durations

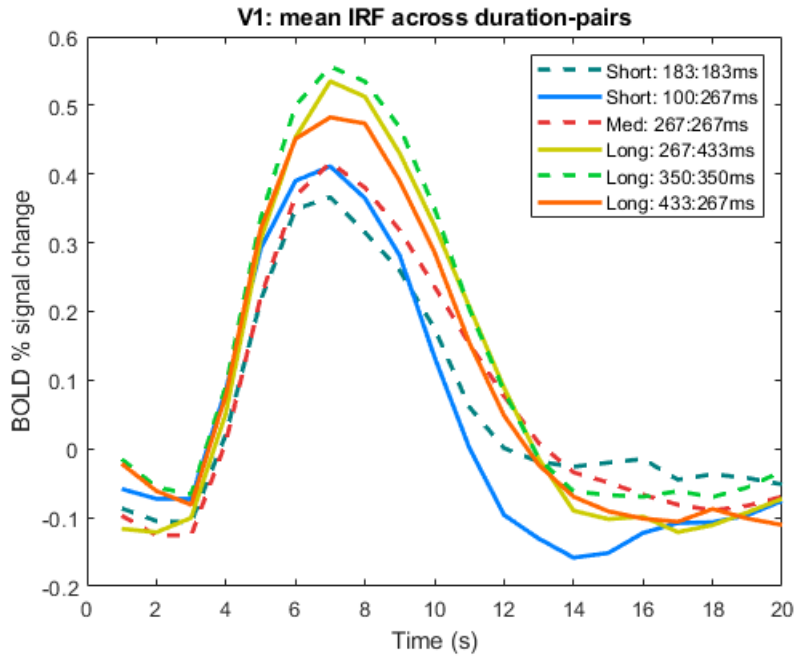

Figure 4.5: Average IRF curves to each condition (see key for colour code) in V1. Y-axis show percent signal change, and x-axis time in seconds.

in V1, V2, V3, LO1, LO2, and V3A/B. Moreover, the figure indicates that there may even be a repetition enhancement within long durations in V3, hV4, LO1, LO2, V3A/B, and V5. However, formal analyses suggest there is no statistical evidence of any difference.

4.4.2.3 Total Duration and the BOLD signal

To further investigate if there were any differences in how shorter and longer durations were processed, the total durations were combined and averaged yielding a short duration, medium duration and long duration. Thereafter we performed a repeated measures ANOVA across the three total durations to assess any evidence for differences of total duration. This was only done for the estimations from the HRF fitted GLM results, as the AUC of IRF analysis yielded no evidence of a total duration effect. Significant differences were found in V1 ($F(2, 16) = 8.464, p = 0.003$) and V5 ($F(2, 16) = 3.837, p = 0.044$), however, these differences did not survive

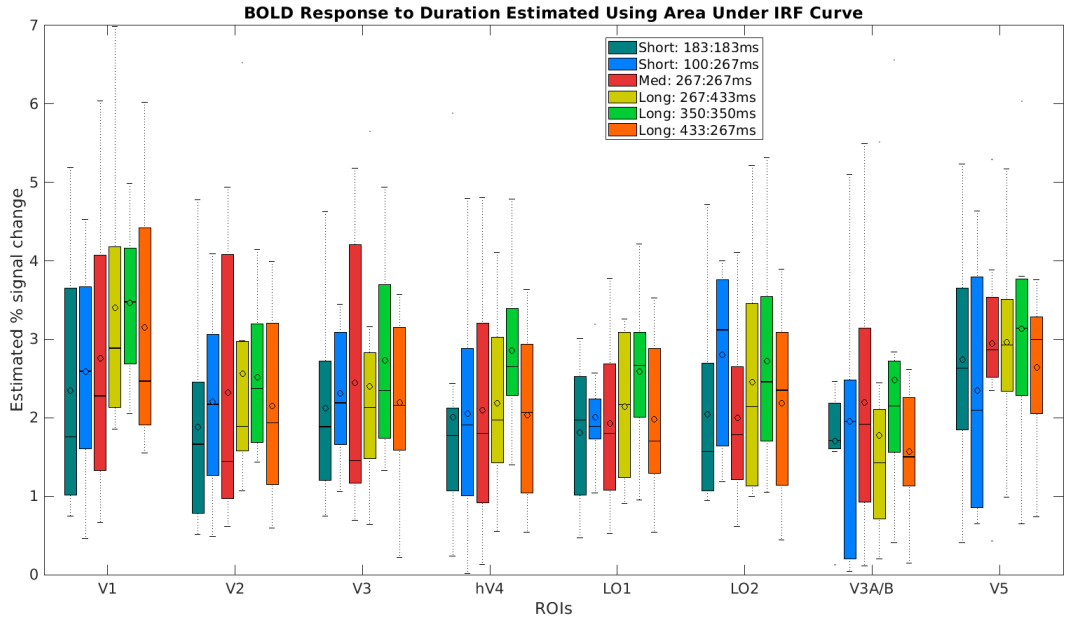

Figure 4.6: Area Under the Curve of IRF: mean percent signal change across conditions and ROI. The figure show estimated percent signal change on the y-axis and ROI on the x-axis. Each ROI has a cluster of boxes indicating the median response (line) as well as mean response (open circle). The box encapsulates the response's interquartile range (see inset for details and colour key). Whiskers include the rest of the data's range, besides outliers which are represented as dots.

the multiple test adjustments (V1: $F(2,16) = 8.464, p = 0.54$, V5: $F(2,16) = 3.837, p = 0.93$).

4.4.2.4 Simulated Duration Data Compared with Measured

We simulated data by convolving duration lengths with the canonical HRF and computed the area under the resulting response curves. We first compared the simulated responses with the response estimates from the beta estimates from the GLM using a canonical HRF by plotting them against each other (see figure 4.8, left panel). There is a linear relationship between the two, consistent with responses solely reflecting overall stimulus duration. There was a slight increase in steepness in signal change between medium and long durations in V1 and V5.

There seems to be an overall linear relationship between the measured data with

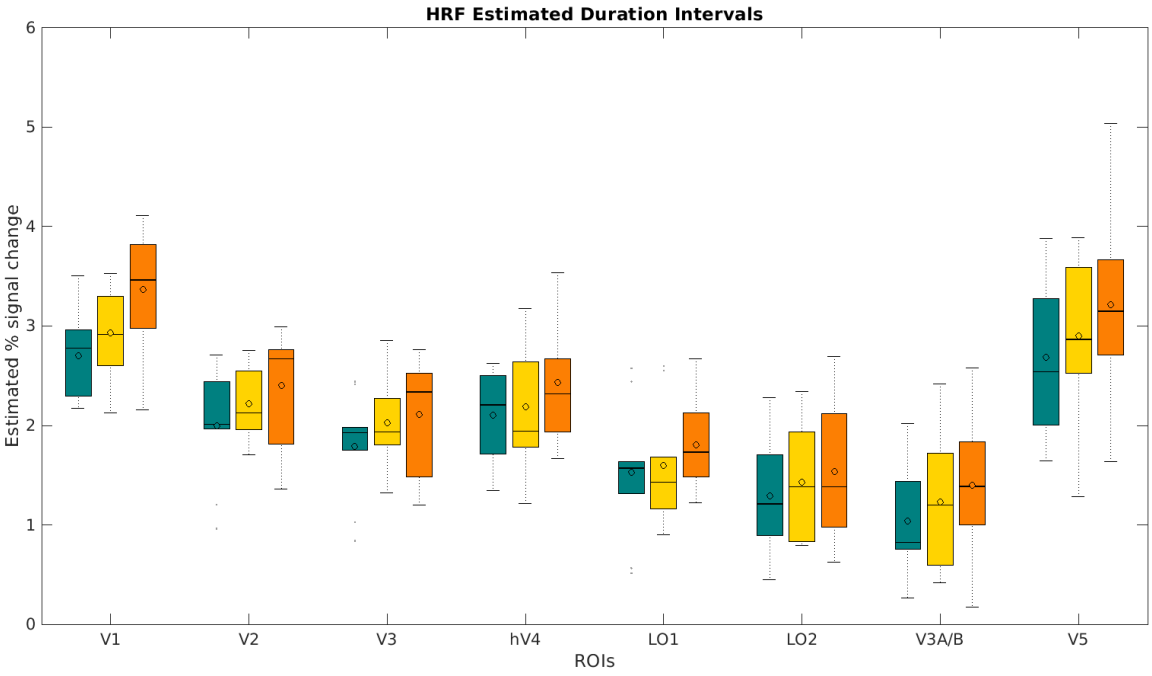

Figure 4.7: Comparing duration intervals (short, medium, and long) within HRF estimated data. The figure show estimated percent signal change on the y-axis and ROI on the x-axis. Each ROI show mean response estimates of short (teal), medium (yellow), and long (orange) durations. Each ROI has a cluster of boxes indicating the median response (line) as well as mean response (open circle). The box encapsulates the response's interquartile range. Whiskers include the rest of the data's range, besides outliers which are represented as dots.

regular GLM analysis and the simulated data.

We then compared the simulated data with the deconvolution data, which made no assumptions of the signal response shape and thus may be more sensitive to responses differences between conditions. As can be seen in figure 4.8, right panel, this indicates a more complex relationship between response duration and magnitude. Only in V1 did the BOLD signal change with increasing duration follow a linear relationship, similar to the HRF data (indicating that responses were proportional to overall response duration). In higher visual areas, notably V5/MT, response magnitudes saturated or decreased at longer durations, indicating that responses were not simply predicted by the overall duration of stimuli.

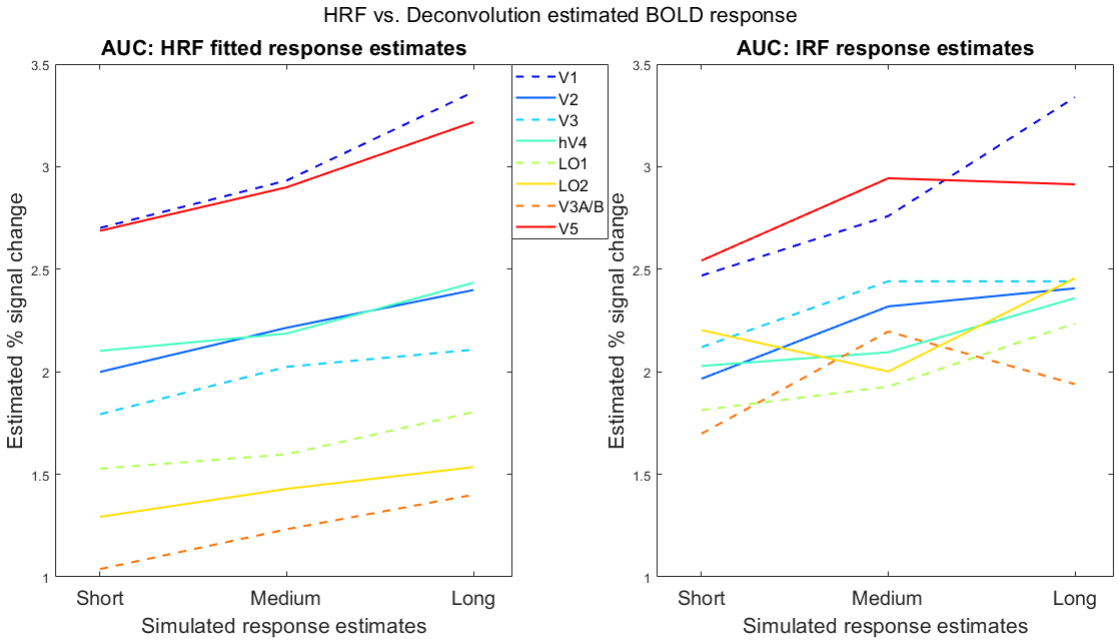

Figure 4.8: Figure showing simulated data vs HRF fitted GLM data (left panel) and IRF estimated deconvolution data (right panel). Percent signal change of measured data analysed with regular GLM vs simulated responses to durations (short, medium, long), as well as the estimated IRF from the deconvolution analysis vs simulated responses

4.5 Discussion

4.5.1 Summary of Results

The results suggest that there is no evidence for RS effects in early visual areas (nor parietal areas), when attention is fully diverted. Moreover, before correcting for multiple comparisons, we observed differences between total durations, suggesting that that small differences in duration can be captured by the BOLD signal (as previously shown by Seiji Ogawa et al., 2000). On the one hand this can be seen as evidence that the absence of RS is not due to a lack of trial-power, however, the diminishing of effects after correcting for multiple tests, indicate that it was a false positive. These findings did not replicate either Durant et al., 2018 or Hayashi et al., 2015. This may suggest that visual duration processing is not automatic, corroborating with Chen et al., 2010. Alternatively, it may be due to the BOLD sig-

nal being more biased during attentional control, or that RS and vMMN paradigms probe distinctly different neural processes. On the other hand, it is important to underscore that this study had 10 participants. Although this sample size has been standard in the field for some time, the increased availability of fMRI has led to the opportunity to increase the sample sizes. Needless to say, a larger sample means increased power and generalisability. The number of participants could be a reason for why the findings did not replicate previous literature. Nevertheless, this study should be viewed for what it is - a pilot. To my knowledge, it is the first of its kind to probe the effects of full attentional diversion on duration perception using RS fMRI, and therefore, I will continue to discuss the current findings further in relation to the literature.

We show that V1 and V5 show strongest signal changes compared to the other areas, as predicted. This is notably the case even when low-level contrast changes that drive V1 and V5 are controlled for. However, when making no assumptions of IRF shape V1 and V5 show different activity pattern across durations, where V1 activity linearly increases with increasing duration while V5 activity seems to saturate after medium duration length. Convolving data with a canonical HRF means that we get an amplitude measure of the initial or early activity, while later amplitude changes are ignored. Thus, any differential curve dispersion and undershoot is modelled away. It is often reasonable to assume a particular response curve shape, however, sometimes these assumptions may not hold (e.g. Handwerker, Ollinger, & D'Esposito, 2004; Henson, Price, Rugg, Turner, & Friston, 2002). For example, in the current study, it may be that the difference between V5 responses in the different analyses is due to IRF shape being different in the medium and long length durations. The fact that V1 show linear responses in both analyses is not surprising as the canonical HRF is heavily modelled on V1 evoked responses.

4.5.2 RS vs vMMN

It is likely that vMMN and RS are mechanistically different although they both rely on adaptation, and that is why the current study find conflicting results compared to Durant et al., 2018. Although, one could argue that the current results are consistent with that of Durant et al., 2018, as we observe duration encoding in V1 whilst diverting attention - especially if MMN and RS are distinct neural processes. In fact, MMN has been used to probe underlying mechanisms of neuropsychiatric diseases (e.g. Haigh, Coffman, Murphy, Ward, & Salisbury, 2017; Rentzsch, Shen, Jockers-Scherübl, Gallinat, & Neuhaus, 2015), and recently it has been observed that Schizophrenia patients show deficits in MMN but not RS (Haigh et al., 2017). This corroborates with the idea that there are some differences between the processes. This is reasonable as MMN asks for detection of stimulus deviance, while RS asks for detection of stimulus repetition (Stefanics, Kremláček, & Czigler, 2016). Hence the current study would benefit replication in EEG to see if the vMMN effects are still present during a RS paradigm – alternatively, the vMMN experiment to be replicated in fMRI to assess presence of this oddball effect is still present in early visual areas.

It is unclear how exactly vMMN and RS are related. Animal electrophysiology has shown that stimulus specific adaptation activity from the macaque IT region generates oddball signals, and not predictions (Kaliukhovich & Vogels, 2014). This is further supported by another primate study showing that auditory MMN signals align with adaptation, and that any deviance detection may arise from higher auditory areas (Fishman & Steinschneider, 2012).

On the other hand, it has been suggested that MMN signals are independent of adaptation (e.g. Fishman & Steinschneider, 2012), and should be seen as a signature of prediction error, or expectation violation (Stefanics et al., 2014; Wacongne

et al., 2012). A recent study showed rat V1 revealing adaptation to regular stimulus presentation, while, however, deviant stimuli drove activity increase in higher areas (latero-intermediate cortex) that could not be accounted for by adaptation (Vinken et al., 2017). The authors suggest that there may by two different processes encoding regular, and irregular, input. This may be analogous to RS and vMMN. Nevertheless, this study did not control for attention, hence the results are not fully comparable to the current thesis study.

However, if it was true that vMMN is akin to an expectation violation, then it is expected that this effect should disappear from the BOLD signal when attention is diverted, while if it is a signature of adaptation the BOLD signal should capture it (Larsson & Smith, 2011). The current study struggles to support either account given the lack of statistical support, thus further studies that directly investigates this question are crucial.

4.5.3 Limitations and Future Directions

One of the issues with this study is, as mentioned, the response score of the attentional task. It is at chance level which indicates that the task was difficult. This is problematic as on the one hand it suggests that the task was difficult enough to divert attention away from the moving stimulus appropriately, or on the other hand, it may indicate that the participants stopped paying attention to the fixation cross and started randomly guessing. Future studies should consider using another task or make the task less demanding. Perhaps using the same attentional diversion task as the second expectation study Larsson and Smith, 2011 - detecting number of a letter in a string of random letters.

Moreover, the level of attentional task difficulty may affect the outcome. Future studies may benefit from manipulating attention level in a more systematic man-

ner. This may explain why Hayashi et al., 2015 find RS effects in their duration paradigm – their attentional task was manipulated by focusing on another feature of the stimuli. Qualitatively one may define attending to the stimuli as no or low attentional diversion and focusing on another dimension of the stimuli as medium level, and focusing on something completely different as high attentional diversion. However, attentional control/diversion may not be a linear process and therefore it is a tricky aspect to control for.

The choice of stimuli may impact the results and may contribute to the diverging results between the current study and the Hayashi et al., 2015 study. Shape stimuli and motion dot field stimuli are different. Studies investigating inherited and intrinsic adaptation effects show that V1 inherit adaptation from V5 (Larsson & Harrison, 2015). To our knowledge, there are no studies on intrinsic and inherited adaptation effects using more complex stimuli such as shapes, and therefore it is difficult to discuss the Hayashi et al., 2015 study. One could reasonably discuss that there is a likelihood that object sensitive areas may process the shape stimuli differently than motion sensitive areas process motion stimuli. The results of this may be that the processing of shapes may overpower any processing of duration leading to the effects Hayashi et al., 2015 observe. Or duration may overpower shape processing.

In fact, a recent study found that different aspects of duration processing are encoded in different regions of the visual system (Stigliani et al., 2019). Specifically, they assessed responses to transient and sustained category stimuli presented at varying durations (from 33ms to 20s). They discovered that laterally located category-selective areas tend to process transient stimuli while ventral category selective areas encode both transient and sustained durations. As there is a widespread dynamic network for processing temporal aspects of categories, then this could facilitate the processing of shapes and hence explain some of Hayashi et al., 2015 results.

In terms of motion stimuli, there is evidence that V5 feeds adaptation effects back to V1 (either cortico-cortically or sub-cortically), and therefore it may be that the RS effects to duration is overpowered by motion input. However, this could just as easily be due to the attentional diversion overwriting any effect that may be observable using fMRI. Especially as Durant et al., 2018 finds RS effects in occipital/occipital-parietal areas using EEG.

4.5.4 Conclusion

The current study did not find any evidence for duration RS effects in early visual areas or parietal areas when attention was diverted. The study shows qualitative differences in total duration, but this is not statistically supported. Since we observe no RS effects, it adds to the inconsistency of the field and underscores the necessity of understanding the differences and similarities RS and vMMN paradigms, the imaging techniques using these, and how they differ with and without attentional diversion.

Chapter 5

Chapter Five: Discussion

5.1 Summary of Thesis Findings

The first experiments presented in this thesis investigated how NVC varies with expectation (experiment 1) and how this is affected by attention (experiment 2). We presented participants with face identities and varied the probability of stimulus repetition between runs. That is, runs with a 75% chance of a repetition (and a 25% chance of an alternation) created an expectation of repetition, whilst runs with these probabilities reversed made a repetition surprising. In the first experiment the participant had to focus on the face stimuli and respond when a face was inverted. In the second experiment, to divert attention away from the face stimuli, the participant had to focus on a demanding letter detection task that was presented at fixation. It was found that BOLD and CBF signals respond differently to expectation levels, specifically that expectation effects are present in CBF signals both when attention is focused and when it is diverted. This is not found in BOLD signals, whereby during focused attention trends towards expectation and RS were detected in V2 and BOLD defined FRA, respectively. When attention was diverted, interaction effects in V2

and V3 were observed. Moreover, it was found that $CMRO_2$ estimates reveal trends towards expectation in V2 and V3 during focused attention, and expectation and RS effects in V2 and V3, respectively, during diverted attention. Furthermore, the n-coupling ratio suggest differential NVC depending on expectation levels in BOLD defined FRA and CBF defined FRA during focused attention, and in CBF defined FRA during diverted attention. Taken together it indicates that the BOLD signal alone may not be sufficient to capture the underlying neural activation pattern, particularly for ES and RS. Additionally, it highlights the utility of measuring the CBF signal alongside the BOLD signal – both to estimate $CMRO_2$ and to understand brain dynamics from another perspective.

A subsequent experiment investigated the relationship between CBF, GABA, and positive and negative BOLD responses. This was done by presenting participants with flickering checkerboard stimuli that were composed of two radial wedges that formed a bowtie shape. These bowties were presented either horizontally or vertically in order to induce positive BOLD responses where the checkerboards were, and negative BOLD responses where the checkerboards were not. We found a positive correlation between BOLD and CBF for positive (in V1 and V3) and negative BOLD responses (in V1), as predicted. Moreover, there was a trend towards a significant positive relationship between GABA and n-coupling, indicating that NVC differs as GABA concentrations differ. Furthermore, we observed that positive responses generate significantly higher $CMRO_2$ levels compared to negative responses.

The final study aimed to replicate an EEG oddball experiment by adapting it to a RS fMRI experiment. The EEG study found that duration is automatically processed in visual areas when attention is diverted away. The current study found no effects of RS for duration in early visual areas, nor a statistically supported effect of total duration when attention is diverted. This means that the final thesis study cannot radically alter the field's understanding of how duration is processed.

We find a trend towards differential n-coupling depending on expectation and GABA concentration (in V1). This is important as it suggests that CBF and $CMRO_2$ are differentially modulated depending on different factors, such as experimental design, but also due to other physiological influences. This further complicates the picture: if CBF and $CMRO_2$ are differentially modulated depending on expectation (as observed in the expectation studies), and if they are also differentially modulated depending on GABA, then these modulations may interact. It would be interesting to measure GABA for the expectation paradigm, as this may shed light on whether individual levels of inhibitory activity affect ES and RS. Indeed, more and more researchers are using GABA as a measure of individual differences (e.g. Matthews et al., 2014), as it has been shown that high levels of GABA is predictive of improved performance in visual intelligence tasks (Cook et al., 2016), contrast discrimination (Hammett et al., submitted), as well as time perception efficiency (Matthews et al., 2014; Terhune, Russo, Near, Stagg, & Kadosh, 2014). These findings may imply that higher GABA concentrations are involved in reducing cortical noise in order to improve perceptual and cognitive processes (as discussed in chapter 3). If GABA is involved in reducing cortical noise, then one would predict that participants with high GABA concentrations would produce stronger suppression effects when trials are repeated or expected. This may also be applicable to the duration study – perhaps participants with high levels of GABA would have stronger suppression of repeated durations.

5.2 Relative vs absolute CBF

The n-coupling ratio is an interesting and potentially very useful way to look at calibrated BOLD data. However, as will be discussed below, the estimation of CBF and $CMRO_2$ has limitations associated with them that can limit the interpretability

of the n-coupling ratio.

It is difficult to determine the validity of the $CMRO_2$ estimates derived from BOLD and CBF measurements as the estimation models in the literature change frequently and are different depending on paradigm (e.g. Griffeth & Buxton, 2011; Moradi & Buxton, 2013, propose slightly different models depending on whether the paradigm is RS or not). The data emerging from that lab underscores the complexity of studying NVC in humans using fMRI, and the difficulty in developing a general $CMRO_2$ estimation model that could capture neural activation in every experimental design. One of the issues when estimating $CMRO_2$ is to appropriately estimate the scaling parameter M (maximal BOLD response) for each participant. This is important as it allows the estimates to be more comparable between participants and between experiments (e.g. Davis et al., 1998). M can greatly vary between individuals because it depends on many physiological factors such as vessel size and geometry, blood volume, oxygenation and deoxygenation at baseline among others (e.g. Huber et al., 2014). Indeed, when Whittaker, Driver, Bright, and Murphy, 2016 investigate the n-coupling parameter they observe that $CMRO_2$ estimates generated from measures of relative CBF change (as in the current experiments) could be confounded if there are inter-participant variations in CBF baselines. They base this on their finding that absolute CBF responses are the same even when baseline CBF varied. Interestingly, M can also vary between brain areas; some brain regions may have differential vascular or neural densities and thus the maximum possible BOLD response would differ. Hence, using relative CBF measures to estimate $CMRO_2$ is not optimal, but this confound can be overcome by incorporating a hypercapnia scan (e.g. Huber et al., 2014; Whittaker et al., 2016). The downside of this is that is limits the feasibility of calibrated BOLD as not every imaging centre has access to the necessary special equipment.

For the current studies we did not include a hypercapnia scan and therefore

the inter-participant CBF variability is unknown. This may mean that some CBF signal changes in response to different levels of expectation or during positive or negative responses are over- or under-estimated, and hence may over- or under-estimate $CMRO_2$. Additionally, there may be vascular and neural density differences between visual areas within each participant, meaning that important regional response differences may have been confounded. Specifically, V1 and V2 can vary in densities within participants leading to e.g. an overestimation of CBF signal change in one area and an underestimate in the other. These experiments could have benefitted from including a hypercapnia scan for absolute CBF measures, especially for the expectation experiments as they have of few trials and effectively halved temporal resolution due to ASL adjustments.

5.3 Who is the star of the show?

As discussed throughout the thesis there is a discrepancy between animal electrophysiological studies and fMRI studies in that animal work cannot replicate ES. Given the literature showing that expectation can affect hemodynamic signals without neural activity (Sirotin & Das, 2009), we set out to investigate hemodynamic contributions to ES. We demonstrate that ES are reflected in hemodynamic signals suggesting that the BOLD signal alone is not suitable for studying this phenomenon. This raises the question as to whether ES have a neural correlate at all. This is not clear from the literature. Perhaps it does not have or require a neural correlate, but it may still have a brain correlate.

Astrocytes are tightly linked with neurons in order to provide them with energy and nutrition – as the astrocytes are also tightly linked with vessels (Fields et al., 2014). Moreover, astrocytes have been shown to be involved in integrating evidence over periods of time to help determine behaviour (Fields et al., 2014; Moore &

Cao, 2008; Mu et al., 2019). Specifically, one recent study used zebrafish to study learned helplessness (Mu et al., 2019). They observed that zebrafish will give up trying to swim when visual flow information is withheld, and they further found that astrocytes calcium levels increased with number of failed swim attempts. As the calcium level reached a certain point, this triggered a suppression of swimming. In other words, astrocytes collect and store information over time and then use this to communicate with the brain that the current behaviour is not useful.

Perhaps this is the missing link. We know that neurons encode and express RS, and we know that ES have repeatedly failed to replicate in electrophysiological experiments. We also know that anticipatory hemodynamic events can occur without neural activity. From the current thesis we know that ES are expressed consistently in CBF signals and not in BOLD signals. Perhaps the information about statistical context, or repetition probability, is stored in astrocytes. Over time these cells may integrate information and recruit CBF accordingly in anticipation. This may explain why ES do not replicate in neural recording studies, as astrocytes are not measured (as they do not engage in electrical transmission of information). This may also explain why hemodynamic anticipatory responses can occur without neural activity – the astrocytes have stored information and are regulating the hemodynamic events. This could also explain how ES are demonstrated in humans using fMRI since the BOLD signal depends on hemodynamic events.

It does not, however, fully explain why ES fail to be observed in the BOLD signal in previous literature when attention is diverted (Larsson & Smith, 2011). However, there is one major hemodynamic signal that the current study did not measure: CBV. It has been shown that CBV tends to operate at a slower temporal scale (by an order of magnitude) compared to $CMRO_2$, CBF, and BOLD signals (e.g. Simon & Buxton, 2015). Moreover, an increase in CBV means an increase in deoxygenation (as most blood is in veins, and veins can accommodate larger

CBV increases compared to arteries), and this results in a slow decrease in BOLD signal over time. Moreover, Goense et al., 2012 observe during negative BOLD responses that CBF decreases, but that CBV increases. The authors attribute this to inhibitory activity since this will reduce excitatory activation leading to reductions in CBF recruitment and BOLD. Yet there is still a lag of blood in arteries and veins from which the inhibitory interneurons can extract energy, and this will lead to a relative increase in CBV.

Attention has been shown to result in differential coupling mechanisms. Moradi et al., 2012 show that when diverting attention the BOLD signals decreases, and CBF signals decrease a lot more in comparison - consistent with the findings in this thesis. They also show that $CMRO_2$ is greatly modulated during attentional tasks and they conclude that attention drives $CMRO_2$ in V1 whilst sensory input (among other processes) drives CBF. Interestingly, attention and GABAergic inhibitory activity are tightly linked, as GABA plays an important role in regulating excitatory activity (e.g. Markram et al., 2004; Paine, Cooke, & Lowes, 2015). Many neuropsychiatric disorders that show deficits in attention, such as ADHD (Kim, Woo, Lee, & Yoon, 2017), depression (Sanacora & Saricicek, 2007) and schizophrenia (Lewis, 2014) express GABA levels and functions that differ from neurotypical individuals.

Considering this and considering that the attentional diversions in the current thesis led to an overall reduction in BOLD signal change, it suggests that the demanding attentional tasks may have required the brain to engage in more inhibitory activation. Specifically, in order to engage with the task and simultaneously ignore the stimuli. Poplawsky, Fukuda, Murphy, and Kim, 2015 found that when they stimulate inhibitory cells then this decreases neural activity, however it increases hemodynamic responses. They observe that CBV increases the most compared to CBF and BOLD, whilst inhibition is increased. In the context of the expectation studies, this may mean that when attention is diverted then inhibitory activation

increases. This would effectively lead to an increase in CBV – and this may diminish some of the differential BOLD responses to expectation when attention is diverted.

In summary, astrocytes regulating hemodynamic responses may be an important process used by the brain to keep track of statistical variation in the external world. Hemodynamic signals are thought to interact differentially during inhibitory activity (Goense et al., 2012; Poplawsky et al., 2015), such as attentional manipulation (e.g. current study). This potentially explains the discrepancy in the literature regarding ES, RS, and attention. In other words, the brain may rely not only on neural information to achieve a task – it may also use glial and vascular information. This is discussed in a review by Moore and Cao, 2008 where they put forward a hypothesis suggesting hemodynamic system is not only a food delivery system, but it is in fact working alongside the neural system to process information. They base this on the observations that hemodynamics are 1) anatomically and functionally positioned to affect neural activity, 2) correlated with neural responses to incoming information and 3) are implicated during neuropathology. This view has been successfully incorporated in some clinical research paradigms that investigate Alzheimer's disease as a vascular rather than a neural disease (e.g. Horsburgh et al., 2018; Shabir, Berwick, & Francis, 2018). Hence, it would be an interesting perspective to adopt in fundamental research as evidence is clear that hemodynamics are vital and essential for neural functioning and existence.

5.4 Summary and Conclusion

We have shown evidence that neural and vascular processes couple differentially depending on expectation, and this may be modulated further by attention, and by putatively high and low inhibitory activity. Moreover, we have demonstrated that attentionally controlled EEG duration MMN effects do not replicate using

attentionally controlled fMRI RS. Although, the latter may be due to RS and MMN being separate processes.

Taken as a whole, the results presented in this thesis demonstrate that the dynamics of the BOLD signal is highly complex and intricate, in line with the literature. Hence, in order to draw conclusions about the underlying neural activity it is not advisable to rely solely on the BOLD signal. This is particularly the case when investigating complex perceptual and cognitive processes such as expectation and attention that may generate various interactions of excitatory and inhibitory activity. Therefore, it is important to either calibrate the BOLD signal using ASL or VASO or, alternatively, be extremely careful when interpreting the BOLD signal. Calibrating the BOLD signal could be of utmost value for researchers interested in understanding feedforward and feedback interactions, attention, memory, and learning as these cognitive and perceptual processes are likely highly complex.

Bibliography

Aguirre, G. K., & Detre, J. A. (2012). The development and future of perfusion fmri for dynamic imaging of human brain activity. *Neuroimage*, *62*(2), 1279–1285.

Andics, A., Gál, V., Vicsi, K., Rudas, G., & Vidnyánszky, Z. (2013). Fmri repetition suppression for voices is modulated by stimulus expectations. *Neuroimage*, *69*, 277–283.

Ascoli, G. A., Alonso-Nanclares, L., Anderson, S. A., Barrionuevo, G., Benav-ides-Piccione, R., Burkhalter, A., ... Fairén, A., et al. (2008). Petilla terminology: Nomenclature of features of gabaergic interneurons of the cerebral cortex. *Nature Reviews Neuroscience*, *9*(7), 557.

Attwell, D., Buchan, A. M., Charpak, S., Lauritzen, M., MacVicar, B. A., & Newman, E. A. (2010). Glial and neuronal control of brain blood flow. *Nature*, *468*(7321), 232.

Attwell, D., & Laughlin, S. B. (2001). An energy budget for signaling in the grey matter of the brain. *Journal of Cerebral Blood Flow & Metabolism*, *21*(10), 1133–1145.

Baker, C. I., Liu, J., Wald, L. L., Kwong, K. K., Benner, T., & Kanwisher, N. (2007). Visual word processing and experiential origins of functional selectivity in human extrastriate cortex. *Proceedings of the Nation-al Academy of Sciences*, *104*(21), 9087–9092.

Bandettini, P. A. (2012). The bold plot thickens: Sign-and layer-dependent hemodynamic changes with activation. *Neuron*, *76*(3), 468–469.

Barbelivien, A., Noël, C., MacKenzie, E. T., & Dauphin, F. (1999). Cerebrovascular evidence for a gabaergic modulation of the cholinergic vasodilatatory basalocortical system in the rat. *Brain research*, *834*(1-2), 223–227.

Barron, H. C., Garvert, M. M., & Behrens, T. E. (2016). Repetition suppression: A means to index neural representations using bold? *Philosophical Transactions of the Royal Society B: Biological Sciences*, *371*(1705), 20150355.

Bastos, A. M., Usrey, W. M., Adams, R. A., Mangun, G. R., Fries, P., & Friston, K. J. (2012). Canonical microcircuits for predictive coding. *Neuron*, *76*(4), 695–711.

Bear, M. F., Connors, B. W., & Paradiso, M. A. (2007). *Neuroscience*. Lippincott Williams & Wilkins.

Behrends, J., & Ten Bruggencate, G. (1993). Cholinergic modulation of synaptic inhibition in the guinea pig hippocampus in vitro: Excitation of gabaergic interneurons and inhibition of gaba-release. *Journal of Neurophysiology*, *69*(2), 626–629.

Bélanger, M., Allaman, I., & Magistretti, P. J. (2011). Brain energy metabolism: Focus on astrocyte-neuron metabolic cooperation. *Cell metabolism*, *14*(6), 724–738.

Benjamini, Y., & Hochberg, Y. (1995). Controlling the false discovery rate: A practical and powerful approach to multiple testing. *Journal of the Royal statistical society: series B (Methodological)*, *57*(1), 289–300.

Blockley, N. P., Griffeth, V. E., & Buxton, R. B. (2012). A general analysis of calibrated bold methodology for measuring cmro2 responses: Comparison of a new approach with existing methods. *Neuroimage*, *60*(1), 279–289.

Blockley, N. P., Griffeth, V. E., Simon, A. B., Dubowitz, D. J., & Buxton, R. B. (2015). Calibrating the bold response without administering gases: Compari-

son of hypercapnia calibration with calibration using an asymmetric spin echo. *Neuroimage*, *104*, 423–429.

Blüml, S. (2013). Magnetic resonance spectroscopy: Basics. In *Mr spectroscopy of pediatric brain disorders* (pp. 11–23). Springer.

Boillat, Y., Xin, L., van der Zwaag, W., & Gruetter, R. (2019). Metabolite concentration changes associated with positive and negative bold responses in the human visual cortex: A functional mrs study at 7 tesla. *Journal of Cerebral Blood Flow & Metabolism*, 0271678X19831022.

Borogovac, A., & Asllani, I. (2012). Arterial spin labeling (asl) fmri: Advantages, theoretical constrains and experimental challenges in neurosciences. *International journal of biomedical imaging*, *2012*.

Burock, M. A., & Dale, A. M. (2000). Estimation and detection of event-related fmri signals with temporally correlated noise: A statistically efficient and unbiased approach. *Human brain mapping*, *11*(4), 249–260.

Buxton, R. B. (2002). Coupling between cbf and cmro2 during neuronal activity. In *International congress series* (Vol. 1235, pp. 23–32). Elsevier.

Buxton, R. B. (2009). *Introduction to functional magnetic resonance imaging: Principles and techniques*. Cambridge university press.

Buxton, R. B., & Frank, L. R. (1997). A model for the coupling between cerebral blood flow and oxygen metabolism during neural stimulation. *Journal of cerebral blood flow & metabolism*, *17*(1), 64–72.

Buxton, R. B., Griffeth, V. E., Simon, A. B., & Moradi, F. (2014). Variability of the coupling of blood flow and oxygen metabolism responses in the brain: A problem for interpreting bold studies but potentially a new window on the underlying neural activity. *Frontiers in neuroscience*, *8*, 139.

Buxton, R. B., Uludağ, K., Dubowitz, D. J., & Liu, T. T. (2004). Modeling the hemodynamic response to brain activation. *Neuroimage*, *23*, S220–S233.

Buzsáki, G., Kaila, K., & Raichle, M. (2007). Inhibition and brain work. *Neuron*, *56*(5), 771–783.

Caesar, K., Offenhauser, N., & Lauritzen, M. (2008). Gamma-aminobutyric acid modulates local brain oxygen consumption and blood flow in rat cerebellar cortex. *Journal of Cerebral Blood Flow & Metabolism*, *28*(5), 906–915.

Chen, Huang, X., Luo, Y., Peng, C., & Liu, C. (2010). Differences in the neural basis of automatic auditory and visual time perception: Erp evidence from an across-modal delayed response oddball task. *Brain research*, *1325*, 100–111.

Chen, & Zhou, X. (2014). Fast transfer of crossmodal time interval training. *Experimental brain research*, *232*(6), 1855–1864.

Chen, & Zhu, X.-H. (1997). Suppression of physiological eye movement artifacts in functional mri using slab presaturation. *Magnetic resonance in medicine*, *38*(4), 546–550.

Cook, E., Hammett, S. T., & Larsson, J. (2016). Gaba predicts visual intelligence. *Neuroscience letters*, *632*, 50–54.

Coull, J. T., Cheng, R.-K., & Meck, W. H. (2011). Neuroanatomical and neurochemical substrates of timing. *Neuropsychopharmacology*, *36*(1), 3.

Curran, W., Benton, C. P., Harris, J. M., Hibbard, P. B., & Beattie, L. (2016). Adapting to time: Duration channels do not mediate human time perception. *Journal of vision*, *16*(5), 4–4.

Davis, T. L., Kwong, K. K., Weisskoff, R. M., & Rosen, B. R. (1998). Calibrated functional mri: Mapping the dynamics of oxidative metabolism. *Proceedings of the National Academy of Sciences*, *95*(4), 1834–1839.

De Baene, W., & Vogels, R. (2009). Effects of adaptation on the stimulus selectivity of macaque inferior temporal spiking activity and local field potentials. *Cerebral Cortex*, *20*(9), 2145–2165.

De Martino, F., Moerel, M., van de Moortele, P.-F., Ugurbil, K., Goebel, R., Yacoub, E., & Formisano, E. (2013). Spatial organization of frequency preference and selectivity in the human inferior colliculus. *Nature communications*, *4*, 1386.

de Lange, F. P., Heilbron, M., & Kok, P. (2018). How do expectations shape perception? *Trends in cognitive sciences*, *22*(9), 764–779.

Demeter, E., Hernandez-Garcia, L., Sarter, M., & Lustig, C. (2011). Challenges to attention: A continuous arterial spin labeling (asl) study of the effects of distraction on sustained attention. *Neuroimage*, *54*(2), 1518–1529.

Derdeyn, C. P., Videen, T. O., Yundt, K. D., Fritsch, S. M., Carpenter, D. A., Grubb, R. L., & Powers, W. J. (2002). Variability of cerebral blood volume and oxygen extraction: Stages of cerebral haemodynamic impairment revisited. *Brain*, *125*(3), 595–607.

Desimone, R. (1996). Neural mechanisms for visual memory and their role in attention. *Proceedings of the National Academy of Sciences*, *93*(24), 13494–13499.

Desimone, R., & Schein, S. J. (1987). Visual properties of neurons in area v4 of the macaque: Sensitivity to stimulus form. *Journal of neurophysiology*, *57*(3), 835–868.

Donahue, M. J., Near, J., Blicher, J. U., & Jezzard, P. (2010). Baseline gaba concentration and fmri response. *Neuroimage*, *53*(2), 392–398.

Donahue, M. J., Rane, S., Hussey, E., Mason, E., Pradhan, S., Waddell, K. W., & Ally, B. A. (2014). Gamma-aminobutyric acid (gaba) concentration inversely correlates with basal perfusion in human occipital lobe. *Journal of Cerebral Blood Flow & Metabolism*, *34*(3), 532–541.

Dougherty, R., Koch, V., Brewer, A., Fischer, B., Modersitzki, J., & Wandell, B. (2003). Visual field representations and locations of visual areas v1/2/3 in human visual cortex. *Journal of vision*, *3*, 586–98.

Duong, T. Q., Yacoub, E., Adriany, G., Hu, X., Ugurbil, K., Vaughan, J. T., ... Kim, S.-G. (2002). High-resolution, spin-echo bold, and cbf fmri at 4 and 7

t. *Magnetic Resonance in Medicine: An Official Journal of the International Society for Magnetic Resonance in Medicine*, *48*(4), 589–593.

Durant, S., Sulykos, I., & Czigler, I. (2018). Automatic detection of the duration of visual static and dynamic stimuli. *Brain research*, *1686*, 34–41.

Edden, R. A., Puts, N. A., Harris, A. D., Barker, P. B., & Evans, C. J. (2014). Gannet: A batch-processing tool for the quantitative analysis of gamma-aminobutyric acid–edited mr spectroscopy spectra. *Journal of Magnetic Resonance Imaging*, *40*(6), 1445–1452.

Eger, E., Schyns, P. G., & Kleinschmidt, A. (2004). Scale invariant adaptation in fusiform face-responsive regions. *Neuroimage*, *22*(1), 232–242.

Ekstrom, A. (2010). How and when the fmri bold signal relates to underlying neural activity: The danger in dissociation. *Brain research reviews*, *62*(2), 233–244.

Epstein, R., & Kanwisher, N. (1998). A cortical representation of the local visual environment. *Nature*, *392*(6676), 598.

Fang, F., Murray, S. O., Kersten, D., & He, S. (2005). Orientation-tuned fmri adaptation in human visual cortex. *Journal of Neurophysiology*, *94*(6), 4188–4195.

Fields, R. D., Araque, A., Johansen-Berg, H., Lim, S.-S., Lynch, G., Nave, K.-A., ... Wake, H. (2014). Glial biology in learning and cognition. *The neuroscientist*, *20*(5), 426–431.

Filosa, J. A., Bonev, A. D., Straub, S. V., Meredith, A. L., Wilkerson, M. K., Aldrich, R. W., & Nelson, M. T. (2006). Local potassium signaling couples neuronal activity to vasodilation in the brain. *Nature neuroscience*, *9*(11), 1397.

Fishman, Y. I., & Steinschneider, M. (2012). Searching for the mismatch negativity in primary auditory cortex of the awake monkey: Deviance detection or stimulus specific adaptation? *Journal of Neuroscience*, *32*(45), 15747–15758.

Fox, S. I. (2006). *Human physiology 9th editon*. McGraw-Hill press, New York, USA.

Fox, Iaria, G., & Barton, J. J. (2009). Defining the face processing network: Optimization of the functional localizer in fmri. *Human brain mapping*, *30*(5), 1637–1651.

Fracasso, A., Luijten, P. R., Dumoulin, S. O., & Petridou, N. (2018). Laminar imaging of positive and negative bold in human visual cortex at 7 t. *NeuroImage*, *164*, 100–111.

Friston, K. (2005). A theory of cortical responses. *Philosophical transactions of the Royal Society B: Biological sciences*, *360*(1456), 815–836.

Gaehtgens, P. (2002). Microcirculation-historical background and conceptual update. In *International congress series* (1235, pp. 3–13).

Gattass, R., Gross, C., & Sandell, J. (1981). Visual topography of v2 in the macaque. *Journal of Comparative Neurology*, *201*(4), 519–539.

Gauthier, C. J., & Hoge, R. D. (2013). A generalized procedure for calibrated mri incorporating hyperoxia and hypercapnia. *Human brain mapping*, *34*(5), 1053–1069.

Gazzaniga, M., & Ivry, R. B. (2013). *Cognitive neuroscience: The biology of the mind: Fourth international student edition*. WW Norton.

Girouard, H., Bonev, A. D., Hannah, R. M., Meredith, A., Aldrich, R. W., & Nelson, M. T. (2010). Astrocytic endfoot ca2+ and bk channels determine both arteriolar dilation and constriction. *Proceedings of the National Academy of Sciences*, *107*(8), 3811–3816.

Goense, J., Merkle, H., & Logothetis, N. K. (2012). High-resolution fmri reveals laminar differences in neurovascular coupling between positive and negative bold responses. *Neuron*, *76*(3), 629–639.

Griffeth, V. E., & Buxton, R. B. (2011). A theoretical framework for estimating cerebral oxygen metabolism changes using the calibrated-bold method: Modeling the effects of blood volume distribution, hematocrit, oxygen extraction

fraction, and tissue signal properties on the bold signal. *Neuroimage*, *58*(1), 198–212.

Griffeth, V. E., Perthen, J. E., & Buxton, R. B. (2011). Prospects for quantitative fmri: Investigating the effects of caffeine on baseline oxygen metabolism and the response to a visual stimulus in humans. *Neuroimage*, *57*(3), 809–816.

Griffeth, V. E., Simon, A. B., & Buxton, R. B. (2015). The coupling of cerebral blood flow and oxygen metabolism with brain activation is similar for simple and complex stimuli in human primary visual cortex. *NeuroImage*, *104*, 156–162.

Grill-Spector, K., Henson, R., & Martin, A. (2006). Repetition and the brain: Neural models of stimulus-specific effects. *Trends in cognitive sciences*, *10*(1), 14–23.

Grill-Spector, K., Kushnir, T., Hendler, T., Edelman, S., Itzchak, Y., & Malach, R. (1998). A sequence of object-processing stages revealed by fmri in the human occipital lobe. *Human brain mapping*, *6*(4), 316–328.

Grill-Spector, K., & Malach, R. (2001). Fmr-adaptation: A tool for studying the functional properties of human cortical neurons. *Acta psychologica*, *107*(1-3), 293–321.

Grill-Spector, K., & Weiner, K. S. (2014). The functional architecture of the ventral temporal cortex and its role in categorization. *Nature Reviews Neuroscience*, *15*(8), 536.

Grondin, S. (2010). Timing and time perception: A review of recent behavioral and neuroscience findings and theoretical directions. *Attention, Perception, & Psychophysics*, *72*(3), 561–582.

Groppe, D. (2020). False discovery rate - benjamini-hochberg method. *MATLAB central file exchange: retrieved 20th of October 2020*, NA.

Grotheer, M., & Kovács, G. (2014). Repetition probability effects depend on prior experiences. *Journal of Neuroscience*, *34*(19), 6640–6646.

Grotheer, M., & Kovács, G. (2016). Can predictive coding explain repetition suppression? *Cortex*, *80*, 113–124.

Haigh, S., Coffman, B., Murphy, T., Ward, K., & Salisbury, D. (2017). 728. deficits in complex mmn to group size deviance in first-episode schizophrenia-spectrum psychosis. *Biological Psychiatry*, *81*(10), S295.

Haller, S., Zaharchuk, G., Thomas, D. L., Lovblad, K.-O., Barkhof, F., & Golay, X. (2016). Arterial spin labeling perfusion of the brain: Emerging clinical applications. *Radiology*, *281*(2), 337–356.

Hammett, S., Cook, E., Hassan, O., Ceri-Ann, H., Rooslien, H., Tizkar, R., & Larsson, J. (submitted). Gaba, noise and gain in human visual cortex. *Current Biology*.

Handwerker, D. A., Ollinger, J. M., & D'Esposito, M. (2004). Variation of bold hemodynamic responses across subjects and brain regions and their effects on statistical analyses. *Neuroimage*, *21*(4), 1639–1651.

Hare, H. V., Blockley, N. P., Gardener, A. G., Clare, S., & Bulte, D. P. (2015). Investigating the field-dependence of the davis model: Calibrated fmri at 1.5, 3 and 7 t. *NeuroImage*, *112*, 189–196.

Harris, A. D., Puts, N. A., Anderson, B. A., Yantis, S., Pekar, J. J., Barker, P. B., & Edden, R. A. (2015). Multi-regional investigation of the relationship between functional mri blood oxygenation level dependent (bold) activation and gaba concentration. *PloS one*, *10*(2), e0117531.

Harrison, R. V., Harel, N., Panesar, J., & Mount, R. J. (2002). Blood capillary distribution correlates with hemodynamic-based functional imaging in cerebral cortex. *Cerebral Cortex*, *12*(3), 225–233.

Harvey, B., Dumoulin, S., & Fracasso, A. (2018). A fronto-parietal network of visual event duration-tuned topographic maps. *Journal of Vision*, *18*(10), 962–962.

Hayashi, M. J., Ditye, T., Harada, T., Hashiguchi, M., Sadato, N., Carlson, S., ... Kanai, R. (2015). Time adaptation shows duration selectivity in the human parietal cortex. *PLoS Biology*, *13*(9), e1002262.

Heeger, D. (2006). Perception lecture notes: Retinal ganglion cells. University Lecture. Department of Psychology, New York University.

Henson, R. N., Price, C. J., Rugg, M. D., Turner, R., & Friston, K. J. (2002). Detecting latency differences in event-related bold responses: Application to words versus nonwords and initial versus repeated face presentations. *Neuroimage*, *15*(1), 83–97.

Heron, J., Aaen-Stockdale, C., Hotchkiss, J., Roach, N. W., McGraw, P. V., & Whitaker, D. (2011). Duration channels mediate human time perception. *Proceedings of the Royal Society B: Biological Sciences*, *279*(1729), 690–698.

Herreras, O. (2016). Local field potentials: Myths and misunderstandings. *Frontiers in neural circuits*, *10*, 101.

Hladky, S. B., & Barrand, M. A. (2016). Fluid and ion transfer across the blood–brain and blood–cerebrospinal fluid barriers; a comparative account of mechanisms and roles. *Fluids and Barriers of the CNS*, *13*(1), 19.

Hoge, R. D. (2012). Calibrated fmri. *NeuroImage*, *62*(2), 930–937.

Horsburgh, K., Wardlaw, J. M., Van Agtmael, T., Allan, S. M., Ashford, M. L., Bath, P. M., ... Carare, R. O., et al. (2018). Small vessels, dementia and chronic diseases–molecular mechanisms and pathophysiology. *Clinical science*, *132*(8), 851–868.

Hu, Chen, X., Gu, H., & Yang, Y. (2013). Resting-state glutamate and gaba concentrations predict task-induced deactivation in the default mode network. *Journal of Neuroscience*, *33*(47), 18566–18573.

Hu, Le, T. H., & Uğurbil, K. (1997). Evaluation of the early response in fmri in individual subjects using short stimulus duration. *Magnetic resonance in medicine*, *37*(6), 877–884.

Hubel, D. H., & Wiesel, T. N. (1959). Receptive fields of single neurones in the cat's striate cortex. *The Journal of physiology*, *148*(3), 574–591.

Hubel, D. H., & Wiesel, T. N. (1962). Receptive fields, binocular interaction and functional architecture in the cat's visual cortex. *The Journal of physiology*, *160*(1), 106–154.

Huber, L., Goense, J., Kennerley, A. J., Ivanov, D., Krieger, S. N., Lepsien, J., ... Möller, H. E. (2014). Investigation of the neurovascular coupling in positive and negative bold responses in human brain at 7 t. *Neuroimage*, *97*, 349–362.

Huber, L., Uludağ, K., & Möller, H. E. (2017). Non-bold contrast for laminar fmri in humans: Cbf, cbv, and cmro2. *NeuroImage*.

Huk, A. C., & Heeger, D. J. (2002). Pattern-motion responses in human visual cortex. *Nature neuroscience*, *5*(1), 72.

Ivry, R. B., & Schlerf, J. E. (2008). Dedicated and intrinsic models of time perception. *Trends in cognitive sciences*, *12*(7), 273–280.

Jenkinson, M., Bannister, P., Brady, M., & Smith, S. (2002). Improved optimization for the robust and accurate linear registration and motion correction of brain images. *Neuroimage*, *17*(2), 825–841.

Kaliukhovich, D. A., & Vogels, R. (2010). Stimulus repetition probability does not affect repetition suppression in macaque inferior temporal cortex. *Cerebral Cortex*, *21*(7), 1547–1558.

Kaliukhovich, D. A., & Vogels, R. (2014). Neurons in macaque inferior temporal cortex show no surprise response to deviants in visual oddball sequences. *Journal of Neuroscience*, *34*(38), 12801–12815.

Kettenmann, H., & Verkhratsky, A. (2011). Neuroglia–living nerve glue. *Fortschritte der Neurologie-Psychiatrie*, *79*(10), 588–597.

Kilner, I., David, O., & Friston, K. (2007). Neuronal models of energetics. *Statistical Parametric Mapping: The Analysis of Functional Brain Images*, 406.

Kim, & Park, J. H. (2019). More about the basic assumptions of t-test: Normality and sample size. *Korean journal of anesthesiology*, *72*(4), 331.

Kim, & Ress, D. (2016). Arterial impulse model for the bold response to brief neural activation. *Neuroimage*, *124*, 394–408.

Kim, Woo, J., Lee, C. J., & Yoon, B.-E. (2017). Decreased glial gaba and tonic inhibition in cerebellum of mouse model for attention-deficit/hyperactivity disorder (adhd). *Experimental neurobiology*, *26*(4), 206–212.

Kohn, A. (2007). Visual adaptation: Physiology, mechanisms, and functional benefits. *Journal of neurophysiology*, *97*(5), 3155–3164.

Kohn, A., & Movshon, J. A. (2003). Neuronal adaptation to visual motion in area mt of the macaque. *Neuron*, *39*(4), 681–691.

Kohn, A., & Movshon, J. A. (2004). Adaptation changes the direction tuning of macaque mt neurons. *Nature neuroscience*, *7*(7), 764.

Kok, P., Jehee, J. F., & De Lange, F. P. (2012). Less is more: Expectation sharpens representations in the primary visual cortex. *Neuron*, *75*(2), 265–270.

Koopmans, P. J., Barth, M., & Norris, D. G. (2010). Layer-specific bold activation in human v1. *Human brain mapping*, *31*(9), 1297–1304.

Kovács, G., Iffland, L., Vidnyánszky, Z., & Greenlee, M. W. (2012). Stimulus repetition probability effects on repetition suppression are position invariant for faces. *Neuroimage*, *60*(4), 2128–2135.

Kovács, G., Kaiser, D., Kaliukhovich, D. A., Vidnyánszky, Z., & Vogels, R. (2013). Repetition probability does not affect fmri repetition suppression for objects. *Journal of Neuroscience*, *33*(23), 9805–9812.

Krause, B. W., Wijtenburg, S. A., Holcomb, H. H., Kochunov, P., Wang, D. J., Hong, L. E., & Rowland, L. M. (2014). Anterior cingulate gaba levels predict whole-brain cerebral blood flow. *Neuroscience letters*, *561*, 188–191.

Krekelberg, B., Boynton, G. M., & van Wezel, R. J. (2006). Adaptation: From single cells to bold signals. *Trends in neurosciences*, *29*(5), 250–256.

Kuffler, S. W. (1953). Discharge patterns and functional organization of mammalian retina. *Journal of neurophysiology*, *16*(1), 37–68.

Larsson, J. (2001). *Imaging vision* (Doctoral dissertation, Karolinska Institute, Stockholm, Sweden).

Larsson, J., & Harrison, S. J. (2015). Spatial specificity and inheritance of adaptation in human visual cortex. *Journal of neurophysiology*, *114*(2), 1211–1226.

Larsson, J., & Heeger, D. J. (2006). Two retinotopic visual areas in human lateral occipital cortex. *Journal of Neuroscience*, *26*(51), 13128–13142.

Larsson, J., Landy, M. S., & Heeger, D. J. (2003). Orientation-selective adaptation to first-and second-order stimuli in human visual cortex measured with fmri. *Science*, *224*, 1260–2.

Larsson, J., & Smith, A. T. (2011). Fmri repetition suppression: Neuronal adaptation or stimulus expectation? *Cerebral Cortex*, *22*(3), 567–576.

Lauritzen, M., Mathiesen, C., Schaefer, K., & Thomsen, K. J. (2012). Neuronal inhibition and excitation, and the dichotomic control of brain hemodynamic and oxygen responses. *Neuroimage*, *62*(2), 1040–1050.

Lee, L. M., Boorman, L., Glendenning, E., Christmas, C., Sharp, P., Redgrave, P., ... Howarth, C. (2019). Key aspects of neurovascular control mediated by specific populations of inhibitory cortical interneurons. *bioRxiv*, 550269.

Lewis, D. A. (2014). Inhibitory neurons in human cortical circuits: Substrate for cognitive dysfunction in schizophrenia. *Current opinion in neurobiology*, *26*, 22–26.

Li, B. S., Wang, H., & Gonen, O. (2003). Metabolite ratios to assumed stable creatine level may confound the quantification of proton brain mr spectroscopy. *Magnetic resonance imaging*, *21*(8), 923–928.

Lin, A.-L., Fox, P. T., Hardies, J., Duong, T. Q., & Gao, J.-H. (2010). Nonlinear coupling between cerebral blood flow, oxygen consumption, and atp produc-

tion in human visual cortex. *Proceedings of the National Academy of Sciences*, *107*(18), 8446–8451.

Lindauer, U., Leithner, C., Kaasch, H., Rohrer, B., Foddis, M., Füchtemeier, M., ... Kohl-Bareis, M., et al. (2010). Neurovascular coupling in rat brain operates independent of hemoglobin deoxygenation. *Journal of cerebral blood flow & metabolism*, *30*(4), 757–768.

Liu, T. T., & Wong, E. C. (2005). A signal processing model for arterial spin labeling functional mri. *Neuroimage*, *24*(1), 207–215.

Logothetis, N. K. (2008). What we can do and what we cannot do with fmri. *Nature*, *453*(7197), 869.

Logothetis, N. K., Pauls, J., Augath, M., Trinath, T., & Oeltermann, A. (2001). Neurophysiological investigation of the basis of the fmri signal. *Nature*, *412*(6843), 150.

Logothetis, N. K., & Wandell, B. A. (2004). Interpreting the bold signal. *Annu. Rev. Physiol. 66*, 735–769.

Mader, S. S. (2008). *Mader's understanding human anatomy & physiology*. McGraw-Hill Higher Education.

Magri, C., Schridde, U., Murayama, Y., Panzeri, S., & Logothetis, N. K. (2012). The amplitude and timing of the bold signal reflects the relationship between local field potential power at different frequencies. *Journal of Neuroscience*, *32*(4), 1395–1407.

Markram, H., Toledo-Rodriguez, M., Wang, Y., Gupta, A., Silberberg, G., & Wu, C. (2004). Interneurons of the neocortical inhibitory system. *Nature reviews neuroscience*, *5*(10), 793.

MATLAB. (2020). *Version 9.8.0 (r2020a)*. Natick, Massachusetts: The MathWorks Inc.

Matthews, W. J., Terhune, D. B., Van Rijn, H., Eagleman, D. M., Sommer, M. A., & Meck, W. H. (2014). Subjective duration as a signature of coding efficiency:

Emerging links among stimulus repetition, predictive coding, and cortical gaba levels. *Timing & Time Perception Reviews*, *1*.

Maunsell, J. H., & Van Essen, D. C. (1983). Functional properties of neurons in middle temporal visual area of the macaque monkey. i. selectivity for stimulus direction, speed, and orientation. *Journal of neurophysiology*, *49*(5), 1127–1147.

Mayrhauser, L., Bergmann, J., Crone, J., & Kronbichler, M. (2014). Neural repetition suppression: Evidence for perceptual expectation in object-selective regions. *Frontiers in human neuroscience*, *8*, 225.

Merola, A., Murphy, K., Stone, A. J., Germuska, M. A., Griffeth, V. E., Blockley, N. P., ... Wise, R. G. (2016). Measurement of oxygen extraction fraction (oef): An optimized bold signal model for use with hypercapnic and hyperoxic calibration. *Neuroimage*, *129*, 159–174.

Metea, M. R., Kofuji, P., & Newman, E. A. (2007). Neurovascular coupling is not mediated by potassium siphoning from glial cells. *Journal of Neuroscience*, *27*(10), 2468–2471.

Mishkin, M., Ungerleider, L. G., & Macko, K. A. (1983). Object vision and spatial vision: Two cortical pathways. *Trends in neurosciences*, *6*, 414–417.

Mohler, H., Fritschy, J., Lüscher, B., Rudolph, U., Benson, J., & Benke, D. (1996). The gaba a receptors. In *Ion channels* (pp. 89–113). Springer.

Moore, C. I., & Cao, R. (2008). The hemo-neural hypothesis: On the role of blood flow in information processing. *Journal of neurophysiology*, *99*(5), 2035–2047.

Moradi, F., Buračas, G. T., & Buxton, R. B. (2012). Attention strongly increases oxygen metabolic response to stimulus in primary visual cortex. *Neuroimage*, *59*(1), 601–607.

Moradi, F., & Buxton, R. B. (2013). Adaptation of cerebral oxygen metabolism and blood flow and modulation of neurovascular coupling with prolonged stimulation in human visual cortex. *Neuroimage*, *82*, 182–189.

Mu, Y., Bennett, D. V., Rubinov, M., Narayan, S., Yang, C.-T., Tanimoto, M., ... Ahrens, M. B. (2019). Glia accumulate evidence that actions are futile and suppress unsuccessful behavior. *Cell*.

Muckli, L. (2010). What are we missing here? brain imaging evidence for higher cognitive functions in primary visual cortex v1. *International Journal of Imaging Systems and Technology*, *20*(2), 131–139.

Muller, T., & Nobre, A. C. (2014). Flow of time: Perceiving the passage of time: Neural possibilities. *Annals of the New York Academy of Sciences*, *1326*(1), 60.

Mulligan, S. J., & MacVicar, B. A. (2004). Calcium transients in astrocyte endfeet cause cerebrovascular constrictions. *Nature*, *431*(7005), 195.

Mullinger, K. J., Mayhew, S. D., Bagshaw, A. P., Bowtell, R., & Francis, S. T. (2014). Evidence that the negative bold response is neuronal in origin: A simultaneous eeg–bold–cbf study in humans. *Neuroimage*, *94*, 263–274.

Murai, Y., Whitaker, D., & Yotsumoto, Y. (2016). The centralized and distributed nature of adaptation-induced misjudgments of time. *Current Opinion in Behavioral Sciences*, *8*, 117–123.

Muthukumaraswamy, S. D., Edden, R. A., Jones, D. K., Swettenham, J. B., & Singh, K. D. (2009). Resting gaba concentration predicts peak gamma frequency and fmri amplitude in response to visual stimulation in humans. *Proceedings of the National Academy of Sciences*, *106*(20), 8356–8361.

Muthukumaraswamy, S. D., Evans, C. J., Edden, R. A., Wise, R. G., & Singh, K. D. (2012). Individual variability in the shape and amplitude of the bold-hrf correlates with endogenous gabaergic inhibition. *Human brain mapping*, *33*(2), 455–465.

Myers, J. F., Nutt, D. J., & Lingford-Hughes, A. R. (2016). Gamma-aminobutyric acid as a metabolite: Interpreting magnetic resonance spectroscopy experiments. *Journal of Psychopharmacology*, *30*(5), 422–427.

Nasrallah, F. A., Kaur, K., Singh, O. R., Yeow, L. Y., & Chuang, K.-H. (2017). Gabaergic effect on resting-state functional connectivity: Dynamics under pharmacological antagonism. *Neuroimage*, *149*, 53–62.

Near, J., Ho, Y.-C. L., Sandberg, K., Kumaragamage, C., & Blicher, J. U. (2014). Long-term reproducibility of gaba magnetic resonance spectroscopy. *Neuroimage*, *99*, 191–196.

Northoff, G., Walter, M., Schulte, R. F., Beck, J., Dydak, U., Henning, A., ... Boesiger, P. (2007). Gaba concentrations in the human anterior cingulate cortex predict negative bold responses in fmri. *Nature neuroscience*, *10*(12), 1515.

Ogawa, S., Menon, R., Tank, D. W., Kim, S., Merkle, H., Ellermann, J., & Ugurbil, K. (1993). Functional brain mapping by blood oxygenation level-dependent contrast magnetic resonance imaging. a comparison of signal characteristics with a biophysical model. *Biophysical journal*, *64*(3), 803–812.

Ogawa, S. [Seiji], Lee, T.-M., Stepnoski, R., Chen, W., Zhu, X.-H., & Ugurbil, K. (2000). An approach to probe some neural systems interaction by functional mri at neural time scale down to milliseconds. *Proceedings of the National Academy of Sciences*, *97*(20), 11026–11031.

Olson, I. R., Rao, H., Moore, K. S., Wang, J., Detre, J. A., & Aguirre, G. K. (2006). Using perfusion fmri to measure continuous changes in neural activity with learning. *Brain and cognition*, *60*(3), 262–271.

Ozeki, H., Finn, I. M., Schaffer, E. S., Miller, K. D., & Ferster, D. (2009). Inhibitory stabilization of the cortical network underlies visual surround suppression. *Neuron*, *62*(4), 578–592.

Paine, T. A., Cooke, E. K., & Lowes, D. C. (2015). Effects of chronic inhibition of gaba synthesis on attention and impulse control. *Pharmacology Biochemistry and Behavior*, *135*, 97–104.

Peelen, M. V., & Downing, P. E. (2017). Category selectivity in human visual cortex: Beyond visual object recognition. *Neuropsychologia*, *105*, 177–183.

Pi, H.-J., Hangya, B., Kvitsiani, D., Sanders, J. I., Huang, Z. J., & Kepecs, A. (2013). Cortical interneurons that specialize in disinhibitory control. *Nature*, *503*(7477), 521.

Pitcher, D., Dilks, D. D., Saxe, R. R., Triantafyllou, C., & Kanwisher, N. (2011). Differential selectivity for dynamic versus static information in face-selective cortical regions. *Neuroimage*, *56*(4), 2356–2363.

Pitcher, D., Duchaine, B., & Walsh, V. (2014). Combined tms and fmri reveal dissociable cortical pathways for dynamic and static face perception. *Current Biology*, *24*(17), 2066–2070.

Poplawsky, A. J., Fukuda, M., Murphy, M., & Kim, S.-G. (2015). Layer-specific fmri responses to excitatory and inhibitory neuronal activities in the olfactory bulb. *Journal of Neuroscience*, *35*(46), 15263–15275.

Preibisch, C., Bührer, M., Riedl, V., et al. (2015). Evaluation of multiband epi acquisitions for resting state fmri. *PloS one*, *10*(9), e0136961.

Puts, N. A., & Edden, R. A. (2012). In vivo magnetic resonance spectroscopy of gaba: A methodological review. *Progress in nuclear magnetic resonance spectroscopy*, *60*, 29.

Ramsey, J. D., Hanson, S. J., Hanson, C., Halchenko, Y. O., Poldrack, R. A., & Glymour, C. (2010). Six problems for causal inference from fmri. *neuroimage*, *49*(2), 1545–1558.

Rao, R. P., & Ballard, D. H. (1999). Predictive coding in the visual cortex: A functional interpretation of some extra-classical receptive-field effects. *Nature neuroscience*, *2*(1), 79.

Rauschecker, J. P. (2018). Where, when, and how: Are they all sensorimotor? towards a unified view of the dorsal pathway in vision and audition. *Cortex*, *98*, 262–268.

Rentzsch, J., Shen, C., Jockers-Scherübl, M. C., Gallinat, J., & Neuhaus, A. H. (2015). Auditory mismatch negativity and repetition suppression deficits in

schizophrenia explained by irregular computation of prediction error. *PloS one*, *10*(5), e0126775.

Reynolds, J. H., Pasternak, T., & Desimone, R. (2000). Attention increases sensitivity of v4 neurons. *Neuron*, *26*(3), 703–714.

Rice, N. J., Valyear, K. F., Goodale, M. A., Milner, A. D., & Culham, J. C. (2007). Orientation sensitivity to graspable objects: An fmri adaptation study. *Neuroimage*, *36*, T87–T93.

Rich, P. (2003). The molecular machinery of keilin's respiratory chain. Portland Press Limited.

Richter, D., Ekman, M., & de Lange, F. P. (2018). Suppressed sensory response to predictable object stimuli throughout the ventral visual stream. *Journal of Neuroscience*, *38*(34), 7452–7461.

Roy, C. S., & Sherrington, C. S. (1890). On the regulation of the blood-supply of the brain. *The Journal of physiology*, *11*(1-2), 85–158.

Sanacora, G., & Saricicek, A. (2007). Gabaergic contributions to the pathophysiology of depression and the mechanism of antidepressant action. *CNS & Neurological Disorders-Drug Targets (Formerly Current Drug Targets-CNS & Neurological Disorders)*, *6*(2), 127–140.

Sanchez-Vives, M. V., Nowak, L. G., & McCormick, D. A. (2000). Membrane mechanisms underlying contrast adaptation in cat area 17in vivo. *Journal of Neuroscience*, *20*(11), 4267–4285.

Schür, R. R., Draisma, L. W., Wijnen, J. P., Boks, M. P., Koevoets, M. G., Joëls, M., ... Vinkers, C. H. (2016). Brain gaba levels across psychiatric disorders: A systematic literature review and meta-analysis of 1h-mrs studies. *Human brain mapping*, *37*(9), 3337–3352.

Segaert, K., Weber, K., de Lange, F. P., Petersson, K. M., & Hagoort, P. (2013). The suppression of repetition enhancement: A review of fmri studies. *Neuropsychologia*, *51*(1), 59–66.

Sereno, M. I., Dale, A., Reppas, J., Kwong, K., Belliveau, J., Brady, T., ... Tootell, R. (1995). Borders of multiple visual areas in humans revealed by functional magnetic resonance imaging. *Science*, *268*(5212), 889–893.

Shabir, O., Berwick, J., & Francis, S. E. (2018). Neurovascular dysfunction in vascular dementia, alzheimer's and atherosclerosis. *BMC neuroscience*, *19*(1), 62.

Shmuel, A., Yacoub, E., Pfeuffer, J., Van de Moortele, P.-F., Adriany, G., Hu, X., & Ugurbil, K. (2002). Sustained negative bold, blood flow and oxygen consumption response and its coupling to the positive response in the human brain. *Neuron*, *36*(6), 1195–1210.

Shulman, R. G., Rothman, D. L., Behar, K. L., & Hyder, F. (2004). Energetic basis of brain activity: Implications for neuroimaging. *Trends in neurosciences*, *27*(8), 489–495.

Siesjö, B., Kjällquist, Å., Pontén, U., & Zwetnow, N. (1968). Extracellular ph in the brain and cerebral blood flow. In *Progress in brain research* (Vol. 30, pp. 93–98). Elsevier.

Simon, A. B., & Buxton, R. B. (2015). Understanding the dynamic relationship between cerebral blood flow and the bold signal: Implications for quantitative functional mri. *Neuroimage*, *116*, 158–167.

Sirotin, Y. B., & Das, A. (2009). Anticipatory haemodynamic signals in sensory cortex not predicted by local neuronal activity. *Nature*, *457*(7228), 475.

Sotelo, C. (1978). Purkinje cell ontogeny: Formation and maintenance of spines. In *Progress in brain research* (Vol. 48, pp. 149–170). Elsevier.

Stagg, C. J., Bachtiar, V., & Johansen-Berg, H. (2011). What are we measuring with gaba magnetic resonance spectroscopy? *Communicative & integrative biology*, *4*(5), 573–575.

Stefanics, G., Kimura, M., & Czigler, I. (2011). Visual mismatch negativity reveals automatic detection of sequential regularity violation. *Frontiers in Human Neuroscience*, *5*, 46.

Stefanics, G., Kremláček, J., & Czigler, I. (2014). Visual mismatch negativity: A predictive coding view. *Frontiers in human neuroscience*, *8*, 666.

Stefanics, G., Kremláček, J., & Czigler, I. (2016). Mismatch negativity and neural adaptation: Two sides of the same coin. response: Commentary: Visual mismatch negativity: A predictive coding view. *Frontiers in human neuroscience*, *10*, 13.

Stigliani, A., Jeska, B., & Grill-Spector, K. (2019). Differential sustained and transient temporal processing across visual streams. *PLoS computational biology*, *15*(5), e1007011.

Summerfield, C., Trittschuh, E. H., Monti, J. M., Mesulam, M.-M., & Egner, T. (2008). Neural repetition suppression reflects fulfilled perceptual expectations. *Nature neuroscience*, *11*(9), 1004.

Summerfield, C., Wyart, V., Mareike Johnen, V., & De Gardelle, V. (2011). Human scalp electroencephalography reveals that repetition suppression varies with expectation. *Frontiers in Human Neuroscience*, *5*, 67.

Tang, M. F., Smout, C. A., Arabzadeh, E., & Mattingley, J. B. (2018). Prediction error and repetition suppression have distinct effects on neural representations of visual information. *Elife*, *7*, e33123.

Team, C. 2. (2011). Cogent 2000. Wellcome Trust Centre for Neuroimaging, UCL London, UK.

Terhune, D. B., Russo, S., Near, J., Stagg, C. J., & Kadosh, R. C. (2014). Gaba predicts time perception. *Journal of Neuroscience*, *34*(12), 4364–4370.

Tjandra, T., Brooks, J. C., Figueiredo, P., Wise, R., Matthews, P. M., & Tracey, I. (2005). Quantitative assessment of the reproducibility of functional activation measured with bold and mr perfusion imaging: Implications for clinical trial design. *Neuroimage*, *27*(2), 393–401.

Todorovic, A., & de Lange, F. P. (2012). Repetition suppression and expectation suppression are dissociable in time in early auditory evoked fields. *Journal of Neuroscience*, *32*(39), 13389–13395.

Todorovic, A., van Ede, F., Maris, E., & de Lange, F. P. (2011). Prior expectation mediates neural adaptation to repeated sounds in the auditory cortex: An meg study. *Journal of Neuroscience*, *31*(25), 9118–9123.

Tolias, A. S., Sultan, F., Augath, M., Oeltermann, A., Tehovnik, E. J., Schiller, P. H., & Logothetis, N. K. (2005). Mapping cortical activity elicited with electrical microstimulation using fmri in the macaque. *Neuron*, *48*(6), 901–911.

Tong, F., Harrison, S. A., Dewey, J. A., & Kamitani, Y. (2012). Relationship between bold amplitude and pattern classification of orientation-selective activity in the human visual cortex. *Neuroimage*, *63*(3), 1212–1222.

Tosetti, M., Schirmer, T., d'Alesio, V., Di Costanzo, A., & Scarabino, T. (2006). Spectroscopy basics. *High Field Brain MRI: Use in Clinical Practice*, 51.

Utzerath, C., John-Saaltink, E. S., Buitelaar, J., & de Lange, F. P. (2017). Repetition suppression to objects is modulated by stimulus-specific expectations. *Scientific reports*, *7*(1), 8781.

Van Rijn, H., Gu, B.-M., & Meck, W. H. (2014). Dedicated clock/timing-circuit theories of time perception and timed performance. In *Neurobiology of interval timing* (pp. 75–99). Springer.

Verkhratsky, A. [Alexei], Zorec, R., & Parpura, V. (2017). Stratification of astrocytes in healthy and diseased brain. *Brain Pathology*, *27*(5), 629–644.

Vinken, K., de Beeck, H. P. O., & Vogels, R. (2018). Face repetition probability does not affect repetition suppression in macaque inferotemporal cortex. *Journal of Neuroscience*, *38*(34), 7492–7504.

Vinken, K., Vogels, R., & de Beeck, H. O. (2017). Recent visual experience shapes visual processing in rats through stimulus-specific adaptation and response enhancement. *Current Biology*, *27*(6), 914–919.

Vogels, R. (2016). Sources of adaptation of inferior temporal cortical responses. *Cortex*, *80*, 185–195.

von Bartheld, C. S., Bahney, J., & Herculano-Houzel, S. (2016). The search for true numbers of neurons and glial cells in the human brain: A review of 150 years of cell counting. *Journal of Comparative Neurology*, *524*(18), 3865–3895.

Wacongne, C., Changeux, J.-P., & Dehaene, S. (2012). A neuronal model of predictive coding accounting for the mismatch negativity. *Journal of Neuroscience*, *32*(11), 3665–3678.

Walsh, K. S., & McGovern, D. P. (2018). Expectation suppression dampens sensory representations of predicted stimuli. *The Journal of Neuroscience*, *38*(50), 10592.

Walter, S., Forsgren, M., Lundengard, K., Simon, R., Nilsson, M., Soderfeldt, B., ... Engstrom, M. (2016). Positive allosteric modulator of gaba lowers bold responses in the cingulate cortex. *PLos ONE*, *11*, 53–62.

Whittaker, J. R., Driver, I. D., Bright, M. G., & Murphy, K. (2016). The absolute cbf response to activation is preserved during elevated perfusion: Implications for neurovascular coupling measures. *Neuroimage*, *125*, 198–207.

Wilson, H. R., & Cowan, J. D. (1972). Excitatory and inhibitory interactions in localized populations of model neurons. *Biophysical journal*, *12*(1), 1–24.

Winkler, A. M., Ridgway, G. R., Webster, M. A., Smith, S. M., & Nichols, T. E. (2014). Permutation inference for the general linear model. *Neuroimage*, *92*, 381–397.

Yaksh, T., & Anderson, R. (1987). In vivo studies on intracellular ph, focal flow, and vessel diameter in the cat cerebral cortex: Effects of altered co2 and electrical stimulation. *Journal of Cerebral Blood Flow & Metabolism*, *7*(3), 332–341.

Zeki, S. M. (1974). Functional organization of a visual area in the posterior bank of the superior temporal sulcus of the rhesus monkey. *The Journal of Physiology*, *236*(3), 549–573.